ลักษณะเฉพาะของลมตามฤดูกาลและกระแสน้ำเนื่องจากลมบริเวณอ่าวไทย

นายประชา ไชยองการ

วิทยานิพนธ์นี้เป็นส่วนหนึ่งของการศึกษาตามหลักสูตรปริญญาวิทยาศาสตรมหาบัณฑิต
สาขาวิชาโลกศาสตร์ ภาควิชาธรณีวิทยา
คณะวิทยาศาสตร์ จุฬาลงกรณ์มหาวิทยาลัย
ปีการศึกษา 2555

CHARACTERISTICS OF SEASONAL WIND AND WIND-DRIVEN CURRENT IN THE GULF OF THAILAND

Mr. Pracha Chaiongkarn

A Thesis Submitted in Partial Fulfillment of the Requirements
for the Degree of Master of Science Program in Earth Sciences
Department of Geology
Faculty of Science
Chulalongkorn University
Academic Year 2012

Thesis Title	CHARACTERISTICS OF SEASONAL WIND AND WIND- DRIVEN CURRENT IN THE GULF OF THAILAND
By	Mr. Pracha Chaiongkarn
Field of Study	Earth Science
Thesis Advisor	Assistant Professor Pramot Sojisuporn, Ph.D.

Accepted by the Faculty of Science, Chulalongkorn University in Partial Fulfillment of the Requirements for the Master's Degree

……Dean of the Faculty of Science
(Professor Supot Hannongbua, Dr.rer.nat)

THESIS COMMITTEE

……Chairman
(Assistant Professor Sombat Yumuang, Ph.D.)

……Thesis Advisor
(Assistant Professor Pramot Sojisuporn, Ph.D.)

……Examiner
(Assistant Professor Srilert Chotpantarat, Ph.D.)

……External Examiner
(Assistant Professor Monton Anongponyoskun, Ph.D.)

ประชา ไชยองการ: ลักษณะเฉพาะของลมตามฤดูกาลและกระแสน้ำเนื่องจากลมบริเวณอ่าวไทย. (CHARACTERISTICS OF SEASONAL WIND AND WIND-DRIVEN CURRENT IN THE GULF OF THAILAND) อ.ที่ปรึกษาวิทยานิพนธ์หลัก: ผศ.ดร. ปราโมทย์ โศจิศุภร, 118 หน้า.

อ่าวไทยตั้งอยู่ระหว่างเส้นละติจูด 6° ถึง 14° เหนือ และลองติจูด 99° ถึง 105° ตะวันออก อยู่ในเขตไหล่ทวีปเชื่อมต่อกับทะเลจีนใต้ทางด้านใต้ เป็นเขตที่ได้รับรังสีจากดวงอาทิตย์สูงเกือบตลอดทั้งปี โดยลมมรสุมตะวันออกเฉียงเหนือและลมมรสุมตะวันตกเฉียงใต้มีบทบาทสำคัญในการควบคุมสภาพภูมิอากาศในพื้นที่ การไหลเวียนของระบบลมมรสุมมีความสัมพันธ์ต่อการเปลี่ยนแปลงของรูปแบบลมและฝนบริเวณประเทศไทย รวมไปถึงการไหลเวียนของกระแสน้ำในอ่าวไทยด้วย

วัตถุประสงค์ของงานวิจัยนี้เพื่อศึกษาการรูปแบบการไหลเวียนของลมและกระแสน้ำเนื่องจากลมบริเวณอ่าวไทยในแต่ละฤดูกาล ตั้งแต่ ปี ค.ศ.2000 ถึง ค.ศ.2002 ซึ่งครอบคลุมปีลานินญ่า, ปีปกติ และปีเอลนินโญ่ โดยทำการจำลองรูปแบบการไหลเวียนของลมด้วยแบบจำลองเชิงตัวเลข WRF ผลที่ได้นำเข้าสู่แบบจำลองการไหลเวียนของกระแสน้ำเพื่อจำลองการไหลเวียนของน้ำเนื่องจากลม จากนั้นทำการหาความสัมพันธ์ของความเร็วทิศทางลมและกระแสน้ำเนื่องจากลมในปีเอลนินโญ่และปีลานินญ่ากับปีปกติ

แบบจำลอง WRF สามารถจำลองความเร็วและทิศทางลมได้ใกล้เคียงกับข้อมูลลมจากดาวเทียม ผลการจำลองกระแสน้ำเนื่องจากลมสอดคล้องกับงานวิจัยอื่นๆ ผลการศึกษาพบว่าการไหลเวียนของน้ำในอ่าวไทยถูกควบคุมด้วยระบบลมมรสุมเป็นหลัก โดยช่วงฤดูฝนมีลมตะวันตกและลมตะวันตกเฉียงใต้พัดแรงเข้ามาจากมหาสมุทรอินเดียส่งผลให้เกิดการไหลเวียนของน้ำแบบตามเข็มนาฬิกาในอ่าวไทยและอ่าวไทยตอนบนและพบกระแสน้ำหมุนวนในหลายพื้นที่ ช่วงฤดูหนาวมีลมพัดแรงมาจากทางทิศตะวันออกเฉียงเหนือและตะวันออกจากที่ราบสูงไซบีเรียผ่านมาทางทะเลจีนใต้ส่งผลให้เกิดการไหลเวียนแบบทวนเข็มนาฬิกาในอ่าวไทยและอ่าวไทยตอนบน ช่วงฤดูร้อนมีลมพัดมาจากทางทิศตะวันออกและทิศตะวันออกเฉียงใต้และจะค่อยๆ เบนเป็นทิศใต้เมื่อเข้าสู่อ่าวไทยตอนบนส่งผลเกิดการไหลเวียนแบบทวนเข็มนาฬิกาเช่นเดียวกับกระแสน้ำในฤดูหนาว ในช่วงที่มีลมตะวันออกแรงบริเวณชายฝั่งอ่าวไทยฝั่งตะวันตกจะเกิดกระแสน้ำไหลเลียบชายฝั่งขึ้นไปทางเหนือ อิทธิพลของปรากฏการณ์เอลนินโญ่ทำให้ความเร็วลมมรสุมมีค่าเพิ่มขึ้นและทิศทางลมเปลี่ยนแปลงไปราว 10 องศา อิทธิพลลานินญ่าทำให้ความเร็วลมมรสุมมีค่าลดลงและทิศทางลมเปลี่ยนแปลงไปเล็กน้อยเช่นกัน รูปแบบการไหลเวียนของน้ำเนื่องจากลมไม่เปลี่ยนแปลงตามอิทธิพลของปรากฏการณ์เอลนินโญ่และลานินญ่า

ภาควิชา ธรณีวิทยา ลายมือชื่อนิสิต .....

สาขาวิชา โลกศาสตร์ ลายมือชื่อ อ.ที่ปรึกษาวิทยานิพนธ์หลัก .....

ปีการศึกษา 2555

5272402023 : MAJOR EARTH SCIENCES

KEYWORDS: WRF MODEL / WIND-DRIVEN CURRENT /SEA SURFACE WIND

PRACHA CHAIONGKARN: CHARACTERISTICS OF SEASONAL WIND AND WIND-DRIVEN CURRENT IN THE GULF OF THAILAND. ADVISOR: ASST. PROF. PRAMOT SOJISUPORN, Ph.D., 118 pp.

The gulf of Thailand is bounded by Latitude 6° to 14°N and Longitude 99° to 105°E. It is located on the continental shelf connecting to South China Sea via the southern entrance. The gulf is border by Thailand, Cambodia and Vietnam on the eastern, northern and western side respectively. The gulf receives high solar radiation throughout the year. The NE and SW monsoon controls the local weather around the gulf. The monsoonal wind plays an important role in controlling the wind pattern, rainfall over Thailand, and also controlling water circulation in the Gulf of Thailand.

The project objective is to simulate wind regime over the gulf and wind-driven circulation in the gulf of Thailand during the year 2000-2002. The study time span cover La Niña, normal and El Niño period respectively. The study is accomplished through to use of WRF model and 2-D water circulation model. Wind regime from WRF model was the input to the water circulation model. Statistical analysis was performed on the wind data in order to study the effect of El Niño and La Niña events on the wind pattern over the gulf of Thailand. Wind pattern from the WRF model was comparable to the satellite (observed) wind. And wind-driven circulation was similar to the results of earlier studies. During rainy season, the westerly and southwesterly wind from the Indian Ocean caused the wind-driven current in the gulf and the upper gulf to flow in a clockwise direction. Small eddies existed some locations in the gulf. During winter, high pressure system from Siberia caused wind in South China Sea to flow from the east to gulf entrance. While inside the gulf, the wind deflected to NE wind and caused the wind-driven circulation in the gulf and the upper gulf to flow in a counterclockwise direction. During summer, wind from South China Sea blew from the east direction. While inside the gulf, the wind deflected to SE wind. And the SE wind deflected to S wind when entering the upper gulf of Thailand. The pattern of wind-driven current in the gulf was similar to that in during the winter. When easterly wind was strong near the lower eastern coast of the gulf, there would be a northward flow of water along the coast.

The effect of the El Niño event increased wind speed over the gulf and deflect the wind direction by 10°. On the other hand, the effect of the La Niña event reduced wind speed over the gulf and deflects the wind direction by the same degree. The wind-driven circulation pattern did not change with the El Niño and La Niña event.

Department: Geology Student's Signature

Field of Study: Earth Sciences Advisor's Signature

Academic Year: 2012

ACKNOWLEDEMENTS

I sincerely thank my Advisor, Assistant Professor Dr. Pramot Sojisuporn, Department of Marine Science, Faculty of Science, Chulalongkorn University for their supports, encouragements, critically advice and reviews of this thesis.

Appreciation is also done to thank Assistant Professor Dr. Sombat Yumuang, Assistant Professor Dr. Srilert Chotpantarat, Department of Geology Science, Faculty of Science, Chulalongkorn University, and Assistant Professor Dr. Monton Anongponyoskun, Thesis Evaluation Committee members who contributed to this thesis by providing useful suggestions and practical advices.

I would like to thank Ms. Boossarasiri Thana, Ms. malatee thiyakup, Department of Geology, Faculty of Science, Chulalongkorn University especially for their valuable suggestion and support. Furthermore, I would like to thank Mr. Kamol Brahmasakha Na Sakolnagara and Mr. Somkuan Tonjan, Numerical Weather Prediction, Meteorological Department of Thailand for technical help on WRF model and visualization software.

I sincerely gratify the Center for Atmospheric Research's (NCAR) Meso-scale and Micro-scale Meteorology (MMM) Division, the National Oceanic and Atmospheric Administration's (NOAA) National Centers for Environmental Prediction (NCEP), for their permission to use software and essential data for this research.

I thank to Mr. julvijit wangprasertkul, Mr. Katawut waiyasusri and all friends for their support throughout my thesis with their valuable suggestions.

Finally, I would like to thank my parents for their support and encouragement throughout my study at the university.

CONTENTS

Page

LIST OF TABLES

LIST OF FIGURES

CHAPTER I
INTRODUCTION

1.1 Background and Statement of the Problem

The Gulf of Thailand is located between Latitude 6° to 14°N and Longitude 99° to 105°E. The gulf is encircled by Thailand, Malaysia, Kingdom of Cambodia and the Socialist Republic of Vietnam on four sides, and open to South China Sea via the southern side. It is a semi-enclosed gulf with about 400-km wide at the mouth and 800-km long along the NW-SE axis. The total area of the gulf is roughly 320,000 km^2. The average depth of the gulf is about 45 m with the maximum depth of 80 m in the middle of the gulf. The gulf aligns in the NW-SE direction (Aschariyaphotha, 2007). The Gulf of Thailand lies in the tropical zone which receives high thermal solar energy throughout the year. The interaction between the atmospheric and ocean surface plays an important role in controlling the local climate stability; in other words, time and spatial variations of the oceanic climate will affect the variability of continental climate conditions. Therefore, climate variability is linked to the changes of weather or regional phenomenon. Located on the Indochina Peninsula that is bordered by the Pacific Ocean on its eastern side and the Indian Ocean on its western side, Thailand is inevitably influenced by the variability of both oceans in terms of climate phenomenon that varies with monsoon regimes. Moreover, climate variability leads to severe weather conditions and natural disasters in both regional and local levels.

Thailand weather is influenced by the NE and SW monsoon seasons. The monsoons also controlled the climatic and oceanographic characteristics of the Gulf of Thailand. People who live around the coast certainly know the changing weather well and have adjusted their activities such as fishing, aquaculture, tourism, transportation accordingly.

To protect the lives and occupations of people against natural disasters, the local climate and oceanographic conditions of the Gulf of Thailand must be known *a priori*. Especially water circulation in the gulf is a very important physical parameter that

controls the rate of water exchange and dispersion of organic and inorganic substances in the water body. The full characteristics of the prevalent currents would help to better understand the behaviors of living organisms and allow for better management of the natural resources in the Gulf (Sojisuporn, 2010).

Circulations in the gulf of Thailand is driven by the reversal monsoonal winds, co-oscillation tide and water density gradients (Singhruck, 2002 by Robinson, 1974). Field data and numerical model results indicated that the predominant monsoonal winds caused eddies, mixing and the exchange of water mass in the gulf (Sojisuporn, 2010 by Robinson, 1974; Siripong, 1984; Buranpratheprat and Bunpapong, 1998; Yanagi and Takao, 1998) and wind is the major contributor to the eddy generation in the gulf, while tidal energy contributed very little in the eddy generation (Singhruck, 2002).

Previous studies on circulations in the Gulf of Thailand have either focused for the entire area of the gulf or just in the Upper Gulf of Thailand which lies in the northern end of the gulf. The driving forces used were also different. For example, Snidvong and Sojisuporn (1997) assumed a steady wind for the entire gulf. Archevarahuprock and Wongwises (1994) used averaged measured wind at some stations in the study area. Lopittayakorn (2012) used averaged measured wind from 9 oceanographic buoys in the gulf. Buranpratheprat and Bunpapong, (1998), Singhruck, (2002) used predicted winds from multi sources.

The wind data used in earlier studies came from 3 sources: 1) measured data from meteorological station whether on land or in the sea, 2) global wind model, and 3) hypothetical data which was usually constant wind field. The bilinear interpolation must be performed on the measured and global wind data which might result in erroneous output for the circulation model while using the constant wind field might not obtain the right circulation pattern. This study will use the regional model to obtain the realistic wind field for the Gulf of Thailand and the wind-driven circulation would be more realistic.

Thus, the accuracy of obtained ocean circulation extremely depended on the accuracy of wind data used. Reliability of wind data becomes very important since the

circulation is very sensitive to the wind patterns (Buranapratherat, 2006). As wind plays a significant role in eddy generation, better accuracy of eddy simulation can be achieved by using regional numerical weather prediction data which should yield better spatial variability than the present global wind data (Singhruck, 2002).

The Weather Research and Forecast (WRF) model is able to produce realistic wind climatology, probabilistic wind distributions and annual cycle. It also reproduces well-known regional winds remarkably well (Menendez, *et al.*, 2012). The performance of the WRF model in wind simulation has been evaluated under different numerical and physical options (Carvalho, 2012). The WRF model is suitable for use in a broad range of applications over wide scales ranging from meters to thousands of kilometers. It includes one-way and two-way moving nested routines and can be coupled with other models including hydrology, land-surface, and ocean models.

The aim of this research is to simulate the regional wind regimes for the Gulf of Thailand using the WRF model. The simulated wind used to drive the 2-D wind-driven current in the Gulf of Thailand under different monsoonal conditions. The result of this study help better understand monsoonal wind and surface ocean circulation variability under the influence of the ENSO conditions. Better options would be obtained from this study and can be used to predict wind field for the Gulf of Thailand in the future.

Real-time wind-driven circulation in the gulf can be obtained if the regional wind forecast is available. Thus prediction of oil spills and search and rescue in the gulf can be done more accurately.

1.2 Objectives of the Research

1. To describe the characteristics of wind and wind-driven circulation in the gulf of Thailand during 2000-2002.

2. To accurately simulate the wind speed and wind direction for the Gulf of Thailand during 2000-2002.

1.3 Scope of the Research

1. Use the global wind gained from the WRF model as input for the simulation of wind characteristics in the Gulf of Thailand during 2000-2002.

2. Use 2-D Numerical model to simulate wind-driven currents in the Gulf of Thailand during 2000-2002.

3. The studied area in the Gulf of Thailand was bounded by Latitude 5°N to 14°N, Longitude 99°E to 107°E (See Figure 1-1).

4. The monsoonal wind variability was caused by ENSO effect only (any effects from the Indian Ocean is omitted).

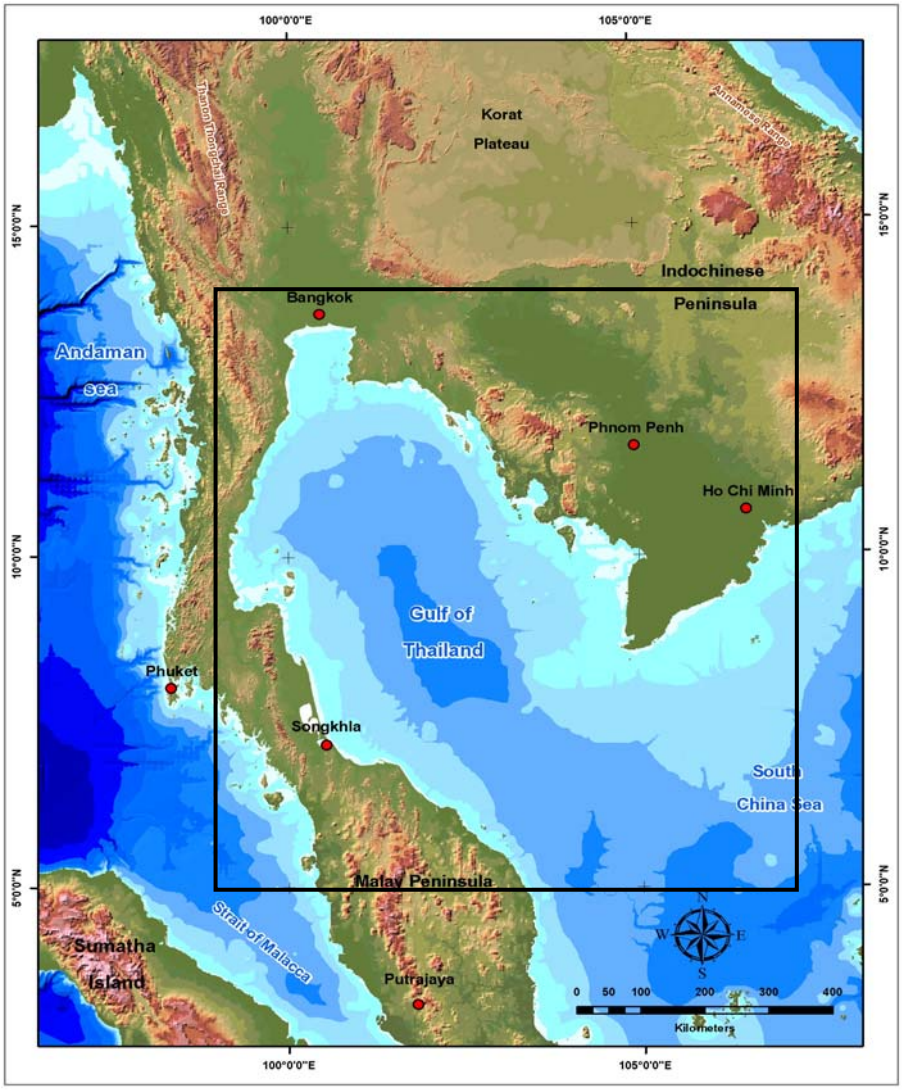

Figure 1-1 The study area.

1.4 Expected Outcomes of the Research

1. Accurate and appropriate simulated wind for the region during 2000-2002.
2. Wind and wind-driven current patterns for the Gulf of Thailand during 2000-2002.
3. Real-time forecast of wind-driven current in the Gulf of Thailand during 2000-2002.

1.5 Research Methodology

To accomplish the aims of this thesis, the research involves five consecutive steps as followed.

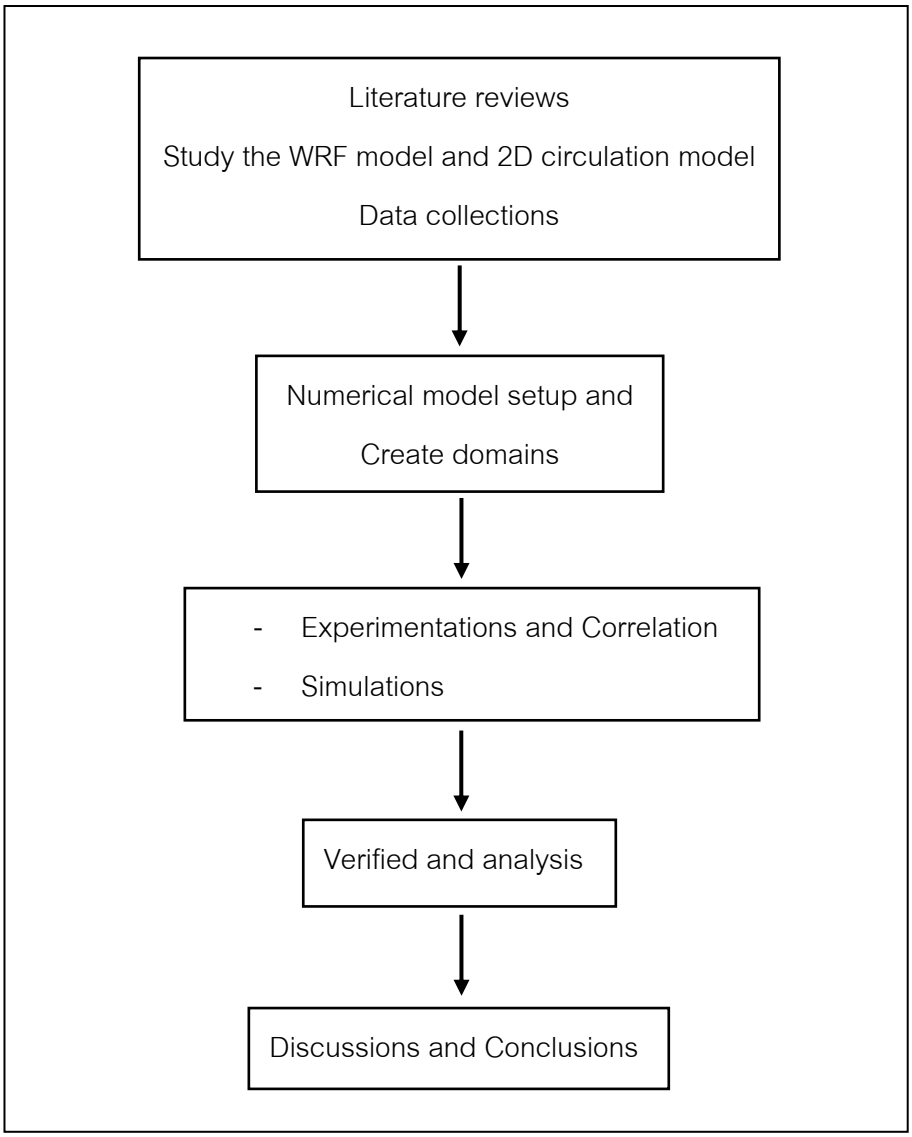

Figure 1-2 The Research Methodology.

1.5.1 Preparation

- Literature reviews of the related research in the study area and surrounding the Gulf of Thailand and South China Sea.
- Study how to run the WRF model and 2-D Numerical model.
- Collect input data for the WRF model.
- Collect satellite data (sea surface wind) covering the Gulf of Thailand.
- Obtains the bottom topography from the 30-second General Bathymetric Chart of the Ocean (GEBCO30).

1.5.2 Numerical model setup

- Install the following software on a PC computer;
    - Fedora 12 (Linux) - C, C++, FORTRAN 90, gFORTRAN compliers
    - WRF model - WRF Domain wizard
    - IDV_3.1u1
- Install the following software on a Laptop computer;
    - Microsoft Windows XP - 2D circulation model
    - Digital visual Fortran 6.5 - Surfer9
    - Grapher8
- Create domain of the study area.
    - Used WRF Domain wizard to create domain for WRF model.
    - Used Surfer9 to provide gridded domain for 2D circulation model.

1.5.3 Simulations and correlation

- Use WRF model to simulate wind patterns over the Gulf of Thailand.
- Try various physical Options in the WRF model which were suggested by many researches performed on other regions.
- Evaluate the WRF model performance using three statistical analyses (RMSE, Bias, and STDE calculation).
- Use the best physical Option to simulate seasonal wind field in the Gulf of Thailand.

- Interpolate the simulated wind field to fit the model area of the Gulf of Thailand.
- Use simulated wind to drive wind-driven circulation on 2D circulation model for the Gulf of Thailand.
- Compare wind-driven circulation under different monsoon seasons and El Niño & La Niña events.
- Plot simulated wind field and wind-driven circulation using SURFER9.

1.5.4 Verification and analysis

- Evaluate fitness of wind regimes from the WRF model with the sea surface wind from the atmospheric satellite data using RMSE, Bias, and STDE values.
- Use the paired t-test to test the mean of wind speed and direction during the normal even with those during the El Niño or La Niña events.
- Verify wind-driven circulation with results from previous studies.

1.5.5 Discussions and Conclusions

- Results of WRF model experiment.
- Results of simulation wind.
- Results of wind-driven current.
- Influence of El Niño and La Niña effects on wind fields and wind-driven current.

1.6 Thesis Chapters

The thesis is composes of 5 chapters, including this introductory Chapter I. Chapter II contains theory and reviews of previous studied. The conceptual idea methodology, the application of 2-D Circulation model and WRF model are also briefly reviewed is given in Chapter III. The study results and discussions will present in Chapters IV. The conclusions and recommendations appear in Chapter V.

CHAPTER II
LITERATURE REVIEWS

2.1 Overview of the Gulf of Thailand

The Gulf of Thailand (GOT) is a shallow semi-enclosed basin on the continental of Sunda Shelf, which is a submerged connection between Southeast Asia, Malaysia, Sumatra, Java, and Borneo (Aschariyaphotha, 2007). Its location is between latitude 6°-14°N and longitude 99°-105°E. The gulf has a roughly rectangular shape with its major axis being 800-km long and aligned in the NW-SE direction. Its minor axis at the mouth is about 400-km long. The averaged depth of the GOT is about 45 m with the deepest spot in the central part of about 80 m. On the northern of the gulf is the shallow Upper Gulf of Thailand where the average depth is only 15 m. The Gulf of Thailand is bordered by Malaysia, Thailand, Cambodia and Vietnam on the western, northern, and eastern sides, respectively (Sojisuporn, 2010).

Thailand's weather is most affected by the monsoon. The word "monsoon" comes from the Arabic word "Mausim", meaning "season" or "the season of wind". And nowadays monsoon is the term used for the seasonal shift in wind direction which usually brings on a different season of weather. Monsoons are characterized by their seasonality, geographical preference, and strength. Monsoon rain and winds are the end results of heating patterns produced by the sun and the distribution of land mass and ocean body (Prakhammintara, 2007).

Thailand is influenced by both the SW and NE monsoon seasons. The SW monsoon usually blows in from the Indian Ocean and the surrounding regions, bringing warm and moist air (thus rainfall) to the mainland. On average, this monsoon starts from the middle of May and lasts till September to mid October. The NE monsoon usually blows in from the continent site in Siberia and the surrounding regions, bringing cold and dry air to Thailand and the region. This monsoon starts from the November and last till mid February.

2.2 Sea surface circulation

Circulation in the Gulf of Thailand is driven by the interplay of wind, co-oscillation tide and water density gradients. The major component of the sea surface circulation appears to be wind induced motion.

2.2.1 Wind-driven current

Wind-driven currents are created by the force of the wind exerting stress on the sea surface. This stress causes the surface water to move and this movement is transmitted to the underlying water to a depth that is dependent mainly on the strength and persistence of the wind. The wind-driven current does not flow in exactly the same direction as the wind, but is deflected by the Earth's rotation. According to the Ekman's theoretical study on the direction effect of wind stress on the ocean current, Ekman current occurs due to the balance between Coriolis acceleration and wind stress terms. The effect of earth's rotation (Coriolis force) is accounted for the deflection of surface current by 45° to the right or left of the wind direction in the northern or southern hemisphere respectively (see Figure 2-1). This theory is based on the assumption of infinitely deep water to avoid the bottom friction effect. For the case finite depth, the angle between wind and surface current direction is not 45°, but it depends on the depth of the sea and latitude.

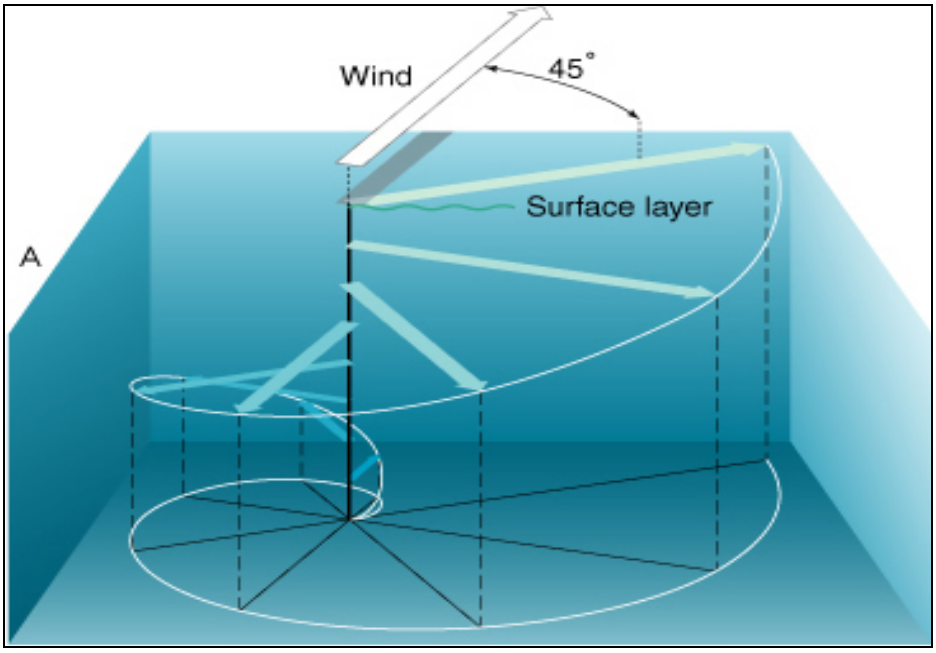

Figure 2-1 Schematic of Ekman spiral for deep water in the Northern Hemisphere.
(http://oceanmotion.org/html/background/ocean-in-motion.htm)

2.2.2 Density-driven current

The density-driven current is driven by the differences in the density of seawater at different locations. The density of seawater depends on its temperature and salinity. As a result, this movement is known as the “thermohaline” circulation (Figure 2-2). Stratification is most developed in March-May due to large sea surface heating and weak sea surface wind, weakened until September-October and it vanishes in the NE monsoon due to sea surface cooling and intense vertical mixing by strong wind. Density-driven current, induced by the horizontal density difference between the head of the Gulf of Thailand and South China Sea, flows offshore in the upper layer and onshore in the lower layer during the stratified period from March to October (Yanagi, 2001). In the Gulf of Thailand, surface temperature and salinity distributions are not related with the surface circulation (Lowwittayakorn, 1998).

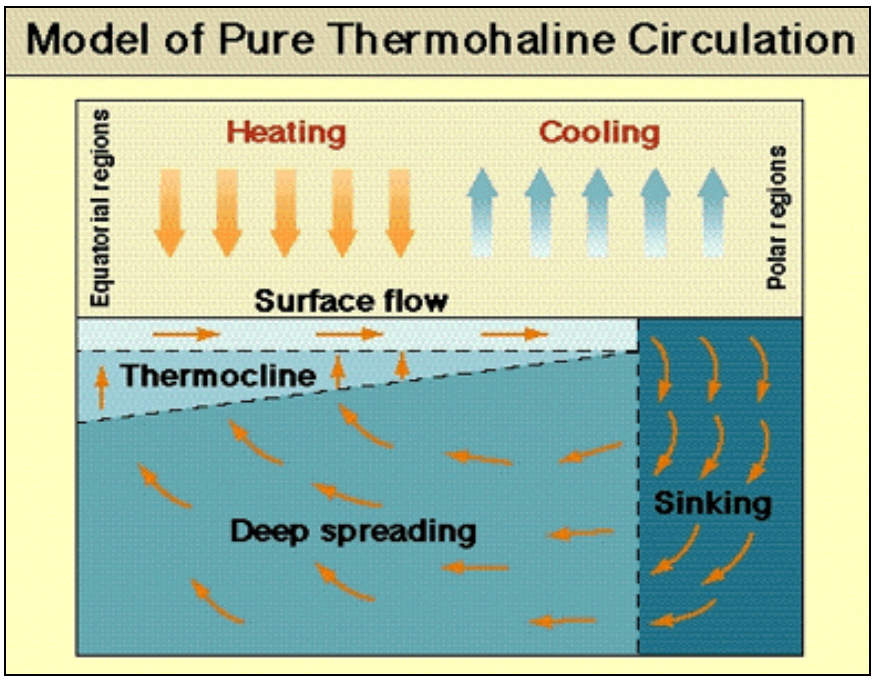

Figure 2-2 Schematic of the thermohaline circulation. (mail.tku.edu.tw)

2.2.3 Tidal current

Tides are the periodic motion of the waters of the sea due to changes in the attractive forces of the Moon and Sun upon the rotating Earth (Figure 2-3). The rise and fall of tide is accompanied by horizontal movement of the water called tidal current. The Moon is the main tide generating body. Due to its greater distance, the Sun's effect is only 46 percent of the Moon's.

Tides in the Gulf of Thailand are the result of tidal waves propagation from South China Sea, which are co-oscillation tides. In general, diurnal components have larger amplitudes than semidiurnal components.

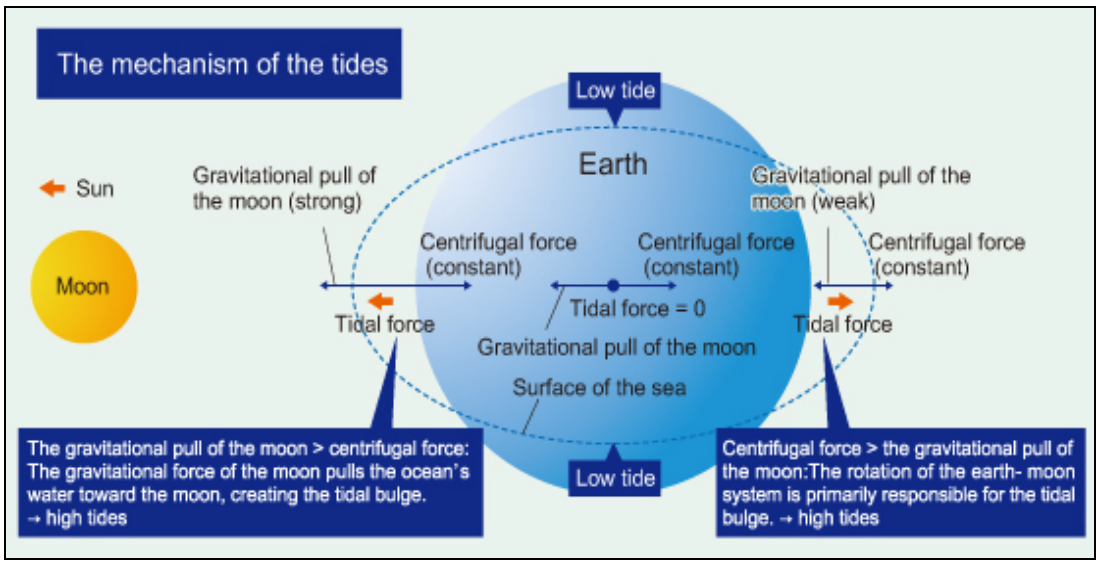

Figure 2-3 The mechanism of the tides.

(http://www.uzunomichi.jp/english/article/0002143.php)

2.3 Horizontal motion

Wind can be defined simply as air in motion. This motion can be in any direction, but in most cases the horizontal component of wind flow greatly exceeds the flow that occurs vertically. Wind develops as a result of spatial differences in atmospheric pressure. Generally, these differences occur because of the uneven absorption of solar radiation at the Earth's surface (Figure 2-4).

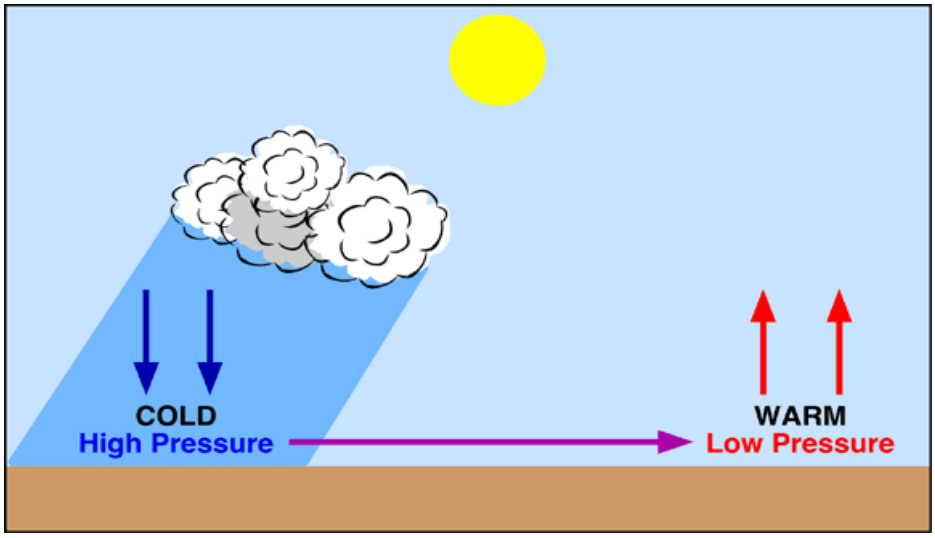

Figure 2-4 Formation of wind as a result of localized temperature differences.

(http://www.physicalgeography.net/fundamentals/7n.html)

Wind is the movement of air across the Earth's surface and is produced by difference in air pressure between the one place to another. Winds are named from the direction from which they originate. For example, a westerly wind is a wind coming from the west and blowing toward the east. Air pressure is created by the motion, size, and number of gas molecules presented in the air. This varies based on the temperature and density of the air mass.

Within the atmosphere, there are several forces that impact the speed and direction of winds which incorporated both "real" and "apparent" forces, stating that the total rate of change of the wind velocity with time was due to a combination of pressure gradient force, friction, gravity (real forces), centrifugal force and Coriolis force (apparent forces). The primary cause of air movement is the development of a horizontal pressure gradient and the fact that such a gradient can persist (rather than being destroyed by air motion towards the low pressure) results from the effect of the earth's rotation which gives rise to the Coriolis force.

2.3.1 The pressure gradient force

The Pressure Gradient Force (PGF) has vertical and horizontal components, the vertical component is more or less in balance with the force of gravity, this mutual balance between the gravity force and vertical pressure gradient is referred to as hydrostatic equilibrium. This state of balance, together with the general stability of the atmosphere and its shallow depth, greatly limits vertical air motion. Horizontal differences in pressure can be due to thermal or mechanical causes (Figure 2-4), and this differences control the horizontal movement of an air mass, force that causes the movement of air away from areas of high pressure and towards areas where it is lower, although other forces prevent air from moving directly across the isobar. The closer of space isobar causes greater the wind speed (see Figure 2-5).

Pressure Gradient Force per unit mass; PGF = $-\frac{m}{\rho}\frac{dp}{dn}$ (2.1)

Where ρ = air density, m =mass, and $\frac{dp}{dn}$ = the horizontal gradient of pressure

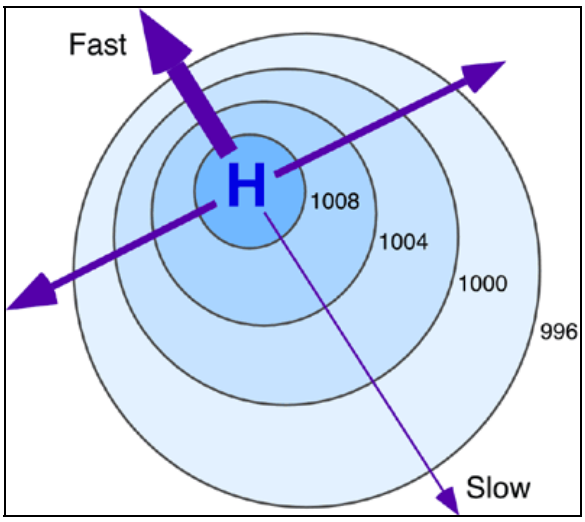

Figure 2-5 Association between wind speed and distance between isobars. In the illustration above thicker arrows represent relatively faster winds. (http://www.physicalgeography.net/fundamentals/7n.html)

2.3.2 The Coriolis force

The Coriolis force arises from the earth's rotational deflective that the movement of masses over the earth's surface is usually referred to a moving co-ordinate system. Figure 2-6 shows the effect of the Coriolis force on a ball moving outward from the centre of the earth. The ball follows a straight path in relation to an inertial frame of reference, but viewed relative to rotating co-ordinates the ball would swing to the right of its initial line of the motion.

The Coriolis force is expressed by $\frac{F_C}{m} = 2\Omega V \sin\phi$ (see Figure 2-7) (2.2)

Force/mass (acceleration) = 2 x angular velocity of earth (1 revolution/day)

x velocity of mass x sine of latitude.

$2\Omega \sin\phi$ is referred to as the Coriolis parameter(f).

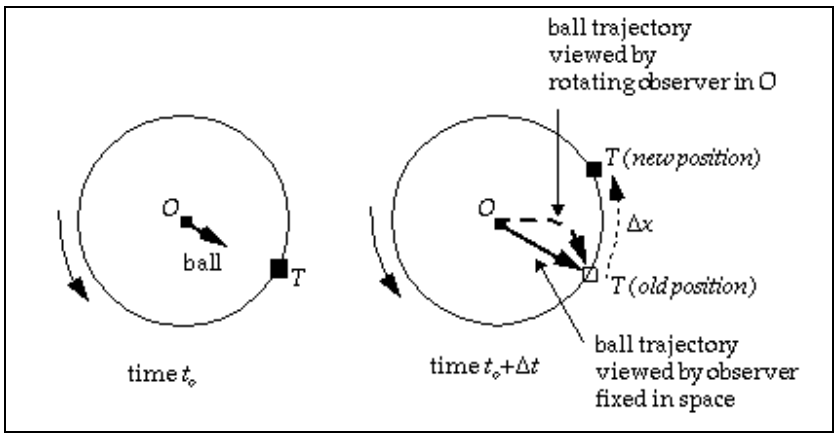

Figure 2-6 The Coriolis force operating on an object moving outward from the center of earth's rotating axis.

(http://acmg.seas.harvard.edu/people/faculty/djj/book/bookchap4.html)

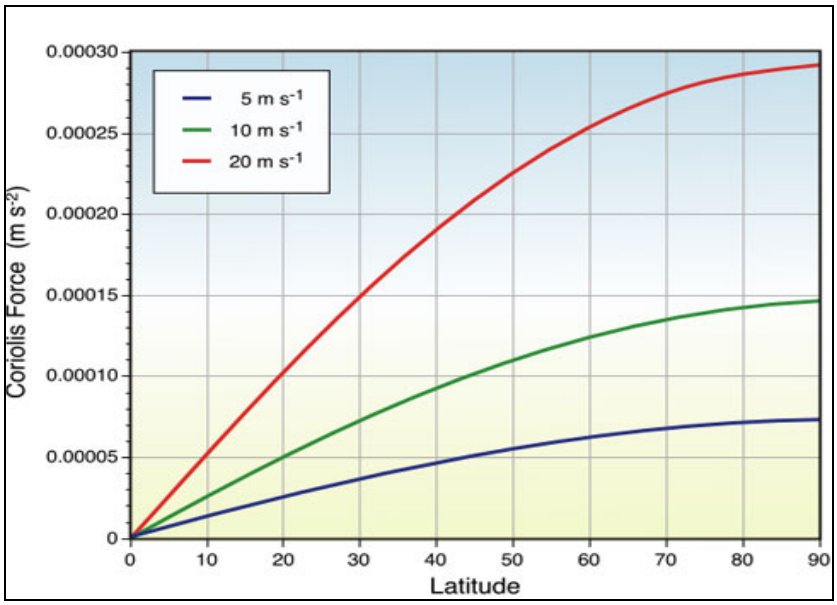

Figure 2-7 The strength of Coriolis force is influenced by latitude and the speed of the moving object.

(http://www.physicalgeography.net/fundamentals/7n.html)

2.3.3 The geostrophic wind

Observations in the free atmosphere, geostrophic motion occurs when there is an exact balance between the pressure gradient force and the Coriolis force, and the air is moving under the action of these two forces only (Figure 2-8). As geostrophic conditions imply no acceleration or friction, we can set these terms to zero in the simplified equations of motion to get the geostrophic wind equations which are given by following (horizontal).

$$0 = -\frac{1}{\rho}\frac{\partial p}{\partial x} + fv_\tau \Rightarrow v_\tau = \frac{1}{\rho f}\cdot\frac{\partial p}{\partial x} \tag{2.3}$$

$$0 = -\frac{1}{\rho}\frac{\partial p}{\partial y} - fu_\tau \Rightarrow u_\tau = -\frac{1}{\rho f}\cdot\frac{\partial p}{\partial y} \tag{2.4}$$

Where v_τ and u_τ are components of the geostrophic winds

We can combine these results to give an equation for the geostrophic wind on a surface chart if we know the perpendicular distance *n* between isobars. Geostrophic wind acts parallel to the isobars (Figure 2-8). The equation is as follows;

$$v_g = \frac{1}{\rho f}\cdot\frac{\partial p}{\partial n} \tag{2.5}$$

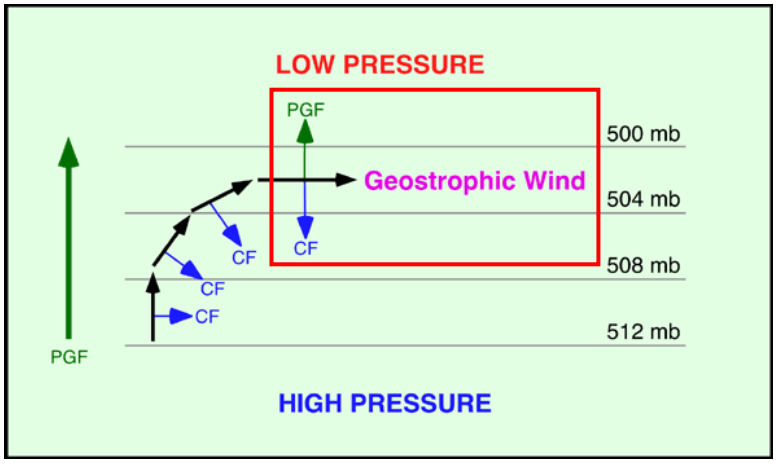

Figure 2-8 A geostrophic wind flows parallel to the isobars (red box) North Hemisphere. (http://www.physicalgeography.net/fundamentals/7n.html)

2.3.4 Centripetal acceleration

Centripetal acceleration is the third force that can act on the moving air. Centripetal acceleration is also another force that can influence the direction of the wind. To follow a curved path there must be an inward acceleration towards the centre of rotation. If the wind flow is curve, thus the pressure gradient force and the Coriolis force must not be in balance with each other. In this case notice that the air's motion is not perpendicular to the two forces. Figure 2-9 (left) shows low pressure system with balanced flow maintaining in a curve when the pressure gradient force is slightly stronger than the Coriolis force. There must be the centripetal force to compensate the difference between these two forces. Similarly, the motion of the air in the high pressure system (Figure 2-9, right) shows the Coriolis force is slightly stronger than the pressure gradient force with the centripetal force to compensate the difference in force.

The residual force that is the difference between the pressure gradient force and Coriolis force gives the net centripetal acceleration inward is called the centripetal force (green arrow in Figure 2-9). The size of the centripetal force depends on the velocity (V) of the moving object and the radius of its curved path (r). The relationship, for an object of mass (m), is

$$\text{Centripetal force } (C_e) = \frac{mV^2}{r} \tag{2.6}$$

When a balance exists between the pressure gradient force, the Coriolis force and the centripetal force, the flow is called gradient flow or gradient wind (V_{gr}).

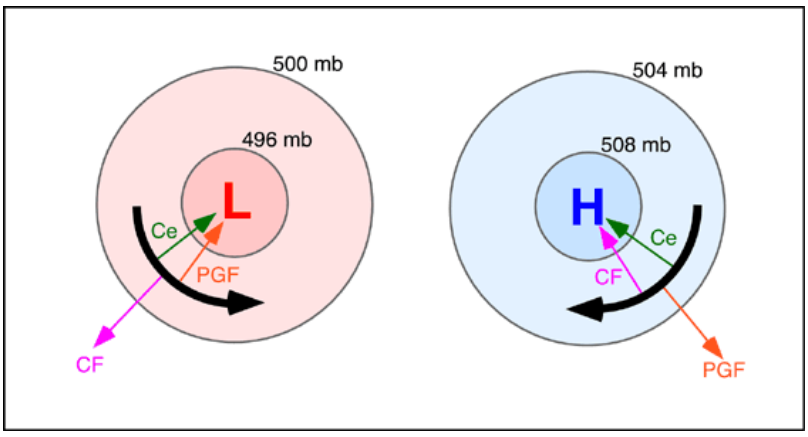

Figure 2-9 The balance of forces that create a gradient wind in the Northern Hemisphere.
(http://www.physicalgeography.net/fundamentals/7n.html)

The gradient wind happens when the Centrifugal Force resulting from curved flow is exactly balanced by the Coriolis forces (C_o) and Pressure Gradient Forces (PGF).

$$C_e = C_o - PGF \tag{2.7}$$

There are 3 cases of the Gradient wind: namely (see Figure 2-10),

- Cyclonic flow
- Anti-cyclonic flow
- Straight flow (V_{gr}=V_g which is a special case)

The equations for the gradient wind depend on whether the flow is cyclonic or anti-cyclonic. For the cyclonic flow,

$$V_{gr} = -rf + \sqrt{\frac{r^2 f^2 + 4rfV_g}{2}} \tag{2.8}$$

Where r is the radius of curvature and V_g is geostrophic wind

And for the anti-cyclonic flow,

$$V_{gr} = rf - \sqrt{\frac{r^2 f^2 - 4rfV_g}{2}} \tag{2.9}$$

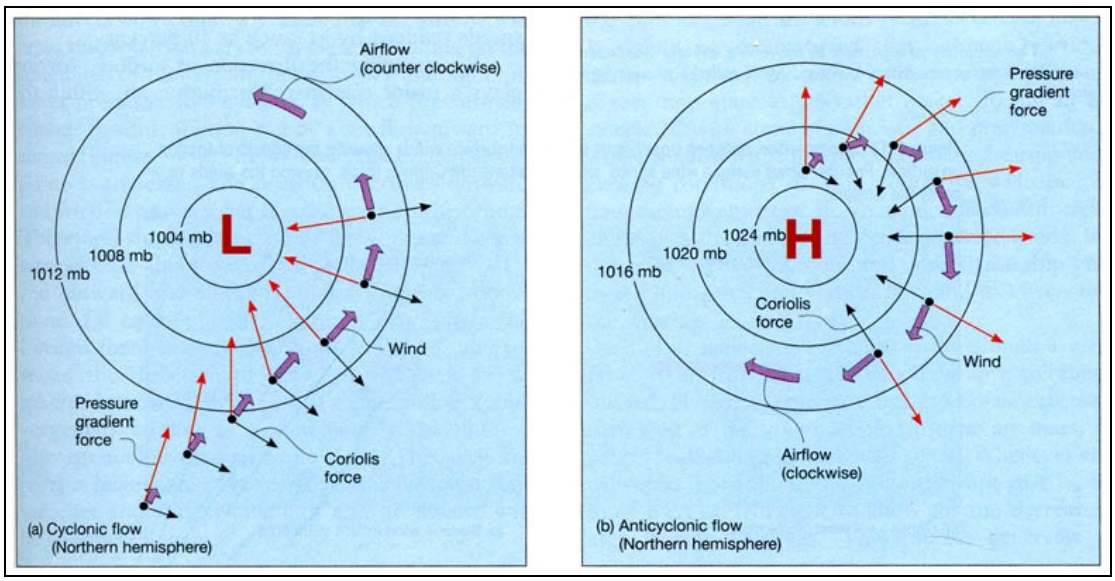

Figure 2-10 Show airflow aloft around low and high pressure centers.
(http://www.ees.rochester.edu/fehnlab/ees215/fig17_5.jpg)

2.3.5 Frictional forces

The last force which has an important effect on air movement is the friction with the earth's surface. If we follow the geostrophic wind near the earth's surface, friction begins to decrease the wind velocity below its geostrophic value. Friction also reduces the magnitude of the Coriolis force. This means that the pressure gradient force is slightly stronger than the Coriolis force, causing the flow somewhat across the isobars toward lower pressure. The friction must be directed opposite to that motion (Figure 2-11). Wind velocity decreases exponentially close to the earth's surface due to the frictional effects produced by surface roughness.

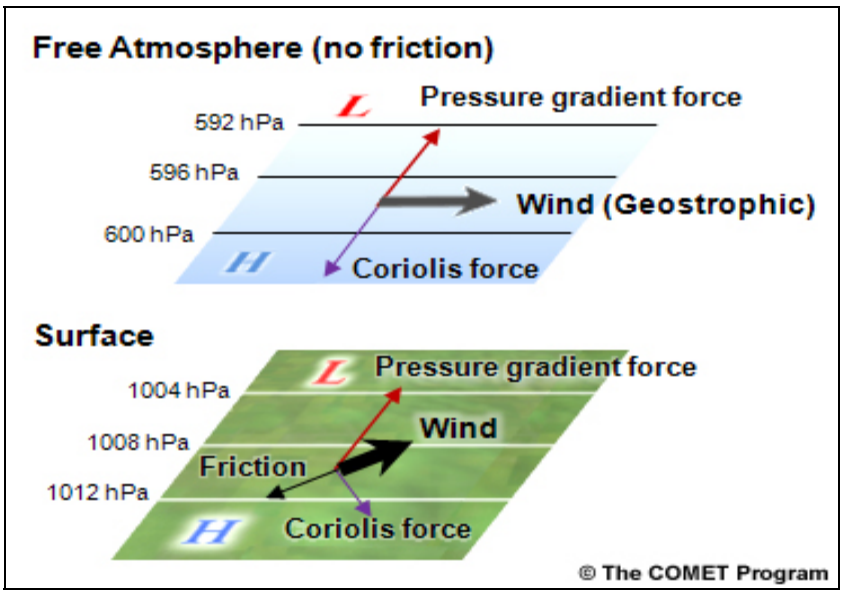

Figure 2-11 Schematic of horizontal forces acting on air parcels near the surface and above the friction layer. (http://www.meted.ucar.edu/tropical/textbook_2nd_edition/navmenu.php?tab=4&page=1.0.0)

In summary, the surface wind (neglecting any curvature effects) represents a balance between the pressure gradient force and the friction parallel to the air motion and between the pressure gradient force and the Coriolis force perpendicular to the air motion.

2.3.6 Equation of motion

By resolving into the different components of a 3-D Cartesian co-ordinate system and using scale analysis we can obtain the general equation of motion as follow,

$$\frac{du}{dt} = -\frac{1}{\rho}\frac{\partial p}{\partial x} + fv \tag{2.10}$$

$$\frac{dv}{dt} = -\frac{1}{\rho}\frac{\partial p}{\partial y} - fu \tag{2.11}$$

$$0 = -\frac{1}{\rho}\frac{\partial p}{\partial z} - g \tag{2.12}$$

Where ρ = density of air

f = Coriolis parameter

2.3.7 Hydrostatic Equation

$$\frac{\partial p}{\partial z} = -g\rho \tag{2.13}$$

And if we are arranged the hydrostatic equation, we can get the following

$$g = -\frac{1}{\rho}\frac{\partial p}{\partial z} \tag{2.14}$$

This equation tell us that if the gravity is a constant, then the rate of change of pressure with height is greater for cold dense air than for warm less dense air when the rate of change of pressure with height is dependent on temperature. The hydrostatic equation mainly use in the measurement of height above ground, if a 'standard' atmosphere is assumed whereby mean sea level temperature is 15°C and the lapse rate is 6.5 °C /km, then a 'standard' distribution of pressure with height results.

2.4 Overview of the El Niño and La Niña

Sea surface temperatures play a major role in global weather and nowhere are that more evident than in El Niño and La Niña events. These types of events often lead to the weather extremes, some of which can be seen in our own backyards. La Niña is described as cooler-than-normal sea surface temperatures in the central and eastern Pacific Ocean, near the equator off the west coast of South America. El Niño is like La Niña's brother, the totally opposite. This is described as warmer-than-normal sea surface temperatures in the same area of the Pacific Ocean.

Easterly trade winds over the equatorial Pacific Ocean are the cause of both phenomenons. For La Niña event, the easterly trade winds strengthen. This blows more warm water west, and allows cold water below the ocean's surface to push towards the top near the South American coast to replace the warm water.

In an El Niño, the opposite occurs. The easterly trade winds become weaker, and can even reverse direction. The warm Pacific Ocean becomes nearly stationary or pushes eastward and gains heat. Besides affecting weather, El Niño has also been known to hurt fishing off the coast of Peru.

El Niño & La Niña phenomenon is associated with the changing atmospheric pressure system, called the variability of the climate in the Southern Hemisphere (Southern Oscillation-"SO"). The degree of the pressure variation is expressed by the "Southern Oscillation Index (SOI)" which is the difference in air pressure between Darwin in the western region and Tahiti in the central Pacific region. The index is calculated using the following formula;

$$\text{SOI} = 10\frac{[Pdiff - Pdiff_{av}]}{SD(Pdiff)} \qquad (2.15)$$

where

Pdiff = (average Tahiti MSL pressure for the month) - (average Darwin MSL pressure for the month),

$Pdiff_{av}$ = long term average of Pdiff for the month in question, and

SD(Pdiff) = long term standard deviation of Pdiff for the month in question.

Sustained negative values of the SOI greater than -8 often indicate El Niño episodes. These negative values associate with the decrease in the strength of the Pacific Trade Winds, and a reduction in winter and spring rainfall over much of eastern Australia and the Top End.

Sustained positive values of the SOI greater than +8 are typical of a La Niña episode. They are associated with stronger Pacific trade winds and warmer sea temperatures to the north of Australia. Waters in the central and eastern tropical Pacific Ocean become cooler during this time. Together these give an increased probability that eastern and northern Australia will be wetter than normal.

Lopittayakorn (2012) In the Gulf of Thailand stated that there are tendency for higher air and sea surface temperature variation occurring during the El Niño event than during the normal year. On the other hand, less air and sea surface temperature variation occurs during the La Niña event. And wind driven circulation patterns in the gulf during El Niño years and La Niña years were similar to that during the moderate

year except that the current speeds were much stronger during the El Niño and La Niña years.

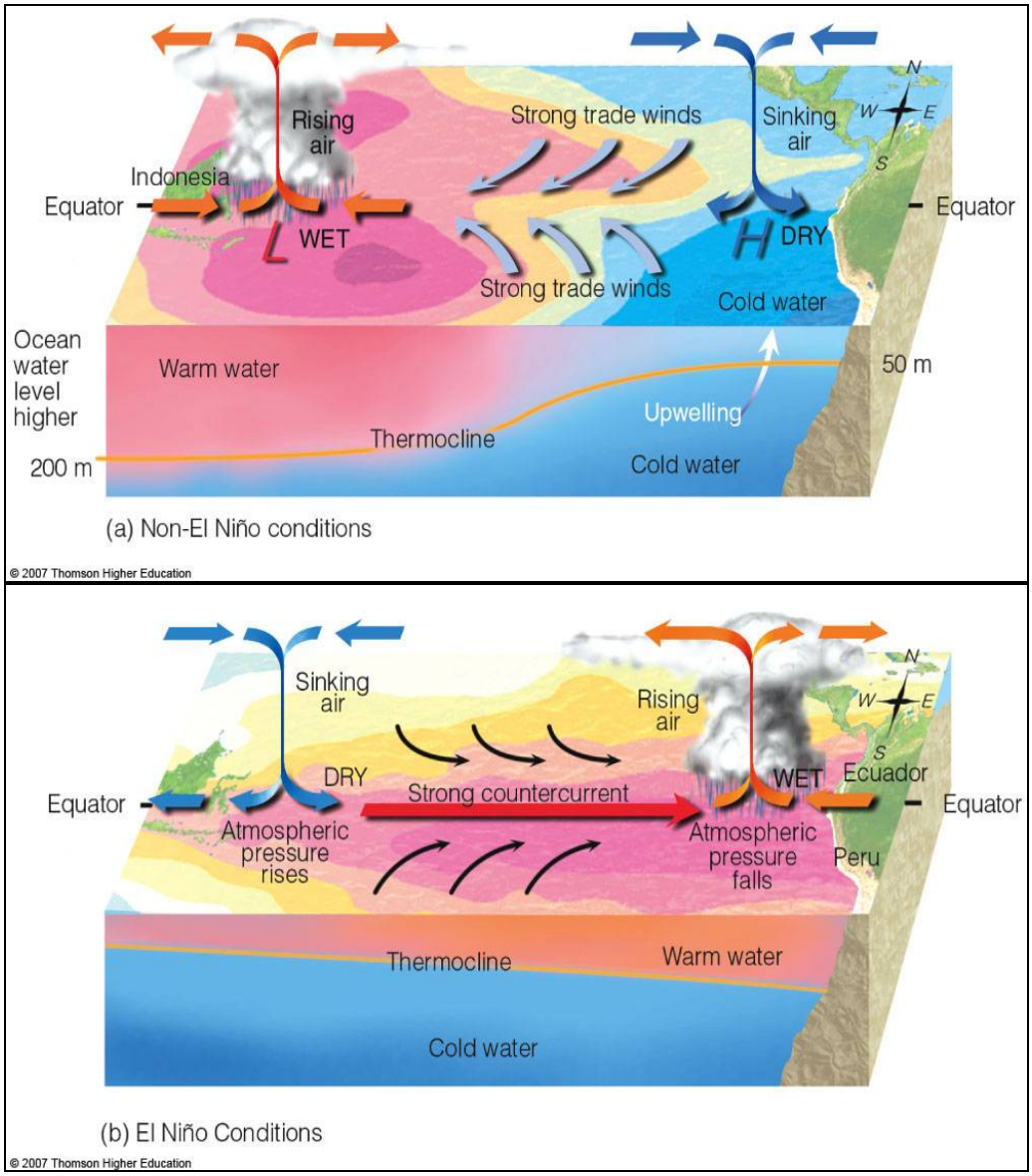

Figure 2-12 The La Niña (a) and El Niño (b) conditions in the equatorial.

(http://apollo.lsc.vsc.edu/classes/met130/notes/chapter10/normalyear_trades.html)

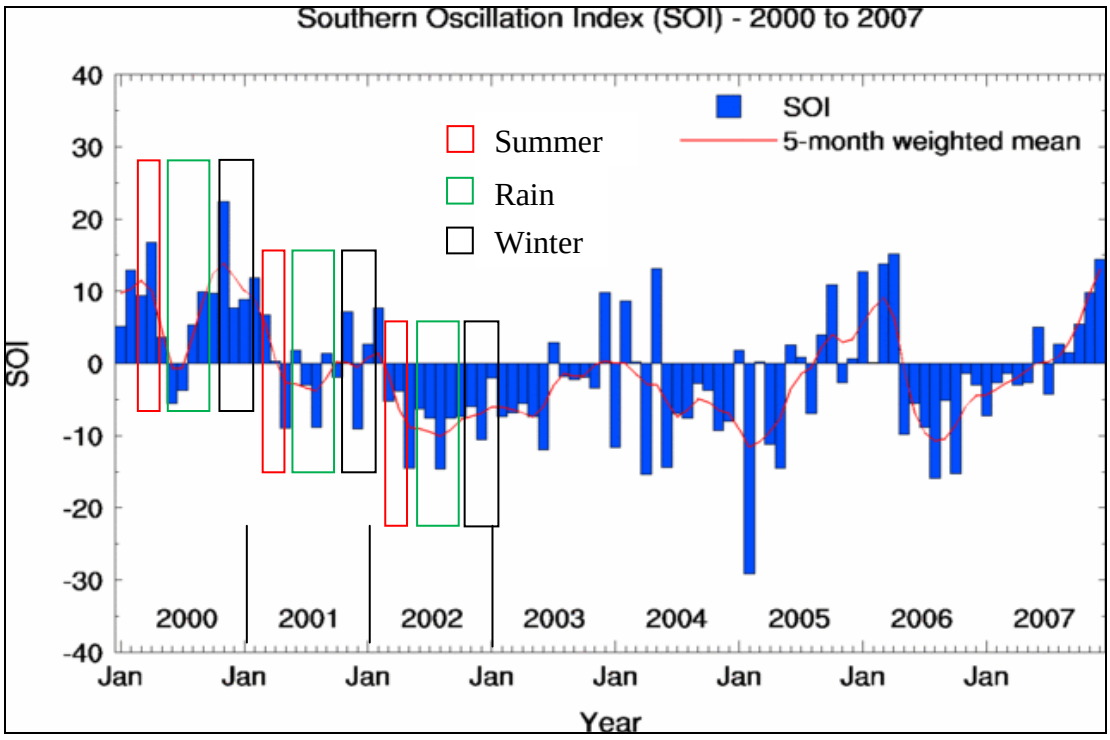

Figure 2-13 Southern Oscillation-Index 2000-2007.

(http://www.bom.gov.au/climate/current/soi-2000-2007.shtml)

	1	2	3	4	5	6	7	8	9	10	11	12
2000												
2001												
2002												
La Niña				Normal					El Niño			

Figure 2-14 El Niño La Niña and normal events in 2000-2002 as suggested by Chaiongkarn, P., [18 April 2556].

2.5 Literature Reviews

2.5.1 Sea surface circulation in the Gulf of Thailand

Snidvongs and Sojisuporn (1997) used three-dimensional hydrodynamic model to investigate the net circulation in the Gulf of Thailand under different monsoon regimes. The circulations were simulated using tri-monthly averaged of observed temperature, salinity, depth, and wind. The sources of temperature and salinity data were come from SEAFDEC, NODC, and JODC. The constant of homogenous wind was used in computation. The results showed that the surface water flowed from South China Sea during the NE monsoon and opposite during the SW monsoon.

Lowwittayakorn (1998) studied the circulation pattern, temperature distribution and salinity of the sea surface in the Gulf of Thailand using a mathematical model and data from oceanographic buoys. The results of study showed that during the SW monsoon, the current entered the gulf from the western side, made a clockwise circulation, and left the gulf through the eastern side. During NE monsoon, the current entered the gulf from the eastern side, made a counterclockwise circulation and left the gulf through the west.

Buranapratheprat and Bunpapong (1998) studied circulation pattern in the Gulf of Thailand using a 2-D hydrodynamic model. Bathymetry data, eight-year averaged wind fields from the European Center for Medium Range Weather Forecast (ECMWF), and the tidal forcing (K1, O1, M2 and S2) at the open boundary were used as major driving forces to water circulation. The results of study from January to September, water flowed into and out of Gulf of Thailand in the southern part and the northern part, respectively. Flow patterns in opposite direction occurred from October to December. Complex flows were generated in June, July and August, when a number of eddies and stronger current occurred. Monthly circulation results suggested that wind be a key factor that controls seasonal circulation patterns.

Booncherm, *et al*., (2001) Studied Sea surface residual flow and water circulation in the Gulf of Thailand using data from oceanographic buoys. He analyzed the data from the upper gulf during 1996 and 1998 and the data from the lower gulf

during 1993 and 1994. The data indicated that the magnitude of the net surface residual current in the gulf was approximately 5 cm/s. In the upper gulf, it had a lower value of 3 cm/s with unpredicted direction pattern. During the NE monsoon, the net surface residual current was large and the pattern of the water circulation in the gulf was counter-clockwise, whereas during the SW monsoon, the residual current was small with a clockwise circulation pattern.

Singharuck (2002) studied eddies in the Gulf of Thailand between January 2000-February 2001 using numerical ocean model in conjunction with satellite remote sensing data. Princeton Ocean model (POM) with 10-km spatial resolution was driven by combined 12-hour wind stress from Navy Operational Global Atmosphere Prediction System and 4 principal tidal constituents (M2, S2, K1, and O1). Numerical experiments showed that wind was the major contributor to the eddy generation in the Gulf of Thailand, while tide is not essential to the eddy generation. However, interaction between wind and tide may account for the location and size of eddies.

Aschariyaphotha (2008) studied seasonal thermohaline feature and the ocean circulation in the Gulf of Thailand based on the Princeton Ocean Model (POM). Model run was executed using wind stress calculated from the climatologically monthly mean wind which has been taking from the European Center for Medium-Range Weather Forecasts (ECMWF). The temperature and salinity fields were taken from Levitus94 data sets. And climatologically monthly mean fresh water flux data was used. During the winter season of Thailand, January, the GOT surface current circulation is generally clockwise with a strong current at the southwest Gulf, Songkla and Patani province' coast. During the summer season of Thailand, April, a weak clockwise current near Pattani and Narathiwat provinces coasts. The model simulates a clockwise eddy in the central GOT during July or the rainy season of Thailand.

Sojisuporn (2010) studied the seasonal variations in the surface water currents within the Gulf of Thailand using the temperature and salinity data derived from the world ocean database, the monthly dynamic heights anomaly from TOPEX/Poseidon and the ERS-2 altimetry data, during 1995-2001. The mean geostrophic current showed

a strong southwestward flow of the South China Sea water along the gulf entrance. Counter-clockwise eddies occurred in the inner gulf and the western side of the gulf entrance. Seasonal geostrophic currents showed a basin-wide counter-clockwise circulation during the SW monsoon season and a clockwise circulation during the NE monsoon season.

Lopittayakorn (2012) studied the effect on atmospheric and oceanographic parameters in the Gulf of Thailand using ENSO indices with air temperature, monthly rainfall from meteorology station, monthly sea surface temperature and sea surface salinity from the oceanographic buoys during 1997-2003. Moreover, circulation patterns in the Gulf of Thailand were also simulated using the Princeton Ocean model. Input to the model was wind from the NAVY Operation Global Atmospheric Prediction System (NOGAPS), sea surface temperature and sea surface salinity data. The simulated circulation patterns were in accordance with the measured current data from the buoys by 60-70%. In the SW monsoon water flowed out of the gulf via the western side with the counter-clockwise eddy existed at the tip of ca Mau peninsular. While in the NE monsoon, the current meandered from the eastern of the gulf and flowed along the gulf's western coast into the gulf.

2.5.2 Surface Wind

Kwun (2009) studied the sensitivity experiments of wind prediction with planetary boundary layer parameterizations using two widely used meso-scale model; namely MM5 and WRF. The capability of three PBL equipped in MM5 (MRF, Eta, Blackadar) and two PBL in WRF (YSU and MYJ) has been analyzed in strong winds days during typhoon Ewiniar in 2006 covering part of East Asia including Korea and Japan. The time series of wind speed from five sensitivity experimental cases were compared with the observations in ASOS and BUOY and QuikSCAT satellite 10-m daily mean winds, the most of the experiments reproducing reliable wind results. However, YSU and MYJ used in the WRF model showed the best agreements with the observation data.

Papanastasiou (2010) studied wind field under sea breeze conditions over the east coast of central Greece using the WRF model. The simulation was carried out for a five-day period. The Monin-Obukov (Eta) scheme, the Mellor-Yamada-Janjic TKE scheme and the Ferrier (new Eta) scheme are used in the WRF model in order to simulate the surface layer, boundary layer processes and atmospheric microphysics procedure respectively. The Kain-Fritsch scheme was used by the model to parameterize cumulus physics, while the Rapid Radiative Transfer Model (RRTM) scheme and the Dudhia scheme were used to simulate the long and short wave radiation fluxes in the atmosphere respectively. The results were compared to the observation data that were collected by a near-surface meteorological station. The model predictions agreed fairly well with the observations taken at a near-surface meteorological station where sea breezes were very frequently developing during the warm period of the year.

Menendez, *et al*., (2012) used the WRF model to generate high resolution offshore wind covering Europe due to ongoing development of offshore wind farms. The Noah scheme, the Yonsei University scheme and the WRF-SM5 scheme were used by WRF model in order to simulate the land surface model, boundary layer processes and atmospheric microphysics procedure respectively. The Grell-Devenyi scheme was used by the model to parameterize cumulus physics, while the Rapid Radiative Transfer Model (RRTM) scheme and the Dudhia scheme are used to simulate the long and short wave radiation fluxes in the atmosphere respectively. The studied results showed that the WRF model was able to produce realistic offshore wind climatology, probabilistic wind distributions and annual cycle. It also reproduced well-known regional winds remarkably well.

Chotamonsak (2012) evaluated the WRF model for regional climate applications over Thailand, focusing on simulated precipitation using various cumulus parameterization schemes available in the WRF model. The model experiments were presented for the year 2005 using four cumulus parameterization schemes, namely Betts-Miller-Janjic (BMJ), Grell-Devenyi (GD), improved Grell-Devenyi (G3D) and KF

(Kain- Fritsch). And fixed physics options used in this study include the WRF Single-Moment6-Class (WSM6) Microphysics scheme, Dudhia shortwave radiation and Rapid Radiative Transfer Modal (RRTM) long-wave radiation, the Yonsei University planetary boundary layer (PBL) scheme, and the Noah Land Surface Model (LSM). The results were compared with the observation data that were collected by a near-surface meteorological station at the Thai Meteorological Department (TMD). The BMJ cumulus scheme yielded the smallest bias relative to the observations.

Amnuaylojaroen and Kreasuwun (2012) investigated the fine and coarse particulate matters from forest fires in Chiang Mai basin in March 2007. Wind over Chiang Mai basin was condition for the particulate matter accumulation. The Noah scheme, the Yonsei University scheme and the WSM6 scheme were used in the WRF model in order to simulate the land surface model, boundary layer processes and atmospheric microphysics procedure respectively. The Kain-Fritsch scheme was used by the model to parameterize cumulus physics, while the Rapid Radiative Transfer Model (RRTM) scheme and the Dudhia scheme were used to simulate the long and short wave radiation fluxes in the atmosphere respectively. The regression results of the simulated and observations were well correlated ($r^2 = 0.71$) for the wind speed.

Cavalho (2012) studied the performance of the WRF model in wind simulation was evaluated under different numerical and physical options for an area of Portugal, located in complex terrain and characterized by its significant wind energy resource. The results show the SL-PBL-LSM parameterization set composed by the schemes MM5-YSU-Noah was the one with better performance for January (winter).

CHAPTER III
RESEARCH METHODOLOGY

3.1 Conceptual basis idea

The study of the characteristics of seasonal wind and wind-driven current in the Gulf of Thailand (GOT) were based on two coupling models. Either measured or forecasting data were used to simulate sea surface wind and 2-D numerical ocean model was used to reproduce the wind-driven current in the GOT under the influence of monsoonal wind over the period of 2000-2002.

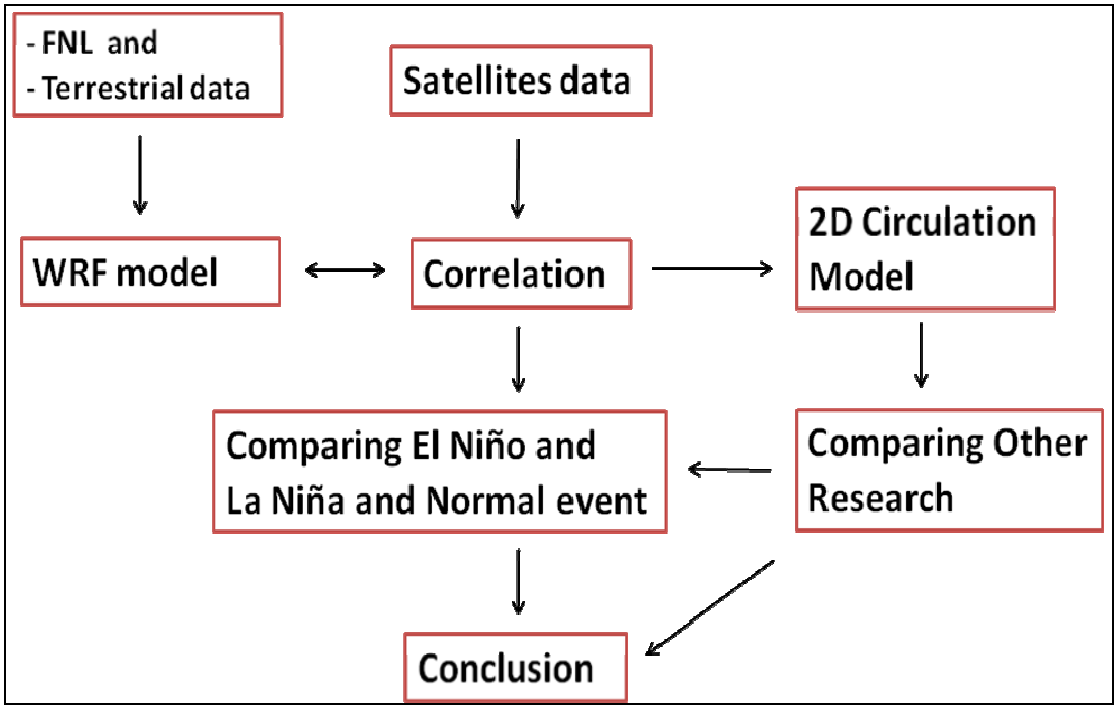

Figure 3-1 Summary of research tasks.

Figure 3-1 shows conceptual basis idea that is used in this study. The WRF model and 2-D Numerical models were setup first. The data obtained from NCEP was used as input to the WRF model. When the outputs of the WRF model came out, the correlation was made between the model output and sea surface wind data from the satellites. After achieving good correlation, the simulated wind was used to drive the wind-driven current in the GOT using the 2-D numerical model. The outputs current

were then compared to results from earlier studies. Both wind and wind-driven current pattern under normal, El Niño and La Niña events were simulated and compared to each other. Finally, the discussion and conclusion were drawn.

3.2 Research tools

3.2.1 Software

- Operating System: Fedora 12 and Microsoft Windows XP
- Application tool: WRF model, 2-D circulation model, WRF Domain wizard
- Compliers: Digital visual Fortran 6.5, C, C++, FORTRAN 90, and gFORTRAN
- Graphic: IDV_3.1u1, Surfer9, Grapher8
- Document: Microsoft Word 2007

3.2.2 Hardware

- PC computer:
  - CPU: AMD Phenom-II
  - RAM: 4 GB
  - Hard disk: 1000 GB
- Laptop computer:
  - CPU: Intel(R) Core™2Duo
  - RAM: 2042 MB
  - Hard disk: 320 GB

3.3 The 2-D Circulation Ocean model

Assuming that the water in the Gulf of Thailand was well-mixed, the 2-D numerical model was employed to simulate the circulation in the Gulf of Thailand during each seasonal period (namely the summer season, the winter season, the rainy season). The governing equations were the vertically integrated momentum equations in the horizontal axes and continuity equation for sea surface fluctuation. The circulation

model was driven by monsoonal wind over the model domain. Mean wind-driven current for 3 seasons were calculated and analyzed.

The momentum equation includes temporal change, the Coriolis effect, Pressure Gradient Force, surface and bottom stress terms, shown as follows:

$$\frac{\partial uD}{\partial t} + \frac{\partial u^2 D}{\partial x} + \frac{\partial uvD}{\partial y} - fvD + gD\frac{\partial \eta}{\partial x} = \tau_x^w - ku(u^2 + v^2)^{1/2} \quad (3.1)$$

$$\frac{\partial vD}{\partial t} + \frac{\partial uvD}{\partial x} + \frac{\partial v^2 D}{\partial y} + fuD + gD\frac{\partial \eta}{\partial y} = \tau_y^w - kv(u^2 + v^2)^{1/2} \quad (3.2)$$

The continuity equation can be used under the assumption that the water density was constant over the water column. The continuity equation can be written as;

$$\frac{\partial \eta}{\partial t} + \frac{\partial uD}{\partial x} + \frac{\partial vD}{\partial y} = 0 \quad (3.3)$$

The velocity components, u & v, are depth-average values and can be defined as;

$$u = \frac{1}{D}\int_{-H}^{\eta} u'dz \; ; \quad v = \frac{1}{D}\int_{-H}^{\eta} v'dz \quad (3.4)$$

where u, v are eastward and northward depth averaged velocity components respectively,

t = time,

D = total depth of water ($D = H + \eta$),

H = the water depth at mean water level,

η = the free surface elevation with respect to mean water level,

f = Coriolis parameter ($2\Omega \sin\phi$),

g = gravity,

k = bottom friction coefficient which is varied with the *Manning's n* value,

τ_x^w, τ_y^w = wind stress in x and y directions

3.3.1 Model grid and bathymetry

The 2-D numerical ocean model domain for the gulf of Thailand extended from latitude 5.5°-14°N and longitude 99°-107.5°E (Figure 3-2). The model used equally spaced grids in latitude and longitude with 6x6 minutes resolution (approximately 11 km), and thus, contained 86x86 grids for the Gulf of Thailand. The bottom topography was sampling from the 30-second General Bathymetric Chart of the Ocean (GEBCO30).

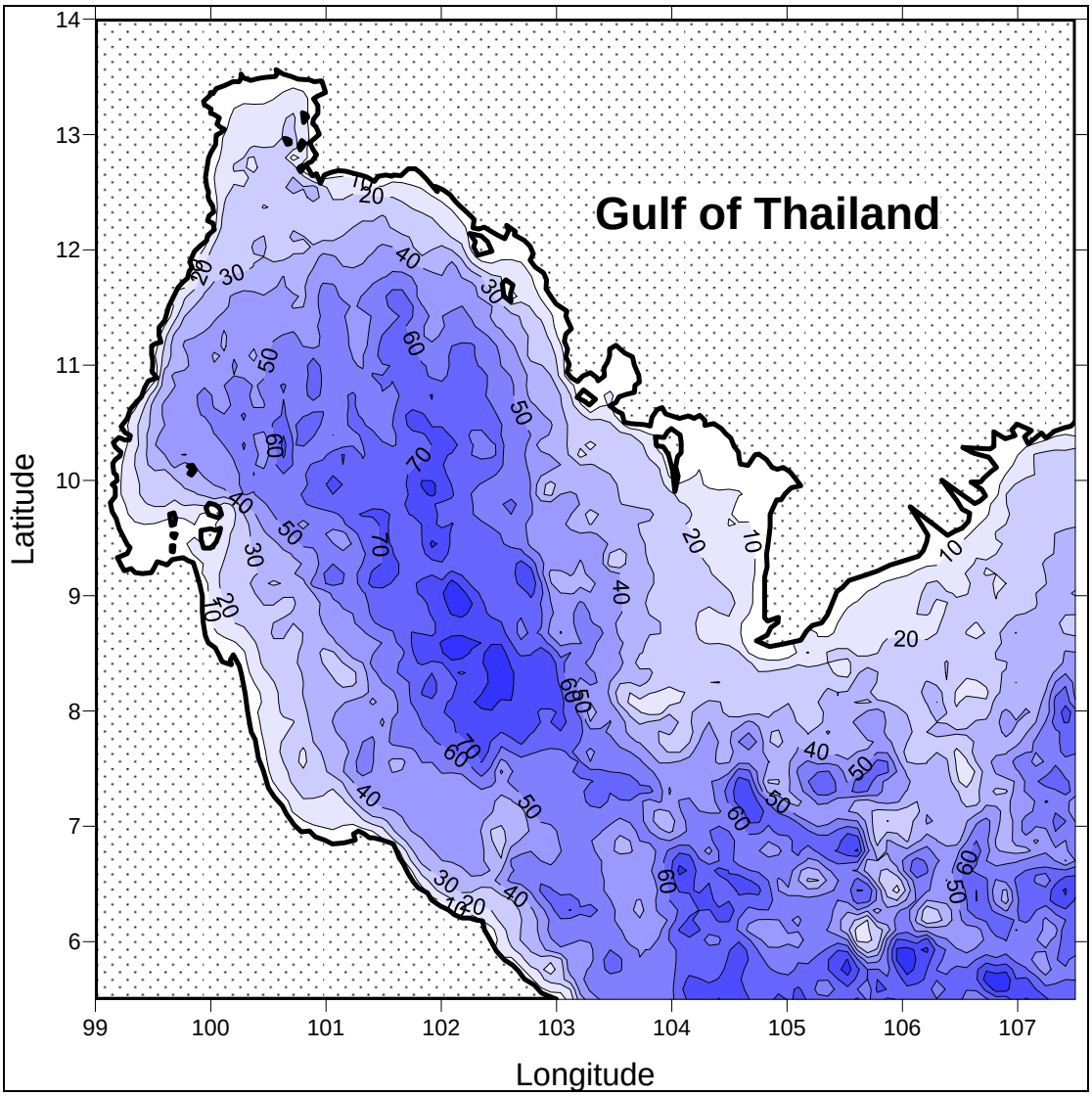

Figure 3-2 The geography and bathymetry (m) of the Gulf of Thailand.

3.3.2 Numerical model application

The model was started initially at rest (still water level with no motion at all grids). Normal component of volume transport was specified as zero along coastal boundary. Averaged seasonal wind fields from WRF model were used as the driving forces to the water circulation.

The friction coefficient at the sea bottom (*Manning's n*) was 0.025, and increased to 0.10 at the open boundary ("cramped" condition). The model time step was 120 sec. The model was run for 30 days to make sure that the model had reached the steady state.

3.4 Weather Research and Forecasting model

The Advanced Research WRF (ARW) modeling system is a model that can be used to simulate and predict the local wind and meso-scale phenomena of the atmospheric conditions. This model was developed by a consortium of government agencies together with the research community. It is used for both operational forecasting research and atmospheric research. And it is widely used as a regional climate model for dynamical downscaling in many regions world-wide. The model used is the Version 3 which is available since April 2008.

The ARW is designed to be a flexible, stat-of-the-art atmospheric simulation system that is portable and efficient on available parallel computing platforms. The WRF ARW model is a fully compressible, non-hydrostatic model (with a hydrostatic option). Its vertical coordinate is a terrain-following hydrostatic pressure coordinate. Features of the WRF include dynamical cores based on finite difference methods and many option for physical parameterizations (microphysics, cumulus parameterization, planetary boundary layers, radiation, and surface model) that are being developed by various groups.

The grid staggering is the Arakawa C-grid. This includes the Runge-Kutta 2nd- and 3rd-order time integration schemes, and 2nd- to 6th-order advection schemes in both horizontal and vertical directions. The ARW is suitable for use in a broad range of applications across scales ranging from meters to thousands of kilometers. It includes

one-way and two-way moving nested and can be coupled with other models including hydrology, land-surface, and ocean model.

The WRF ARW model Version 3 supports a variety of capabilities. These include:

- Idealized simulations
- Parameterization research
- Data assimilation research
- Forecast research
- Real-time NWP
- Coupled-model applications
- Etc.

The output of WRF model consists of many parameters. For this study, wind speed and direction at 10 m was used. To characteristics of wind pattern during year 2000-2002 covered all normal, El Niño and La Niña events.

The WRF Modeling System Program Components

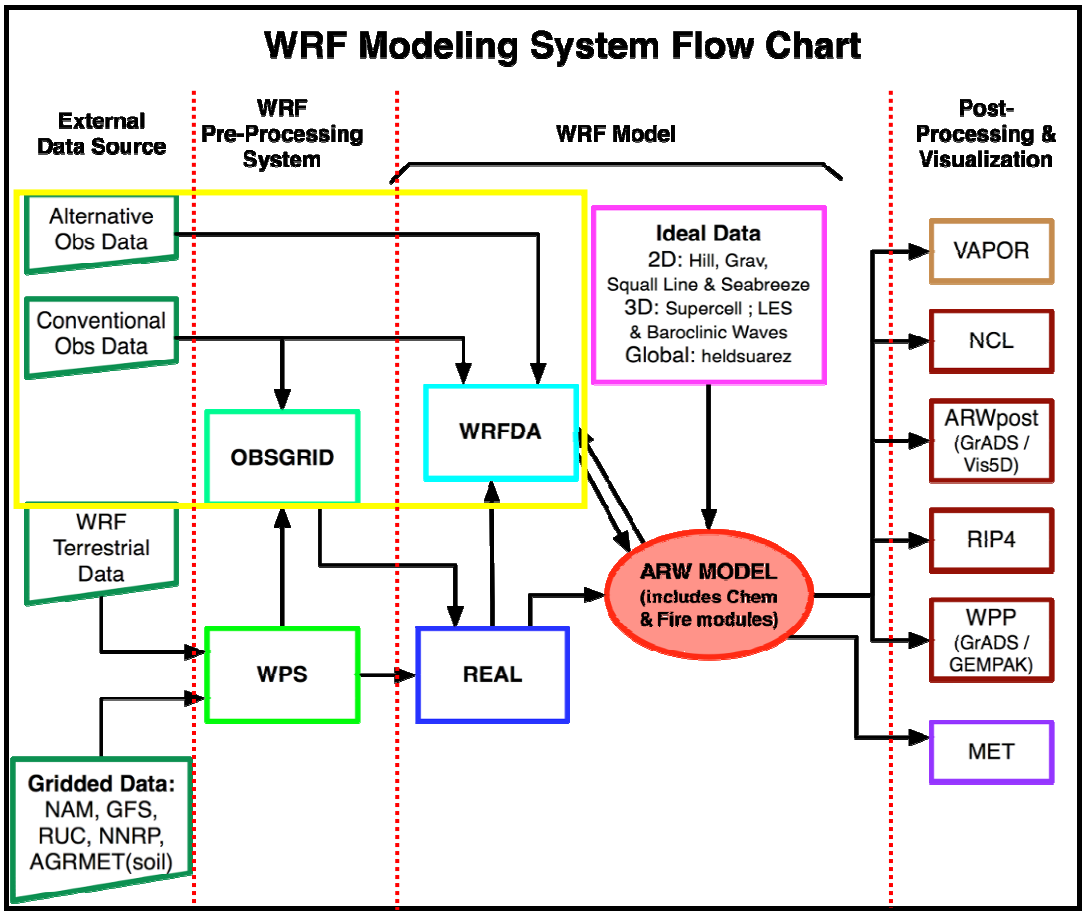

Figure 3-3 The flowchart for the WRF Modeling System Version 3. The yellow box encircles data assimilation steps which was not included in this study. (www.mmm.ucar.edu)

3.4.1 External Data Source

- WRF Terrestrial Data, the sets of static fields (topography, land use, soil types, land-water masks, albedo) global 25-category data with a 30-second resolution.

- Gridded Data (meteorological data), the initial and boundary conditions supplied to the model were driven by the National Centers for Environmental Prediction (NCEP) Final Operational Global Analysis, with 1° of spatial resolution and 6 hr of temporal sampling.

3.4.2 The WRF Preprocessing System (WPS)

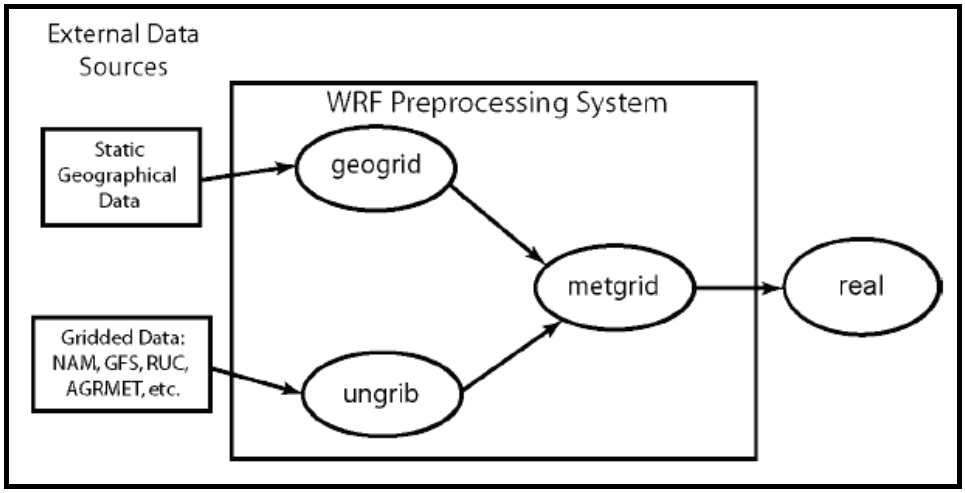

Figure 3-4 The WRF Preprocessing System. (www.mmm.ucar.edu)

The WRF Preprocessing System (WPS) is a set of three programs whose collective role is to prepare input to the *real* program. Each of the programs performs one stage of the preparation:

geogrid program defines model domains (Map projection, Geographic location, Dimensions) and interpolates static geographical data to the grids which ***geogrid*** provides values for static (time-invariant) fields at each model grid point. The program computes latitude, longitude, map scale factor, and Coriolis parameters at each grid point. The programs also horizontally interpolate static terrestrial data (topography height, land use, soil type, vegetation fraction, surface albedo).

ungrib program reads GRIB files, "degribs" the data, and extract meteorological fields. GRIB is a WMO standard file format for storing regularly-distributed fields ("General Regularly-distributed Information in Binary").

metgrid program horizontally interpolates the meteorological data that are extracted by the ***ungrib*** program onto the simulation domains defined by the ***geogrid*** program. Grid Staggering for ARW model (Arakawa C grid stagger), wind U-component interpolated to "U" staggering, wind V-component interpolated to "V" staggering and other meteorological fields interpolated to "θ" staggering (Figure 3-5).

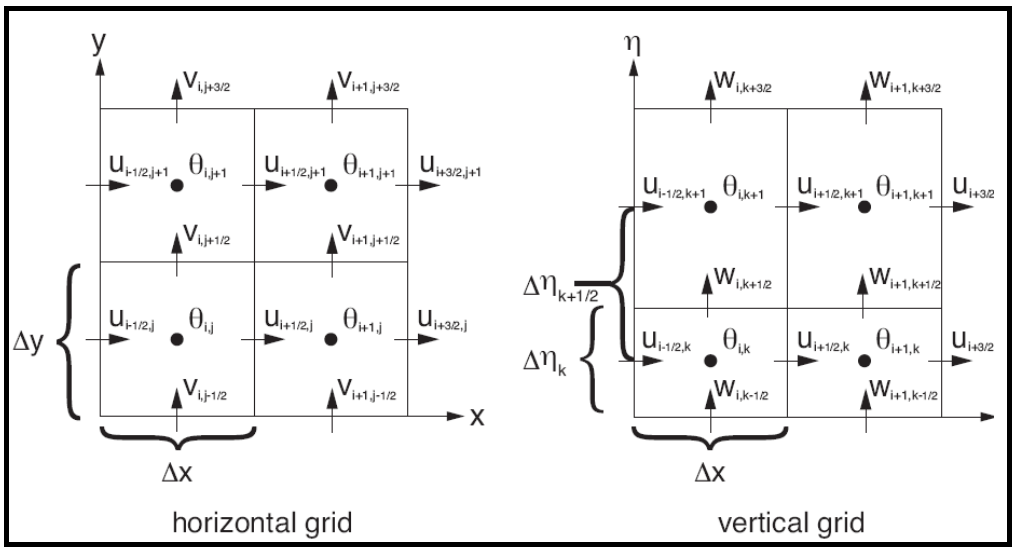

Figure 3-5 The Arakawa C grid stagger. (www.mmm.ucar.edu)

(Horizontal and Vertical grid cell, with "U", "V", and "θ" points labeled.)

3.4.3 WRF model

real or ***real_nmm*** program vertically interpolates meteorological field to WRF eta levels. They compute a base state/reference profile for geopotential and column pressure and compute the perturbations from the base state for geopotential and column pressure. The program initializes meteorological variables: u, v, potential temperature and vapor mixing ratio. It also initializes static fields for the map projection and the physical surface, and defines a vertical coordinate and interpolates data to the model's vertical coordinate.

ARW model offers multiple physics options that can be combined in any way. The options typically range from simple and efficient, to sophisticated and more computationally costly, and from newly developed schemes, to well-tried schemes such as those in current operational models.

Major physic Options that available in ARW, included;

1. Radiation

    1.1. Longwave (ra_lw_physics)

    1.2. Shortwave (ra_sw_physics)

2. Surface

2.1. Surface layer (sf_sfclay_physics)

2.2. Land/water surface (sf_surface_physics)

3. Planetary Boundary layer (bl_pbl_physics)

4. Cumulus convection parameterization (cu_physics)

5. Microphysics (mp_physics)

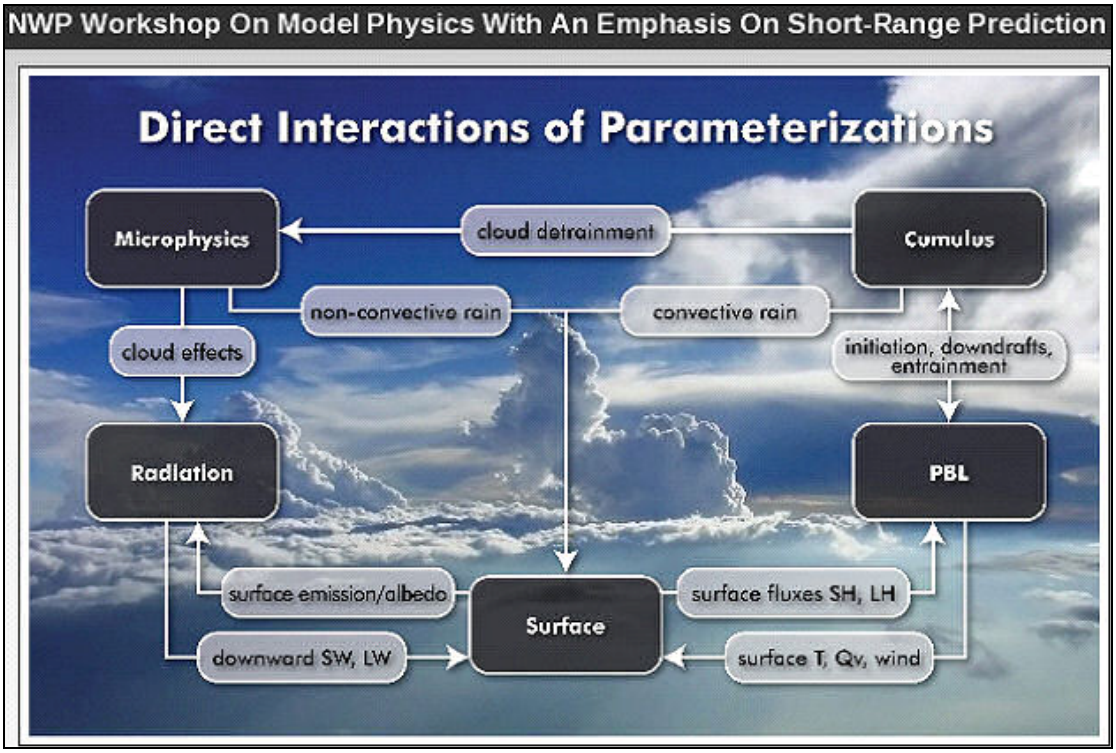

Figure 3-6 Direct Interactions of Parameterizations. (www.ncep.noaa.gov)

1. Radiation

Provides atmospheric heating due to radiative flux divergence and surface downward longwave and shortwave radiation for the ground heat budget which within the atmosphere the radiation responds to model predicted cloud and water vapor distributions, as well as specified carbon dioxide, ozone, and (optionally) trace gas concentrations.

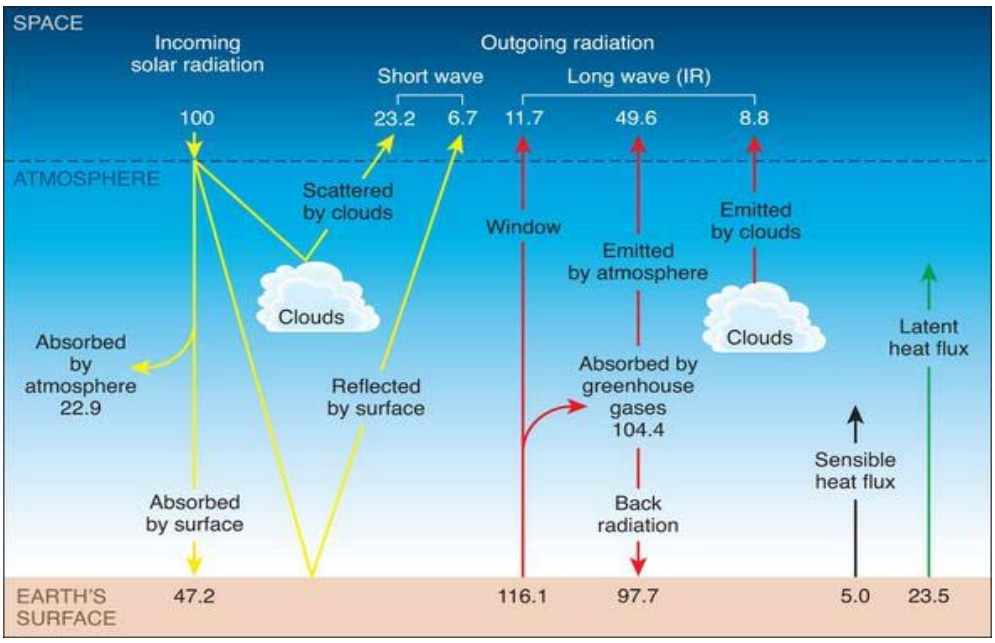

Figure 3-7 Radiation as part of the entire model energy budget.

(serc.carleton.edu)

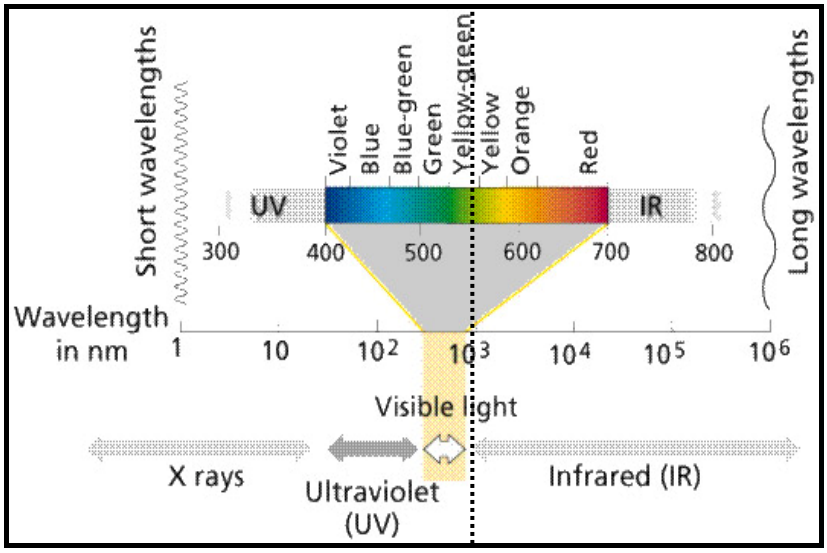

Figure 3-8 The electromagnetic spectrum.

(http://www.emc.maricopa.edu/)

1.1. Longwave (ra_lw_physics)

Compute clear-sky and cloud upward and downward radiation fluxes, downward flux at surface important in land energy budget.

Longwave radiation includes infrared or thermal radiation absorbed and emitted by gases and surfaces. Upward longwave radiative flux from the ground is determined by the surface emissivity that in turn depends upon land-use type, as well as the ground temperature. Infrared radiation generally leads to cooling in clear air, stronger cooling at cloud tops and warming at cloud base.

Table 3-1 Longwave Radiation schemes.

ra_lw_physics	Schemes	References
1	RRTM	Mlawer, *et al*., (1997, JGR)
3	CAM	Collins, *et al*., (2004, NCAR Tech. Note)
4	RRTMG	Iacono, *et al*., (2008, JGR)
99	GFDL	Fels and Schwarzkopf (1981, JGR)

RRTM = Rapid Radiative Transfer Model, RRTMG is new version of RRTM

CAM = Community Atmosphere Model, GFDL = Geophysical Fluid Dynamics Laboratory

1.2. Shortwave (ra_sw_physics)

Compute clear-sky and cloudy solar fluxes, most consider downward and upward (reflected) fluxes. Include annual and diurnal solar cycles which it is important component of surface energy balance.

Shortwave radiation includes visible and surrounding wavelengths that make up the solar spectrum. Hence, the only source is the Sun, but processes include absorption, reflection, and scattering in the atmosphere and at surfaces.

Table 3-2 Shortwave Radiation schemes.

ra_sw_physics	Schemes	References
1	Dudhia	Dudhia (1989, JAS)
2	Goddard	Chou and Suarez (1994, NASA Tech Memo)
3	CAM	Collins, *et al*., (2004, NCAR Tech Note)
4	RRTMG	Iacono, *et al*., (2008, JGR)
99	GFDL	Fels and Schwarzkopf (1981, JGR)

2. Surface

Include surface layer of atmosphere (exchange and transfer coefficients) and land/water-surface (soil temperature and moisture, snow cover, and canopy properties etc.)

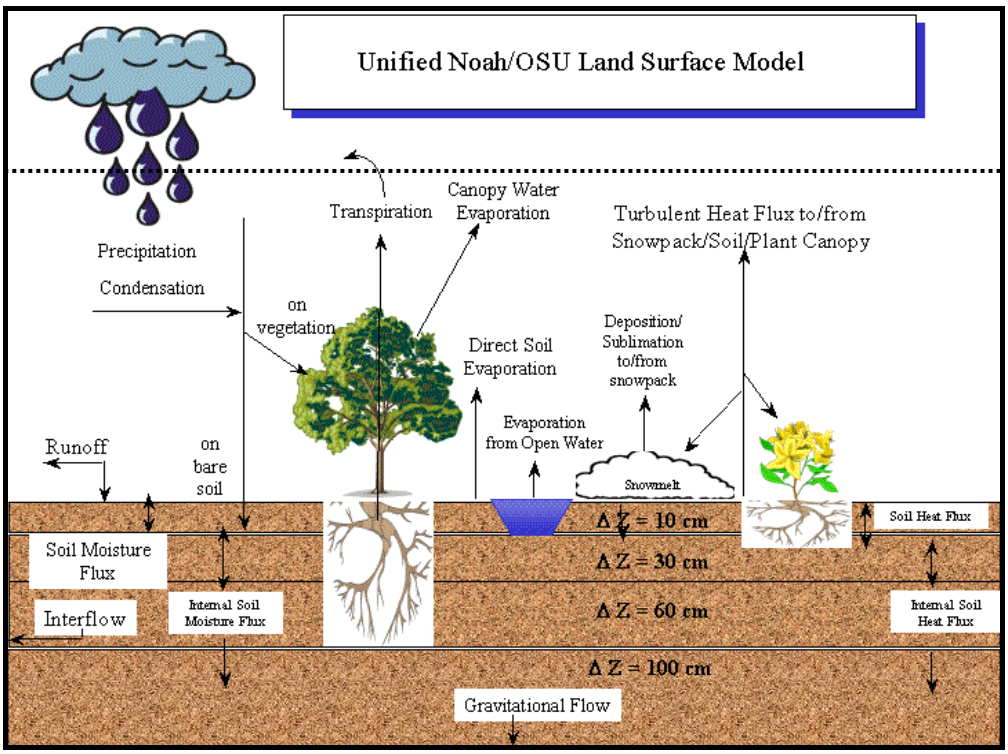

Figure 3-9 The processes of land surface model and surface layer. (www.mmm.ucar.edu)

2.1. Surface layer (sf_sfclay_physics)

Calculate friction velocities and exchange coefficients that enable the calculation of surface heat and moisture fluxes by the land/water-surface and surface stress in the planetary boundary layer scheme. Over water surfaces, the surface fluxes and surface diagnostic fields are computed in the surface layer scheme itself. The schemes provide no tendencies, only the stability dependent information about the surface layer for the land-surface and planetary boundary layer scheme.

Table 3-3 Surface layer schemes.

sf_sfclay_physics	Schemes	References
1	MM5 surface layer	Beljaars (1994)
2	Eta model surface layer	Janjic (1996, 2002)
4	QNSE surface layer	-
5	MYNN surface layer	-
7	Pleim-Xiu surface layer	Pleim (2006)

2.2. Land/water surface (sf_surface_physics)

The land/water-surface models use atmospheric information from the surface layer scheme, radiative forcing from the radiation scheme, and precipitation forcing from the microphysics and cumulus parameterization scheme, together with internal information on the land's state variables and land/water-surface properties, to provide heat and moisture fluxes over land points and sea-ice points. These fluxes provide a lower boundary condition for the vertical transport done in the PBL scheme. The land/water-surface model have various degrees of sophistication in dealing with thermal and moisture fluxes in multiple layers of the soil and also may handle vegetation, root, and canopy effects and surface snow cover prediction. The land surface model provides no tendencies, but dose update the land's state variables which include the ground temperature, soil temperature profile, soil moisture profile, snow cover, and possibly canopy properties.

Table 3-4 Land/water surface schemes.

sf_surface_physics	Schemes	References
1	5-layer thermal diffusion	-
2	Noah land surface model	Chen and Dudhia (2001)
3	RUC land surface model	Smirnova, *et al.*, (1997, 2000)
7	Pleim-Xiu land surface model	Pleim and Xiu (1995)

3. Planetary Boundary layer (bl_pbl_physics)

Planetary Boundary layer (PBL) purpose is to distribute surface fluxes with boundary layer eddy fluxes and allow for PBL growth by entrainment these schemes also do vertical diffusion due to turbulence which (responsible for vertical sub-grid-scale fluxes due to eddy transports) provides boundary layer fluxes and vertical diffusion in the whole atmospheric column (heat, moisture, momentum), not just the boundary layer. The most appropriate horizontal diffusion choices are those based on horizontal deformation or constant Kh (vertical mixing) values where horizontal and vertical mixing are treated independently.

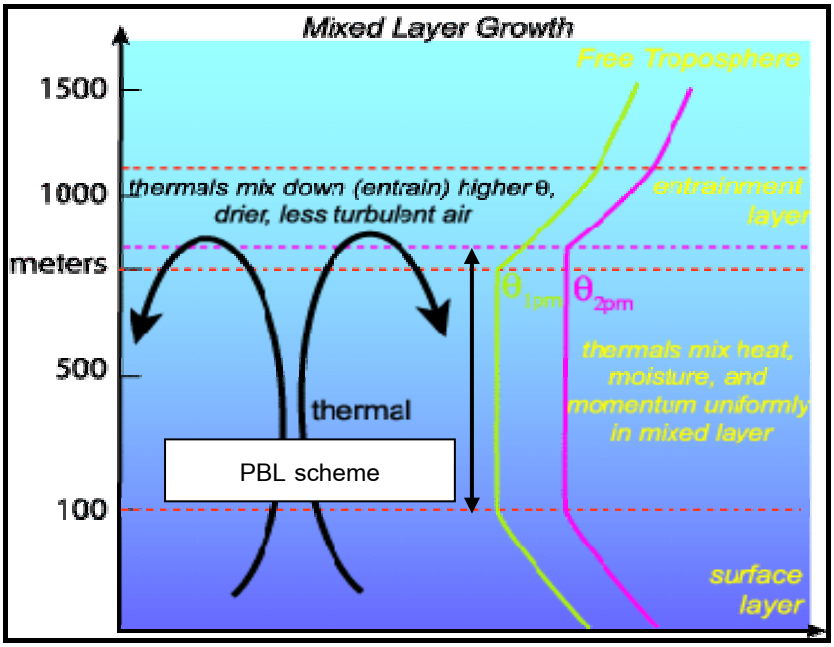

Figure 3-10 Processes of planetary Boundary layer.

(www.mmm.ucar.edu)

Table 3-5 Planetary Boundary layer schemes.

bl_pbl_physics	Schemes	References
1	YSU	Hong, Noh and Dudhia (2006, MWR)
2	MYJ	Janjic (1994, MWR)
4	QNSE	Sukoriansky, Galperin, and Perov (2005, BLM)
5	MYNN2.5	Nakanishi and Niino (2006, BLM)
6	MYNN3	Nakanishi and Niino (2006, BLM)
7	ACM2	Pleim (2007, JAMC)
8	BouLac	Bougeault and Lacarrere (1989, MWR)
99	MRF	Hong and Pan (1996, MWR)

4. Cumulus convective parameterization (cu_physics)

A cumulus convective parameterization based on mass fluxes, convective-scale vertical velocities, and meso-scale effects has been incorporated in an atmospheric general circulation model (GCM). Most contemporary cumulus parameterizations are based on convective mass fluxes. This parameterization augments mass fluxes with convective scale vertical velocities (transport surface air to top of cloud and include subsidence) as a means of providing a method for incorporating cumulus microphysics using vertical velocities at physically appropriate (sub-grid) scales. Convective-scale microphysics provides a key source of material for meso-scale circulations associated with deep convection, along with meso-scale in situ microphysical processes. The latter depend on simple, parameterized meso-scale dynamics. Consistent treatment of convection, microphysics, and radiation is crucial for modeling global-scale interactions involving clouds and radiation.

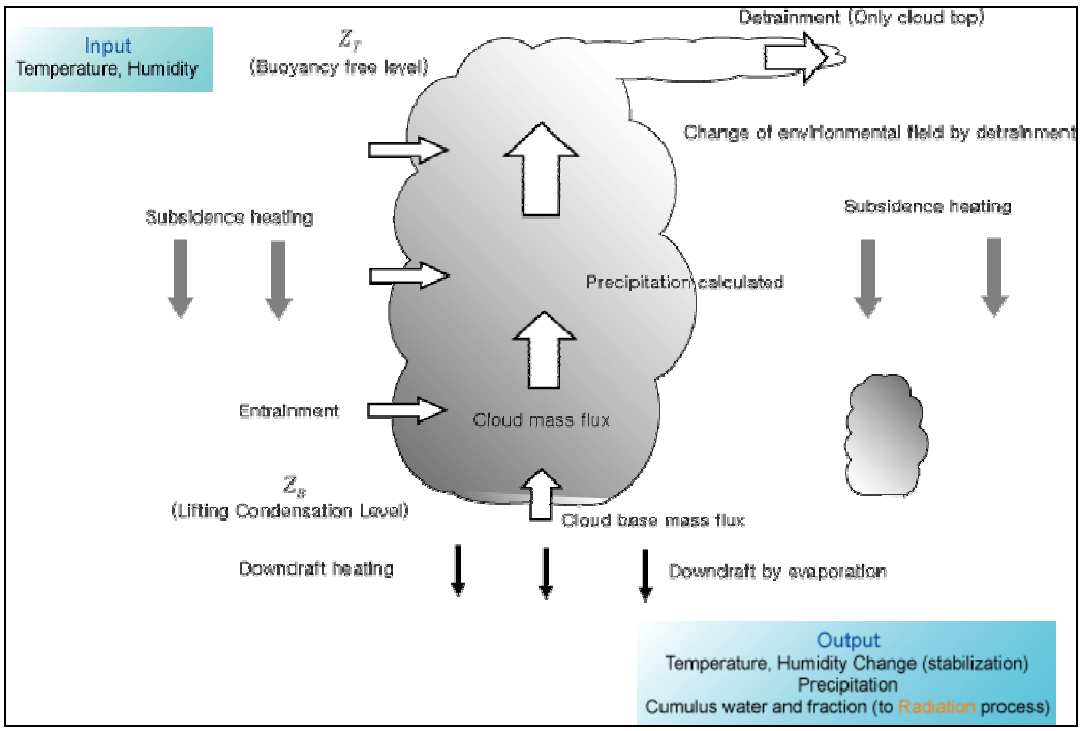

Figure 3-11 The cumulus convective processes.

(http://climate.snu.ac.kr/gcmdocu/Phy_Cum.htm)

Table 3-6 The cumulus convective parameterization schemes.

cu_physics	Schemes	References
1	Kain-Fritsch	Kain (2004, JAM)
2	Betts-Miller-Janjic	Janjic (1994,MWR; 2000, JAS)
3	Grell-Devenyi	Grell and Devenyi (2002, GRL)
4	Simplified Arakawa-Schubert	Grell, *et al.*, (1994, MM5 NCAR Tech Note)
5	Grell-3	Grell and Devenyi (2002, GRL)
99	Old Kain-Fritsch	Kain and Fritsch (1990, JAS; 1993 Meteo, Monogr.)

5. Microphysics (mp_physics)

The processes control formation of cloud droplets and ice crystals their growth and fallout as precipitation formed by radiative, dynamical or convective processes. The prognostic variables for these schemes include Qv, Qc, Qr, Qi, Qs, Qh, Qg (mixing ratio for water vapor, cloud, rain, ice, snow, hail, and graupel respectively).

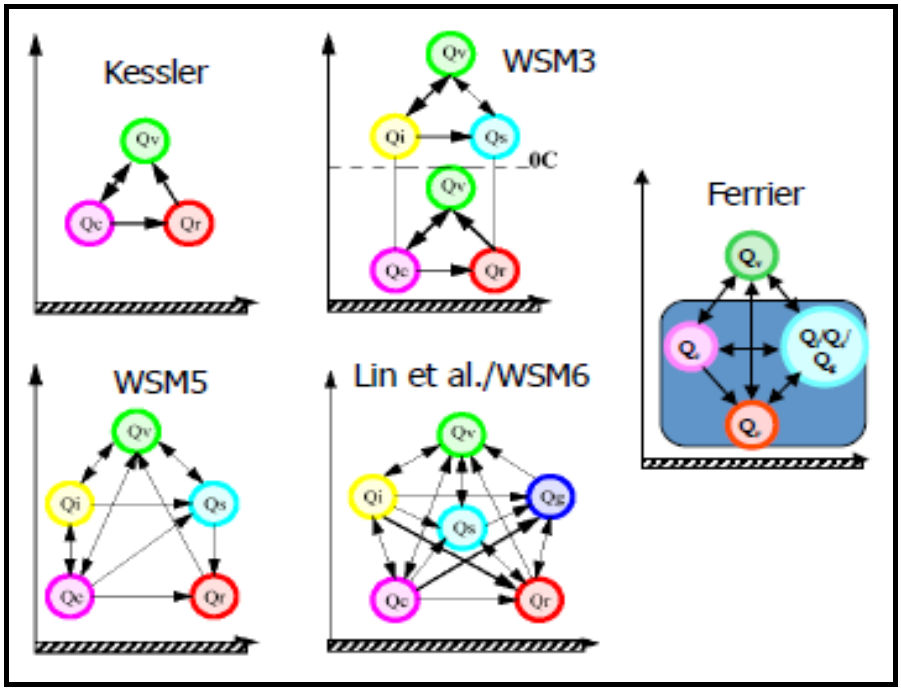

Figure 3-12 Example microphysics processes. (www.mmm.ucar.edu)

Table 3-7 Microphysics schemes.

mp_physics	Schemes	References
1	Kessler	Kessler (1969)
2	Lin (Purdue)	Lin, Farley, and Orville (1983, JCAM)
3	WSM3	Hong, Dudhia, and Chen (2004, MWR)
4	WSM5	Hong, Dudhia, and Chen (2004, MWR)
5	Eta (Ferrier)	Rogers, Black, and Ferrier, *et al.*, (2001)
6	WSM6	Hong and Lim (2006, JKMS)
7	Goddard	Tao, Simpson, and McCumber (1989, MWR)
8	Thompson	Thompson, *et al.*, (2008, MWR)

9	Milbrandt-2-mom	Milbrandt and Yau (2005, JAS)
10	Morrison 2-mom	Hong and Pan (1996, MWR)
14	WDM5	Lim and Hong (2010)
16	WDM6	Lim and Hong (2010)

3.4.4 Post processing and visualization

There are a number of visualization tools available to display ARW model data. Model data in netCDF format, can essentially be displayed using any tool capable of displaying this data format. Currently the following post-processing utilities are supported: NCL, RIP4, ARWpost (converter to GrADS), WPP, and VAPOR. NCL, RIP4, ARWpost and VAPOR can currently only read data in netCDF format, while WPP can read data in netCDF and binary format, netCDF stands for Network Common Data Form. This format is platform independent, i.e., data files can be read on both big-endian and little-endian computers, regardless of where the file was created. To use the netCDF libraries, ensure that the paths to these libraries are set correct in your login scripts as well as all Make files.

Additional libraries required by each of the supported post-processing packages:

- NCL (*http://www.ncl.ucar.edu*)
- GrADS (*http://grads.iges.org/home.html*)
- GEMPAK (*http://www.unidata.ucar.edu/software/gempak/*)
- VAPOR (*http://www.vapor.ucar.edu*)

3.4.5 Set Domain

WRF Domain Wizard used to define the region and projection of a domain on the map and define any nested interface used in the WPS. WRF Domain Wizard stores its information in namelist.wps and namelist.input (inside core ARW). It enables users to easily define and localize domains (cases) by selecting a region of the Earth and choosing a map projection. Users can also define nests using the nests editor. The

research is carried out over the areas of the Southeast Asia within latitude 4°S to 22.5°N and longitude 92°E to 112.5°E (Figure 3.13). There are 2 areas in this study. Area 1 is between latitude 4°S to 22.5°N and longitude 92°E to 112.5°E. Area 2 is between latitude 3.5°N to 15.5°N and longitude 98°E to 107°E. The domain of area 2 is chosen so that it can accommodate the study domain of the 2-D circulation model.

Table 3-8 WRF Domains.

Domains	Map projection	Grid size (km)	Vertical level	Terrain resolutions	Periods
Domain 1 (Test)	Mercator	90	27	10 m	Winter2009
Domain 2 (Test)	Mercator	30	27	10 m	Winter2009
Domain 1	Mercator	30	27	10 m	2000-2002
Domain 2	Mercator	10	27	5 m	2000-2002

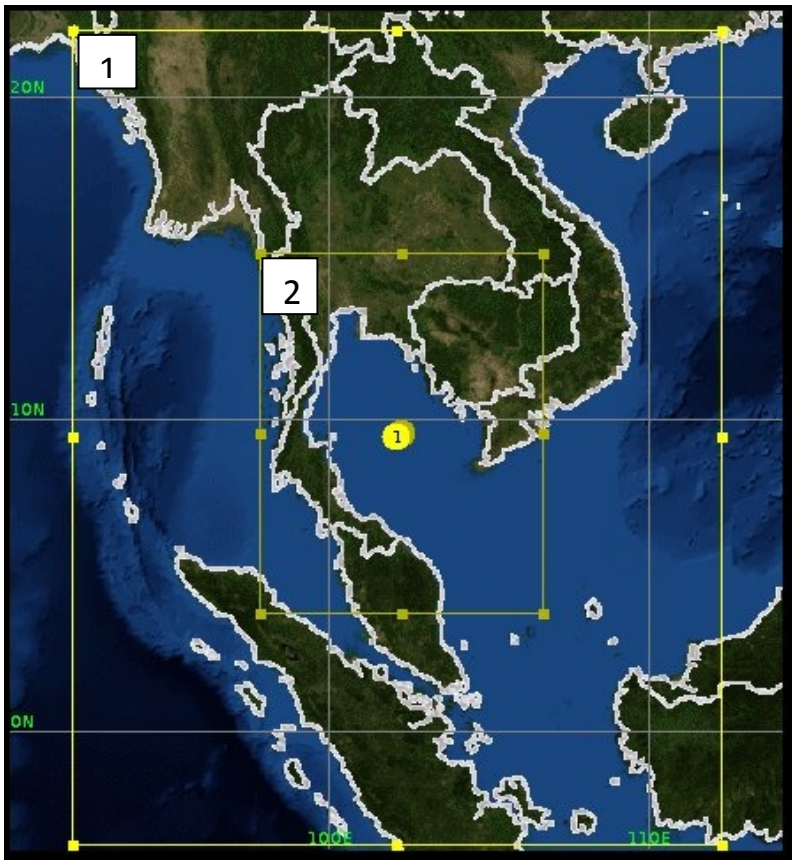

Figure 3-13 The domain in WRF model.

3.4.6 Physical options

After the determination of the numerical configuration of the model and setup domain, next step is to determine which set of physical options (parameterizations) offers the best results, for a winter season are presented Table 3.9. The different sets of parameterizations schemes regarding fixed the boundary layer (SL, PBL and LSM) and radiation scheme (SW and LW) (Carvalho, 2012), which varies cumulus scheme and microphysics scheme were tests. In this study not use nudging techniques on the simulations. The nudging is an option of WRF in its Four-dimensional data assimilation (FDDA) system, show in Figure 3-3 (yellow box).

Table 3-9 WRF model sensitivity test options.

simulations	WRF Physical Options					
Case No.	Land Surface Model	Planetary Boundary Layer	Radiation	Micro-physics	Cumulus convective	references
GT.1	Noah LSM	YSU	RRTM (lw) Dudhia (sw)	Ferrier (Eta)	Kain-Fritsch	Kwun, H. J., 2009.
GT.2	Noah LSM	YSU	RRTM (lw) Dudhia (sw)	WSM5-class	Grell-Devenyi	Menendez, *et al*., 2012.
GT.3	Noah LSM	YSU	RRTM (lw) Dudhia (sw)	WSM6-class	Betts-Miller-Janjic	Chotamon-sak, 2012.
GT.4	Noah LSM	YSU	RRTM (lw) Dudhia (sw)	WSM6-class	Kain-Fritsch	Amnuayloja roen, 2011.
GT.5	Noah LSM	YSU	RRTM (lw) Dudhia (sw)	Ferrier (Eta)	Grell 3D	Papanas-tasiou, 2010.

3.4.7 Validations of the model

The Weather Research and Forecasting model can be validated according to different methodologies that, all together, complement themselves. In the present case, the goal is to validate the model using meteorological observations that represent the real state of the variables to simulate. To evaluate the model performance, three statistical parameters will be used (Carvalho, 2012).

3.4.7.1 The Root Mean Squared Error (RMSE),

$$\text{RMSE} = \left[\frac{1}{N} \sum_{i=1}^{N} (d_i')^2 \right]^{\frac{1}{2}} \tag{3.5}$$

Where

$$d_i' = d_i^m - d_i^{obs} \tag{3.6}$$

Represent the deviation between one individual value of the wind speed simulation and the observed wind speed in the same place and time instant and *N* is the total number of both of values simulation and observation.

For the wind direction, which is a circular variable and not a linear one, d' takes a different expression due to the fact that the absolute deviation of the wind direction cannot exceed 180° in modulus.

$$d_i' = d_i^m - d_i^{obs} \left[1 - 360 / \left| d_i^m - d_i^{obs} \right| \right], \text{ if } \left| d_i^m - d_i^{obs} \right| > 180^\circ \tag{3.7}$$

It is also defined that, for northern Hemisphere, a positive d' represents a clockwise deviation and a negative d' counterclockwise deviation.

3.4.7.2 The Bias,

$$\text{Bias} = \frac{1}{N} \sum_{i=1}^{N} (d_i') \tag{3.8}$$

Allows the evaluation of the data tendency, if it is positive the simulated values tend to be an overestimation of the real values, if it is negative the simulated values tend to be an underestimation of the real ones. For the wind direction, a positive/negative Bias means a clockwise/counter clockwise deviation.

3.4.7.3 The Standard Deviation Error (STDE),

$$\text{STDE} = \left[\frac{1}{N} \sum_{i=1}^{N} \left(d_i' - \frac{1}{N} \sum_{i=1}^{N} d_i' \right)^2 \right]^{\frac{1}{2}} \quad (3.9)$$

is very useful to evaluate the dispersion of the error.

Priority will be given to the values of STDE, and this assumption comes from the fact that, even if a simulation has a high RMSE or Bias, if the STDE is low it means that the error is somewhat constant and can be seen as a kind of offset and the simulation physics is correct. If a simulation has a high STDE, the error is random and the simulation has low physical meaning, even if ha a relatively low RMSE or Bias (Carvalho, 2012).

3.5 Data collection

3.5.1 Atmospheric Satellite data

The Blended Sea Winds contain globally gridded, high resolution ocean surface vector winds and wind stresses on a global 0.25° grid, and multiple time resolutions of 6-hourly, daily, monthly climatologically monthlies. The period of record is July 1987 - present. The wind speeds were generated by blending observations from multiple satellites (up to six satellites). The wind directions came from two sources depending on the products: for the research products the source is the NCEP Reanalysis 2 (NRA-2) and for near real-time products the source is the ECMWF NWP. The wind directions were interpolated onto the blended speed grids. The blending of multiple satellite observations fill in the data gaps (in both time and space) of the individual satellite samplings and reduce the sub-sampling aliases and random errors. The development of these products is in response to the demand for increasingly higher resolution global datasets. For example, scientists want to make more accurate forecasts of ocean and weather conditions.

Table 3-10 Available of Atmospheric satellite data.

Database	Resolution	Period	Source for download
winds and wind-stresses data	0.25 degree	1999-2002	http://www.ncdc.noaa.gov/oa/rsad/air-sea/seawinds.html

3.5.2 Initial and boundary data

- NCEP FNL

These NCEP FNL (Final) Operational Global Analysis data are on 1.0x1.0 degree grids prepared operationally every six hours. This product is from the Global Data Assimilation System (GDAS), which continuously collects observational data from the Global Telecommunications System (GTS), and other sources, for many analyses. The FNL are made with the same model which NCEP uses in the Global Forecast System (GFS), but the FNL are prepared about an hour or so after the GFS is initialized. The FNL are delayed so that more observational data can be used. The GFS is run earlier in support of time critical forecast needs, and uses the FNL from the previous 6 hour cycle as part of its initialization.

The analyses are available on the surface, at 26 mandatory (and other pressure) levels from 1000mb to 10mb, in the surface boundary layer and at some sigma layers, the tropopause and a few others. Parameters include surface pressure, sea level pressure, geopotential height, temperature, sea surface temperature, soil values, ice cover, relative humidity, u- and v- winds, vertical motion, vorticity, and ozone.

- Terrestrial Data

Terrestrial Data are sets of static fields (topography, land use, soil types, land-water masks, albedo) global 25-category data with a 30-second resolution.

Table 3-11 Available of initial and boundary data.

Database	Resolutions	Periods	Sources for download
NCEP Final Analysis (FNL from GFS)	1 degree	1999-2002	http://www.mmm.ucar.edu/ wrf/users/download/free_data.html
Terrestrial Data	30 second	2009	http://www.mmm.ucar.edu/wrf/ users/ download/get_source.html

CHAPTER IV
RESULTS AND DISCUSSIONS

4.1 Model verification

Time series of wind speed and direction from five simulations described in chapter 3 (3.4.6) were compared with the observed data during the winter season only and the statistical analysis results are given in Table 4-1 and Figure 4-1 to 4-2. For the verification of sea surface wind, the 10-m daily mean wind speed and direction from QuikSCAT satellite data (Menendez, *et al*., 2012) was used in the RMSE, Bias and STDE analysis (Carvalho, 2012).

Table 4-1 Statistical analysis performed on 5 simulations of wind speed and direction during winter 2009.

WRF model	Wind speed (m/s)			Wind directions (degree)		
Simulations	RMSE	Bias	STDE	RMSE	Bias	STDE
GT.1	2.941	1.470	2.547	34.9	-24.7	24.6
GT.2	2.359	0.701	2.252	29.5	-14.0	25.9
GT.3	2.291	0.822	2.139	28.2	-10.9	26.0
GT.4	2.861	1.172	2.610	36.3	-25.9	25.4
GT.5	2.656	1.280	2.328	35.6	-25.3	25.0

The Physics Options used in the 5 experiments were chosen from the best options used in earlier studies by other researchers. The boundary layer (SL, PBL and LSM) and radiation scheme (SW and LW) which deal with cumulus scheme and microphysics scheme were similar to what Carvalho (2012) used. They found that the RMSE, Bias, and STDE values were lowest during winter season. Thus, according to their study, I chose to do the experiment for the Gulf of Thailand during winter.

It was noticeable that the model was able to accurately reproduce the local wind regime, both in terms of speed and direction. The model tended to overestimate

wind speed while underestimate wind direction. There was tendency for the deviation of wind direction to be anti-clockwise (left, negative d'). The GT.3 seemed to give wind speed & direction values closest to the observed ones (lowest RMSE, Bias, and STDE in Table 4-1). Figure 4-1 and Figure 4-2 showed scattering plots of the simulation data .vs. the observed data. The GT.3 simulation also gave the highest R^2 (0.37).

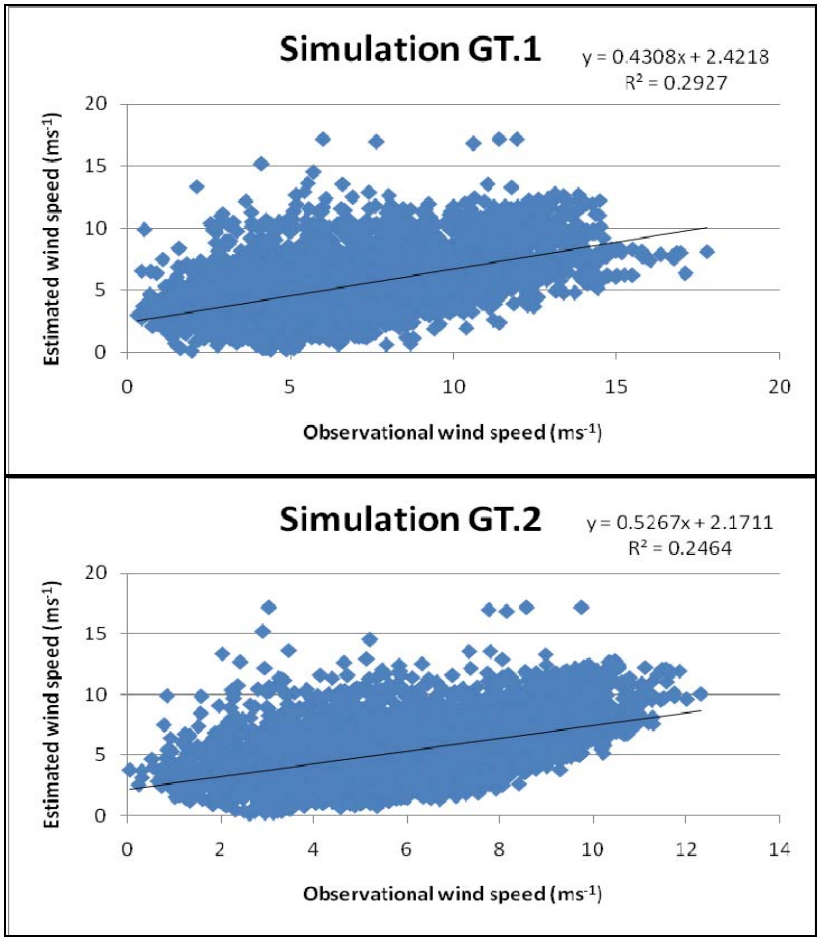

Figure 4-1 Correlation of the observed wind speed with simulated winds (GT.1 and GT.2).

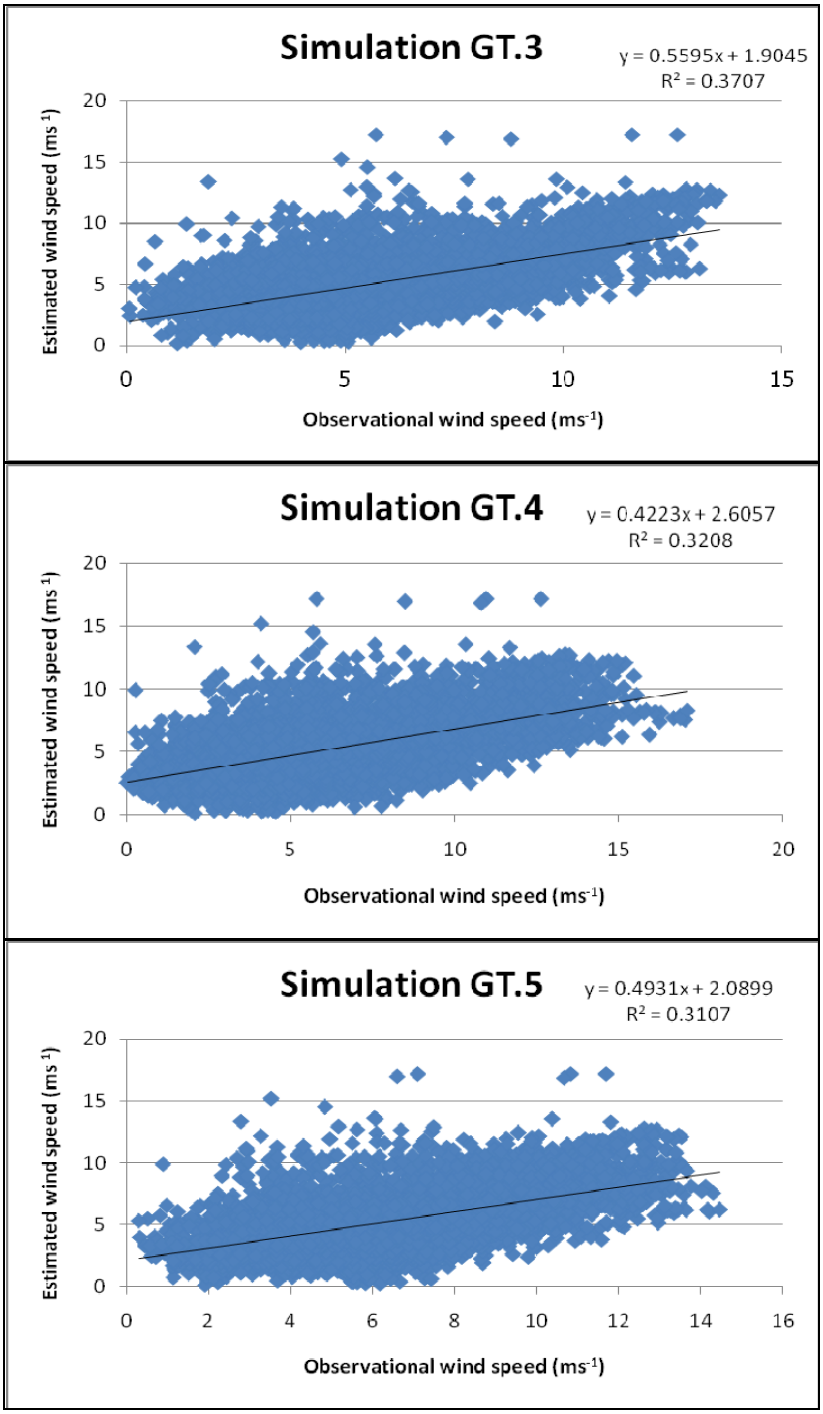

Figure 4-2 Correlation of the observed wind speed with simulated winds (GT.3 to GT.5).

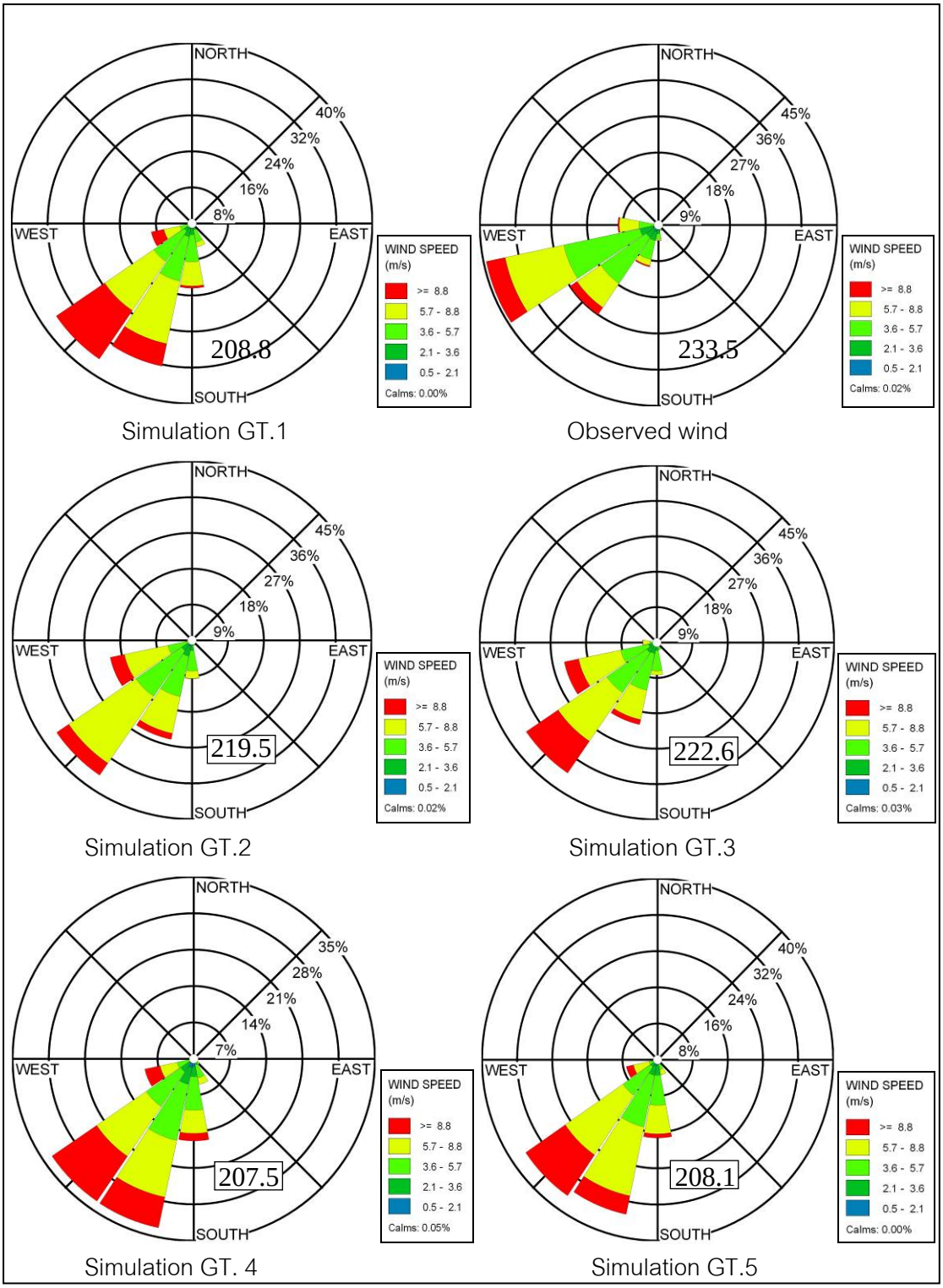

Figure 4-3 The wind rose of observed and 5 simulation wind (GT.1 to GT.5).

Figure 4-3 displayed wind roses of the observed wind and 5 simulated wind and Figure 4-4 and Figure 4-5 displayed frequency of the observed wind speed and the simulated wind speeds respectively. The simulated wind tended to give higher wind speed and lower mean wind direction than the observed one. About 48% of wind in simulation GT.1 fell in 195-225° range with the average value of 208.8° and mean wind speed in 5.7-8.8 m/s range (about 38%). About 44% of wind in simulation GT.2 fell in 225-255° range with the average value of 219.5° and mean wind speed in 5.7-8.8 m/s range (about 43%).

About 46% of wind in simulation GT.3 fell in 225-255° range with the average value of 222.6° and mean wind speed in 3.6-5.7 m/s range (about 37%). About 47% of wind in simulation GT.4 fell in 195-225° range with the average value of 207.5° and mean wind speed in 3.6-5.7 m/s and 5.7-8.8 m/s ranges (about 32%). About 52% of wind in simulation GT.5 fell in 195-225° range with the average value of 208.1° and mean wind speed in 5.7-8.8 m/s range (about 43%). About 54% of the observed wind fell in 225-255° range with the average value of 233.5° and mean wind speed in 3.6-57 m/s range (about 45%).

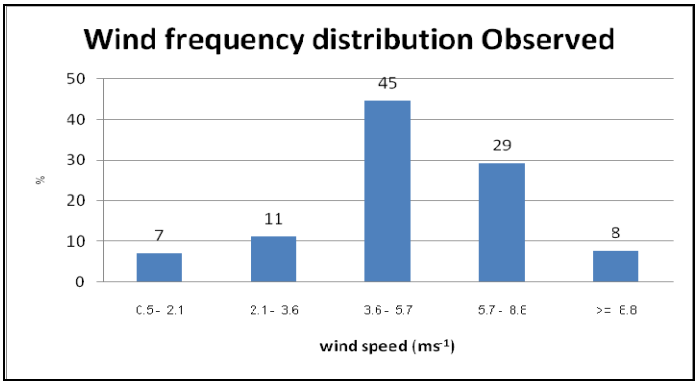

Figure 4-4 Frequency distribution of the observed wind speed (winter 2009).

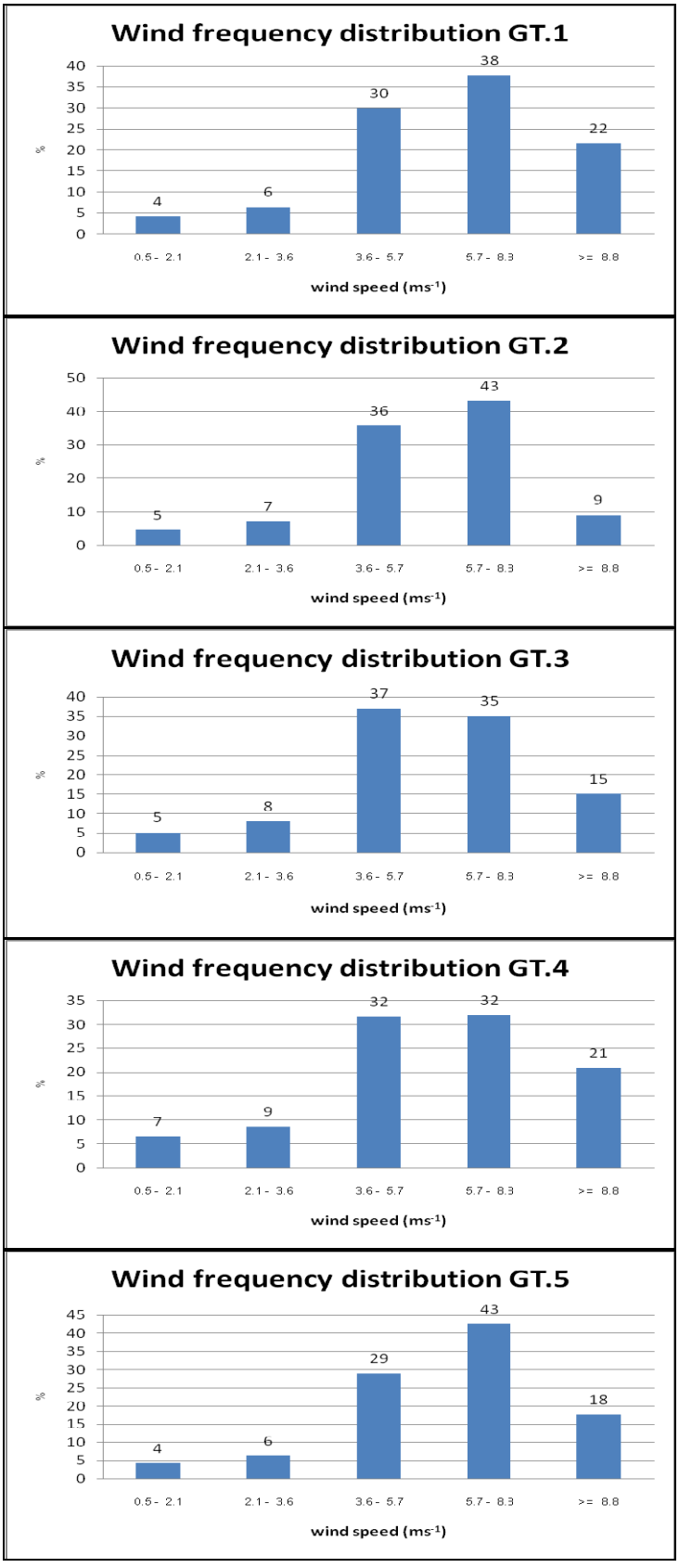

Figure 4-5 The wind frequency distribution of GT.1 to GT.5 (winter 2009).

Table 4-2 compared the mean wind speed and direction of the GT.3 simulation with those of the observed data. Except for the summer 2000, the mean wind speeds from the WRF model were lower than those of the observed data, but the differences were less than 1 m/s. And except for the winter 2001, the mean wind directions from the WRF model were lower than those of the observed data, but the deviations were in the range of 2 to 15 degree. Statistical analysis (RMSE, Bias and STDE) performed on wind speed and wind direction from the model .vs. the observed data were presented in Table 4-3. Bias is the difference of the mean while RMSE and STDE indicate variation of the mean. The RMSE and STDE of the wind speed data were less than 2 which were acceptable while those of the wind direction varied from 9 to 69 degree. Summer wind direction had higher RMSE and STDE values due to the fact that the wind was rather weak during this season, thus its direction can be effected by land topography and other atmospheric effects.

Table 4-2 Comparison of the mean wind speed and direction of the WRF model with those of the observed data during 2000-2002.

Seasonally	Average (model) Speed/Direction	Average (obs.) Speed/Direction
Summer 2000	2.524/114.4	2.476/127.1
Summer 2001	2.404/104.7	2.603/120.6
Summer 2002	2.874/102.8	3.549/120.5
Rainy season 2000	4.097/227.2	5.063/238.4
Rainy season 2001	5.142/230.6	5.616/244.8
Rainy season 2002	5.276/227.8	6.140/237.8
Winter season 2000	4.413/56.4	5.237/58.0
Winter season 2001	5.289/54.0	5.626/50.2
Winter season 2002	5.223/64.0	5.477/65.9

Table 4-3 Statistical analysis performed on seasonal wind speed and direction during 2000-2002.

	Wind speed (m/s)			Wind directions (degree)		
Seasonally	RMSE	Bias	STDE	RMSE	Bias	STDE
Summer 2000	1.358	0.048	1.357	68.8	-6.3	68.5
Summer 2001	1.583	-0.199	1.571	57.0	-12.6	55.5
Summer 2002	1.996	-0.675	1.879	66.7	-4.0	66.6
Rainy 2000	1.786	-0.966	1.502	24.2	-11.7	21.2
Rainy 2001	1.965	-0.474	1.907	24.0	-14.7	19.0
Rainy 2002	2.202	-0.863	2.026	26.2	-11.1	23.7
Winter 2000	1.825	-0.824	1.629	12.3	-1.5	12.2
Winter 2001	1.959	-0.437	1.909	10.0	3.2	9.5
Winter 2002	2.009	-0.254	1.993	11.0	-2.3	10.8

Table 4-4 Acceptable Benchmark of the Meteorological Model Evaluation.

(Adapted from Emery, *et al*., 2001)

	Benchmark	
Parameters	Bias	RMSE
Wind speed	$\leq \pm$ 0.5 m/s	$\leq$ 2.0
Wind direction	$\leq \pm$ 10 deg.	

Table 4-4 lists acceptable benchmark for the model evaluation as suggested by Emery, *et al*., (2001). These benchmark values are derived based on performance statistics of MM5 model from a number of studies over the U.S. domain (mostly at a horizontal grid resolution of 4 and 12 Km). This benchmark will be adopted for this study.

Table 4-1 showed the options used in the WRF model in order to get the simulated wind speed and direction. The resolution of the large domain area was 90 km, and then the resolution for the small domain area was 30 km (Table 3-8). The model evaluation was performed only during the winter 2009. Option GT.3 (Noah lands surface

model, YSU, RRTM and Duhia, WSM6-class, and Kain-Frisch scheme) gave the best statistics but the numbers were beyond the acceptable ranges. Thus, the model resolution was further reduced to 10 km, and it gave better statistic as shown in Table 4-3.

In Table 4-3, statistics for wind speed and direction during summer and winter fell in the acceptable ranges. However, most statistics for those during rainy period were beyond the acceptable ranges. In this study, we calibrated the WRF model for winter period and used this optimum option for rainy season and summer. Further effort should be spent to find the optimum option for other seasons too.

Table 4-5 Paired t-test of the simulated/observed wind speed and direction during 2000-2002.

Wind speed (S-O)	t-test	Average	SD	Sig(2-tailed)	α
Summer2000	0.56	2.52/2.47	1.35	1.65	0.05
Summer2001	-2.02	2.40/2.60	1.57	-1.65	0.05
Summer2002	-5.73	2.87/3.55	1.88	-1.65	0.05
Rainy2000	-10.27	4.09/5.06	1.50	-1.65	0.05
Rainy2001	-3.96	5.14/5.61	1.91	-1.65	0.05
Rainy2002	-6.81	5.27/6.14	2.03	-1.65	0.05
Winter2000	-8.07	4.41/5.24	1.63	-1.65	0.05
Winter2001	-3.01	5.28/5.63	1.80	-1.65	0.05
Winter2002	-0.20	5.22/5.47	1.99	-1.65	0.05
Wind direction (S-O)	t-test	Average	SD	Sig(2-tailed)	α
Summer2000	-3.02	114/127	70.79	-1.65	0.05
Summer2001	-5.42	105/120	66.26	-1.65	0.05
Summer2002	-6.02	103/120	66.85	-1.65	0.05
Rainy2000	-8.79	227/238	21.28	-1.65	0.05
Rainy2001	-12.35	230/244	19.03	-1.65	0.05
Rainy2002	-7.46	228/238	23.77	-1.65	0.05
Winter2000	-2.00	56/58	12.21	-1.65	0.05
Winter2001	5.43	54/50	9.49	1.65	0.05
Winter2002	-3.36	64/66	10.81	-1.65	0.05

4.2 Characteristics of seasonal wind in the Gulf of Thailand

Northeast and Southwest monsoon controlled wind characteristics over the Gulf of Thailand. The rainy season starts from May and end in September when low pressure in the Indian Ocean controls the weather over the region. October is the inter-monsoon period when the SW monsoon is weak and the NE monsoon gains strength. The winter season starts from November to February when high pressure in the Siberia controls the weather over the Asian continent. And March-April is the summer period where the wind blows from South China Sea in the SE direction.

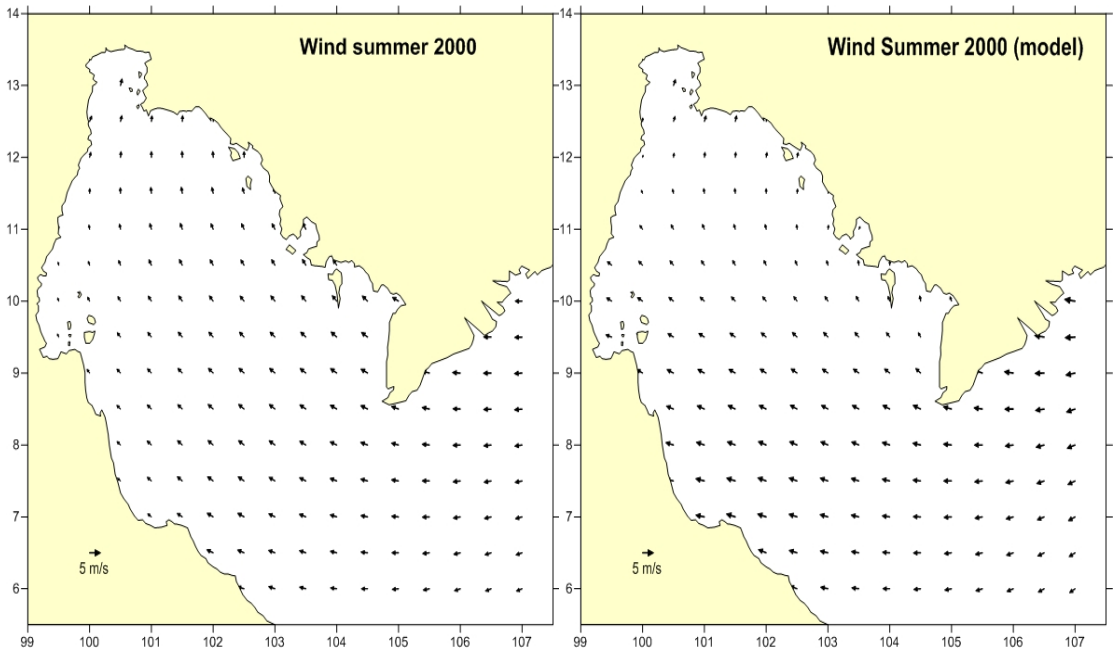

Figure 4-6 Mean sea surface wind (satellite) and simulated wind over the Gulf of Thailand in summer season 2000.

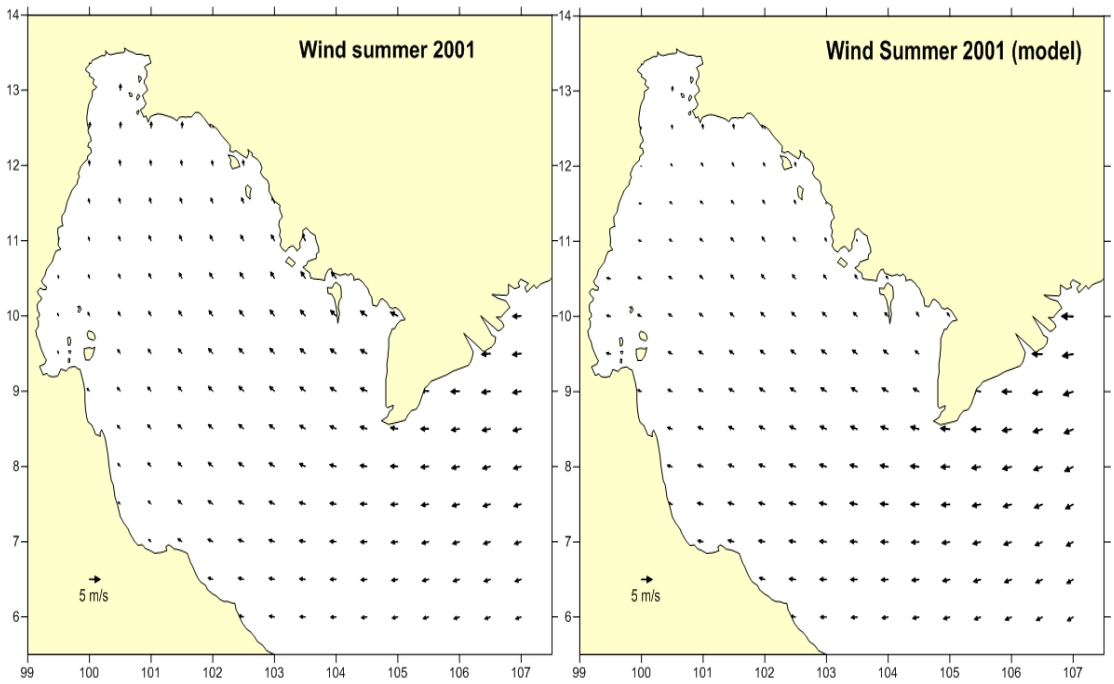

Figure 4-7 Mean sea surface wind (satellite) and simulated wind over the Gulf of Thailand in summer season 2001.

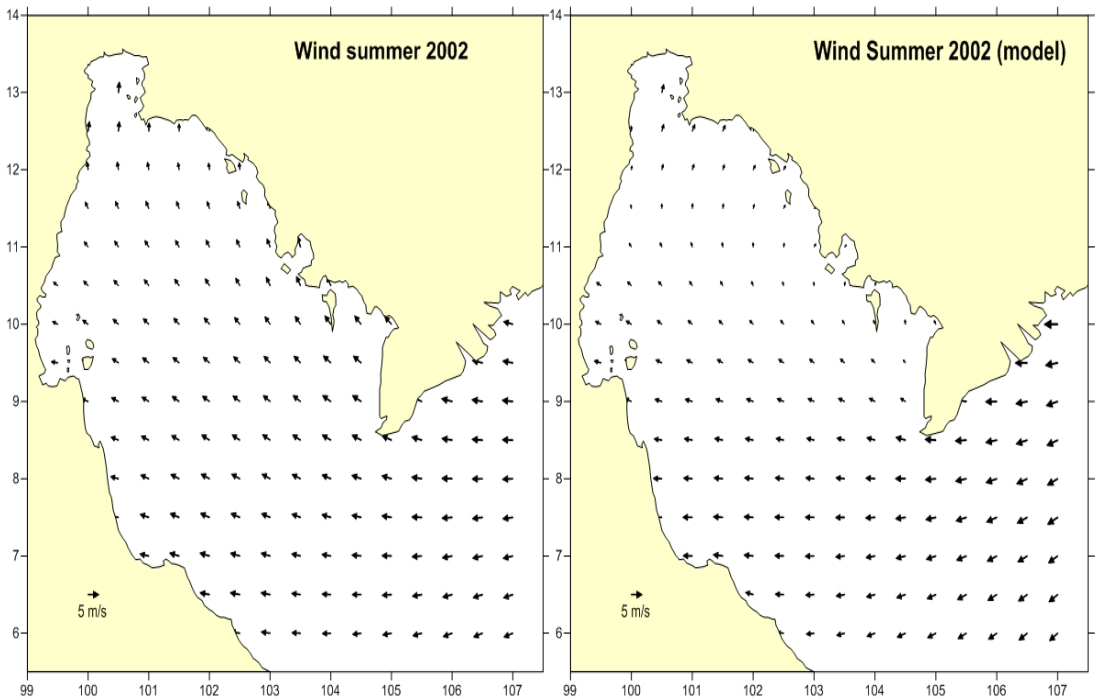

Figure 4-8 Mean sea surface wind (satellite) and simulated wind over the Gulf of Thailand in summer season 2002.

Figure 4-6 to Figure 4-8 compared mean sea surface wind from the satellite (observed wind) with the simulated wind during summer 2000-2002. This was the first inter-monsoon period where wind blew from South China Sea in the east direction with the mean wind speed of 3.2 m/s. The E wind turned into the SE wind when entering the lower Gulf of Thailand with the mean wind speed of 2.9 m/s. The SE wind turned into the S wind when entering the upper Gulf of Thailand with the mean wind speed of 2.3 m/s.

From Table 4-2 wind speeds from WRF model were lower than those from the observed data except during summer 2000, but the differences were not high. Paired t-test in Table 4-5 indicated that only the mean wind speed for summer 2000 was not significantly different. Figure 4-9 showed distribution of wind speeds and directions for the summer 2000-2002. The observed data dispersed unevenly in quadrant II while the model data lumped around E direction. The mean wind direction for the observed data veered to the left (anti-clockwise) of the model directions for all 3 years. Paired t-test of the wind direction (Table 4-5) indicated that wind direction from the model differed significantly with that from the observed data.

Table 4-6 Summary results of summer 2000-2002.

	Wind speed (m/s)				Wind directions (degree)			
Season	RMSE	Bias	t-test	Average	RMSE	Bias	t-test	Average
Summer2000	1.358	0.048	0.56	2.524	68.8	-6.3	-3.02	114.4
Summer2001	1.583	-0.199	-2.02	2.404	57.0	-12.6	-5.42	104.7
Summer2002	1.996	-0.675	-5.73	2.874	66.7	-4.0	-6.02	102.8

Summary from Table 4-6 and Figures 4-6 to 4-8, wind in the Gulf of Thailand during summer blew mainly from the SE direction. The bias values for wind directions for summer 2000, 2001, and 2002 were negative, indicating that the average wind direction of the simulated data was lower than that of the satellite data (anti-clockwise). While the t-test values were less than -1.65, meaning that the simulated wind direction differed significantly from the observed one.

The bias value for wind speed for summer 2000 was positive and the t-test value was also positive and less than 1.65, indicating that simulated wind speed was greater than the satellite one but the difference was not significant. On the other hand, the bias values for wind speed for summer 2001 and 2002 were weaker than the satellite data and t-test results indicated that the differences were significant statistically.

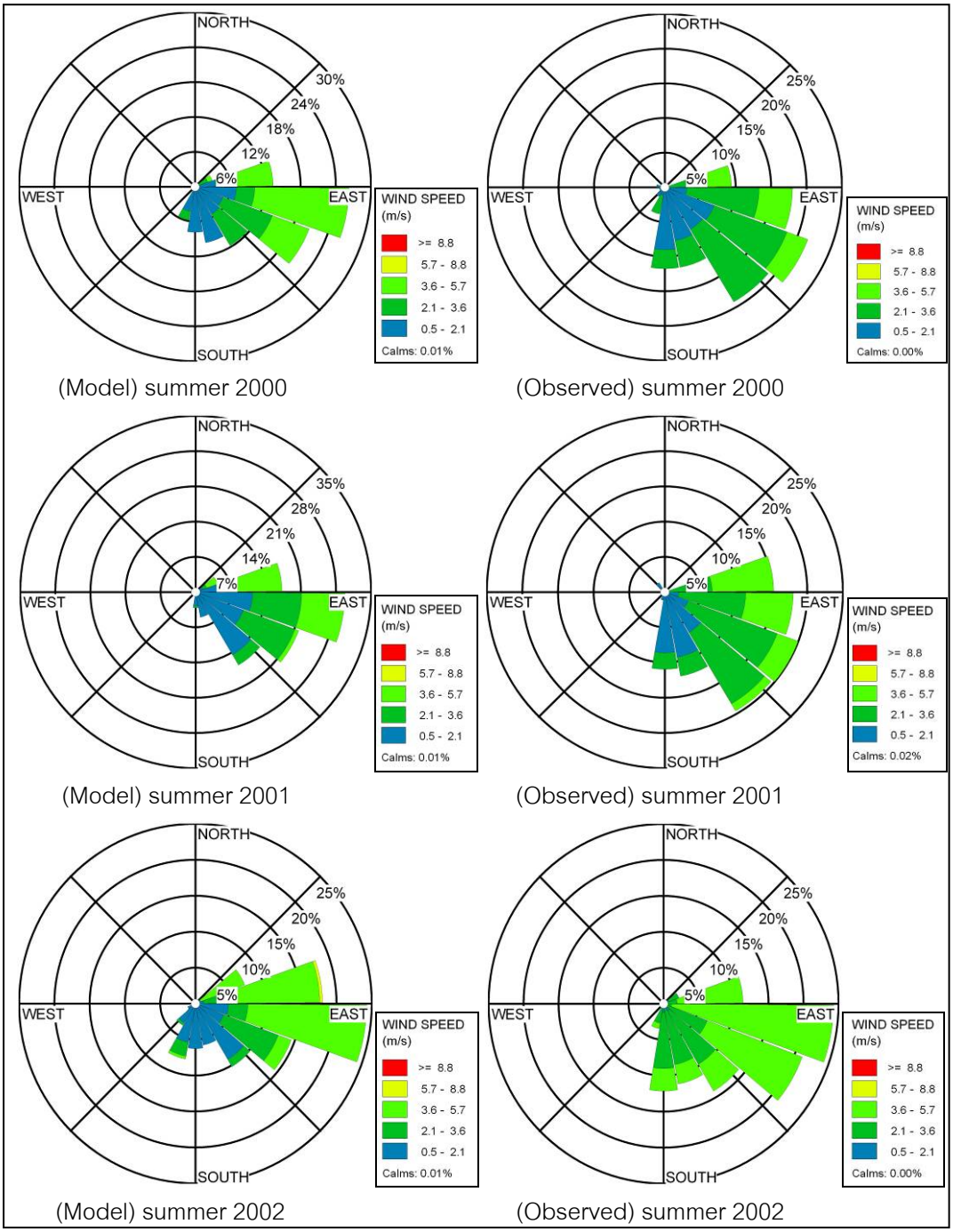

Figure 4-9 The wind rose over the Gulf of Thailand in summer season 2000 to 2002.

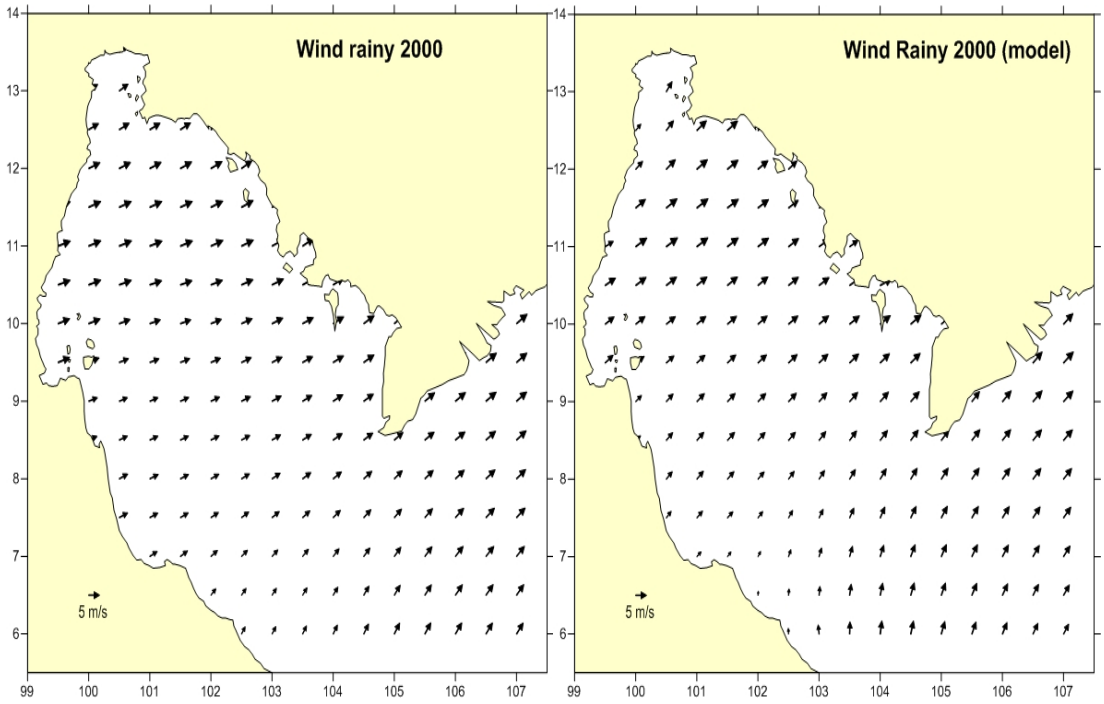

Figure 4-10 Mean sea surface wind (satellite) and simulated wind over the Gulf of Thailand in rainy season 2000.

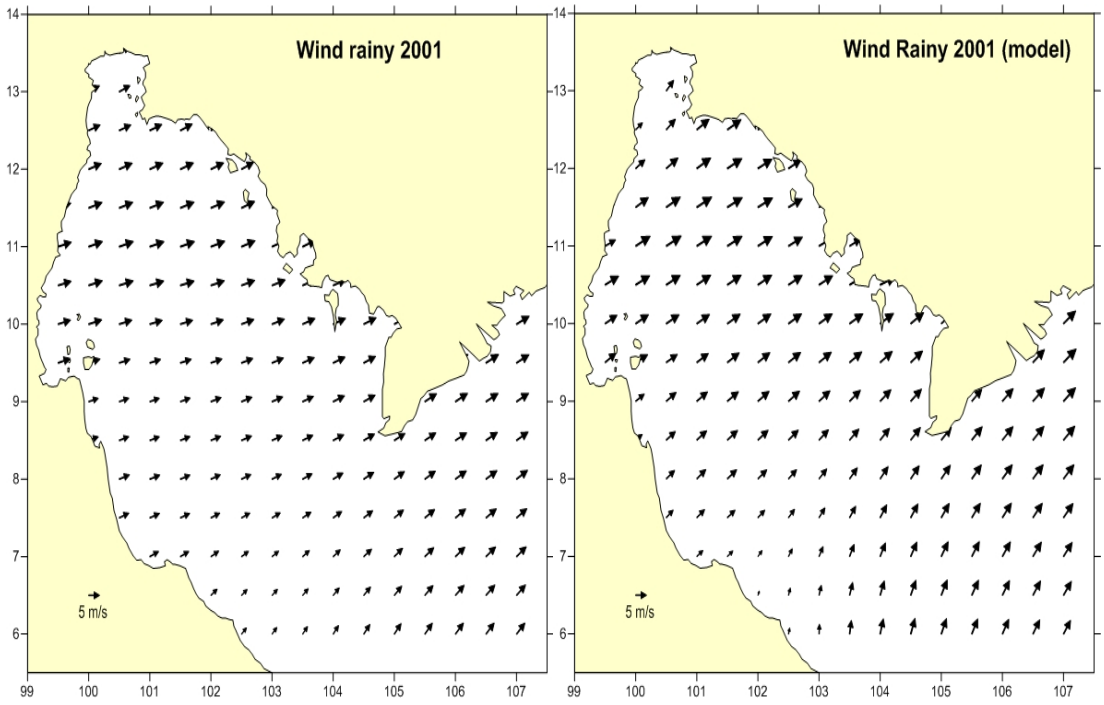

Figure 4-11 Mean sea surface wind (satellite) and simulated wind over the Gulf of Thailand in rainy season 2001.

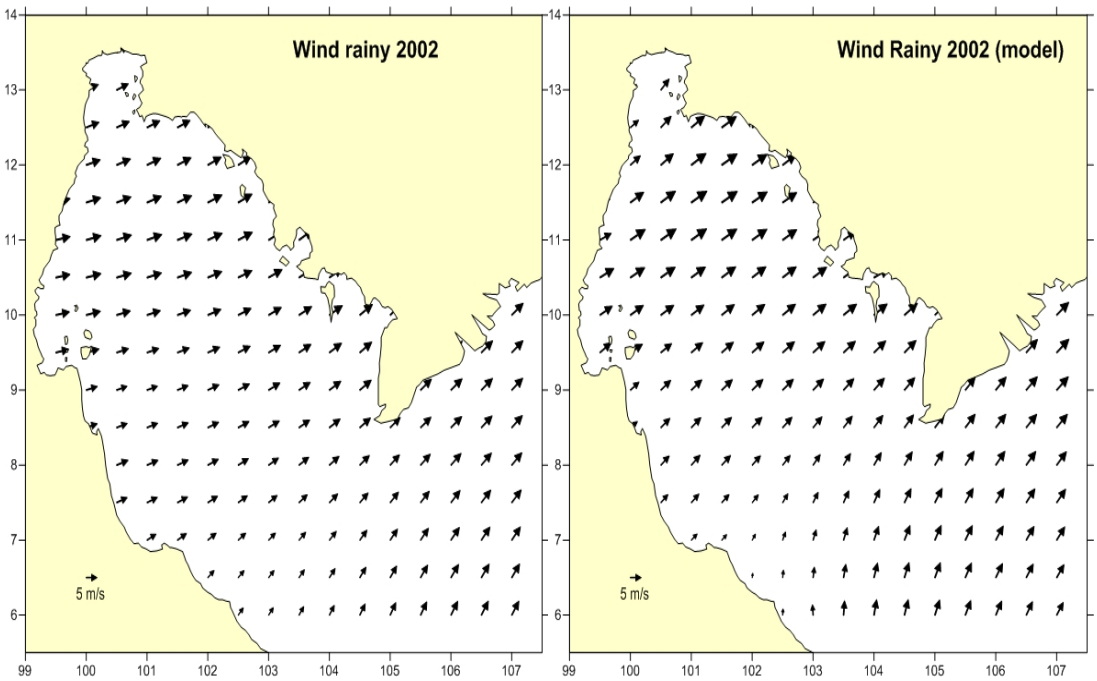

Figure 4-12 Mean sea surface wind (satellite) and simulated wind over the Gulf of Thailand in rainy season 2002.

Figure 4-10 to Figure 4-12 compared wind patterns from the satellite (observed) with those from the WRF model for the rainy season 2000-2002. The wind originated from the Indian Ocean and blew over the Gulf of Thailand. The wind directions over the gulf were in the WSW direction with the mean wind speed of 6.1 m/s while those over South China Sea were in the SW direction with the mean wind speed of 4.9 m/s.

From Table 4-2, wind speeds from WRF model were lower than those from the observed data. Table 4-5 paired t-test indicated that the differences in wind speed were significant for all these 3-year period. Stronger wind occurred in 2002 which was classified as the El Niño period. Figure 4-13 showed distribution of wind speeds and directions for the rainy season 2000-2002. The observed wind data blew mainly from the SW direction while wind in the model also varied around the SW direction. The mean wind direction of the WRF model veered to the right (clockwise) of the observed data. Paired t-test (Table 4-5) indicated that wind direction from the model differed significantly with that from the observed data.

Table 4-7 Summary results of rainy 2000-2002.

	Wind speed (m/s)				Wind directions (degree)			
Season	RMSE	Bias	t-test	Average	RMSE	Bias	t-test	Average
Rainy 2000	1.786	-0.966	-10.27	4.097	24.2	-11.7	-8.79	227.2
Rainy 2001	1.965	-0.474	-3.96	5.142	24.0	-14.7	-12.35	230.6
Rainy 2002	2.202	-0.863	-6.81	5.276	26.2	-11.1	-7.46	227.8

Summary from Table 4-7 and Figures 4-10 to 4-12, wind in the Gulf of Thailand during winter blew mainly from the SW direction. The bias values for wind directions for rainy season 2000-2002 were negative, indicating that the average wind direction of the simulated data was lower than that of the satellite data (anti-clockwise). While the t-test values were less than -1.65, meaning that the simulated wind direction differed significantly from the observed one.

The bias value for wind speed for rainy season 2000-2002 were also negative and the t-test values were also negative and less than 1.65, indicating that simulated wind speed was weaker than the satellite one and the differences were significant statistically.

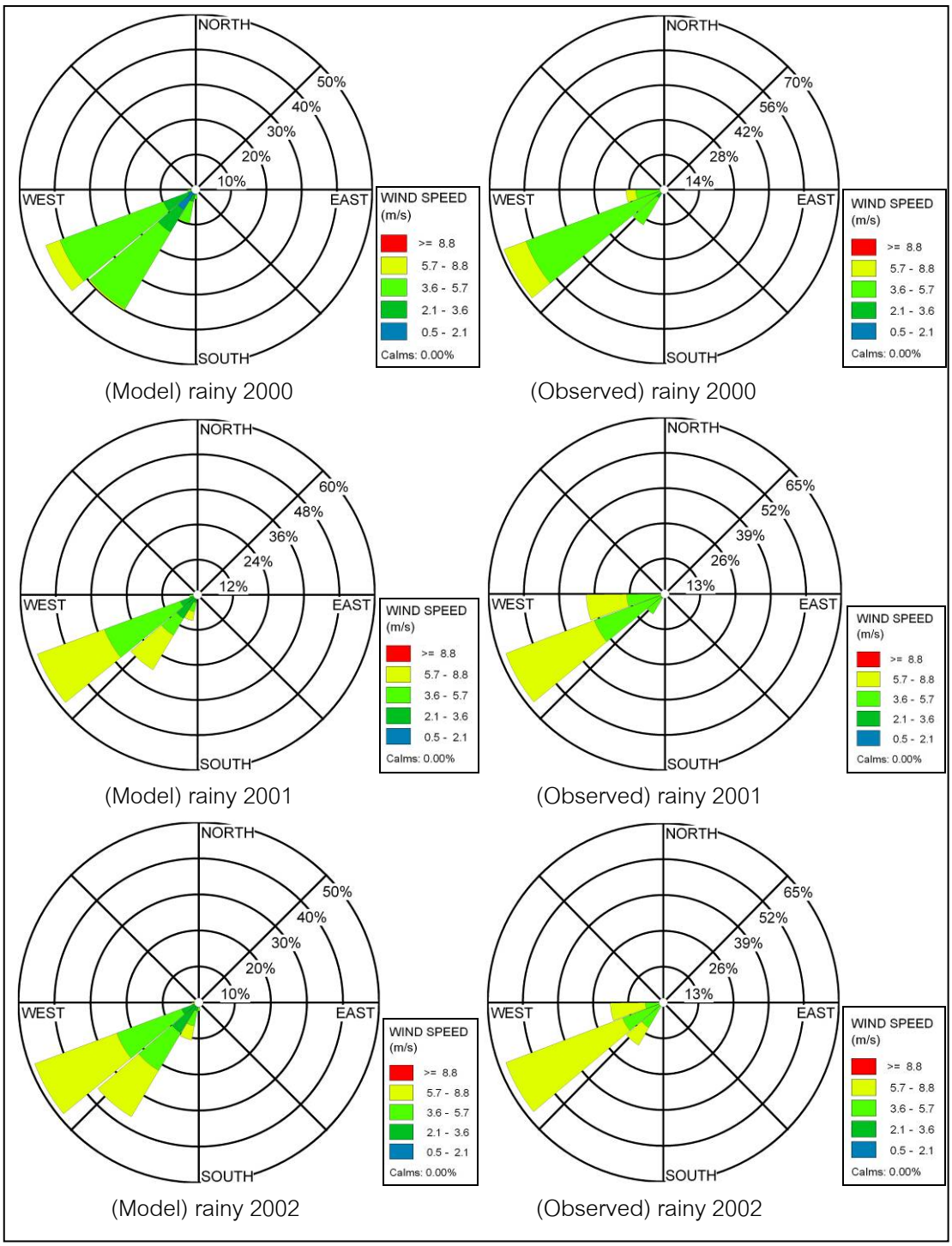

Figure 4.13 Wind rose over the Gulf of Thailand in rainy season from 2000 to 2002.

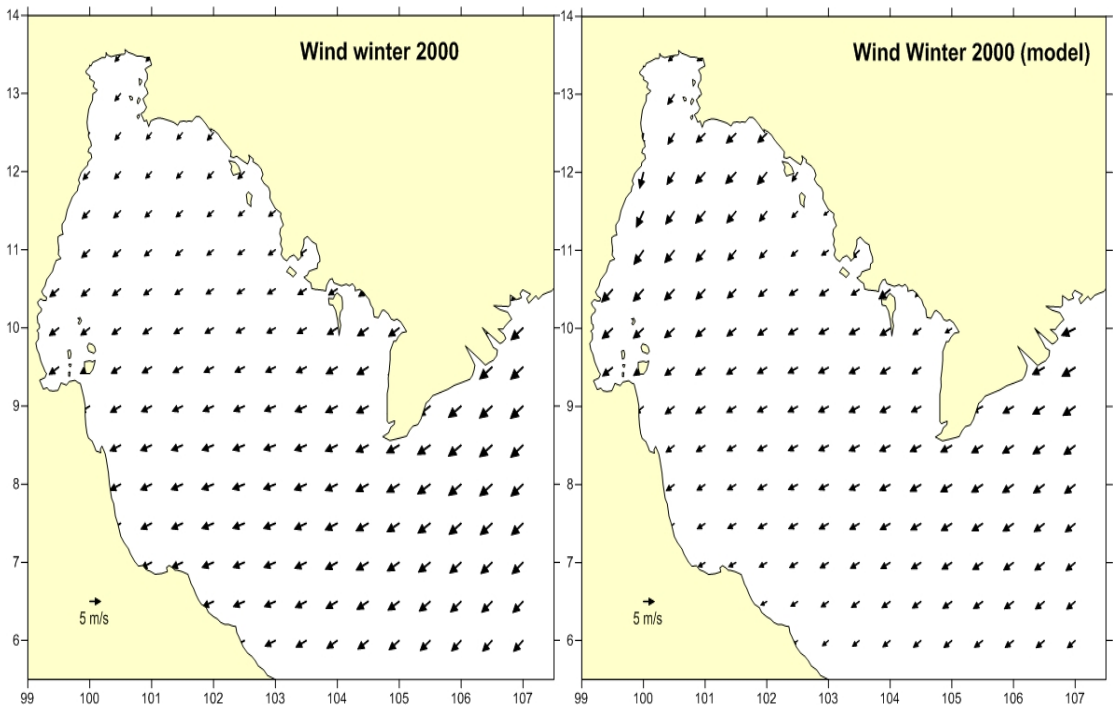

Figure 4-14 Mean sea surface wind (satellite) and simulated wind over the Gulf of Thailand in winter season 2000.

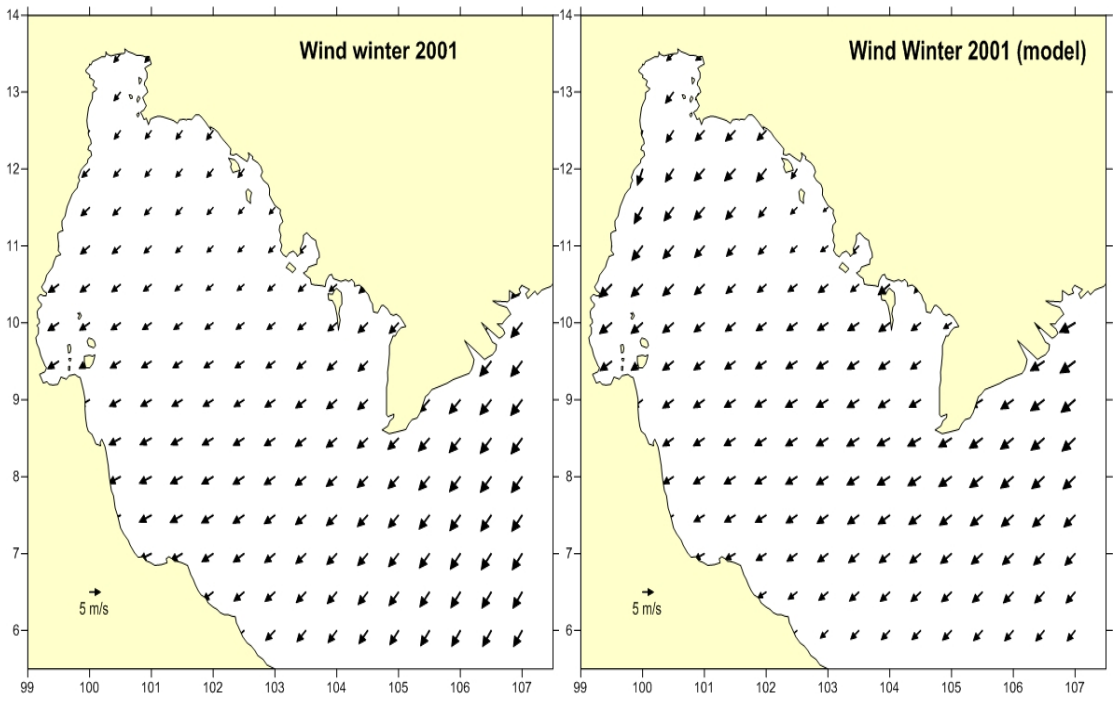

Figure 4-15 Mean sea surface wind (satellite) and simulated wind over the Gulf of Thailand in winter season 2001.

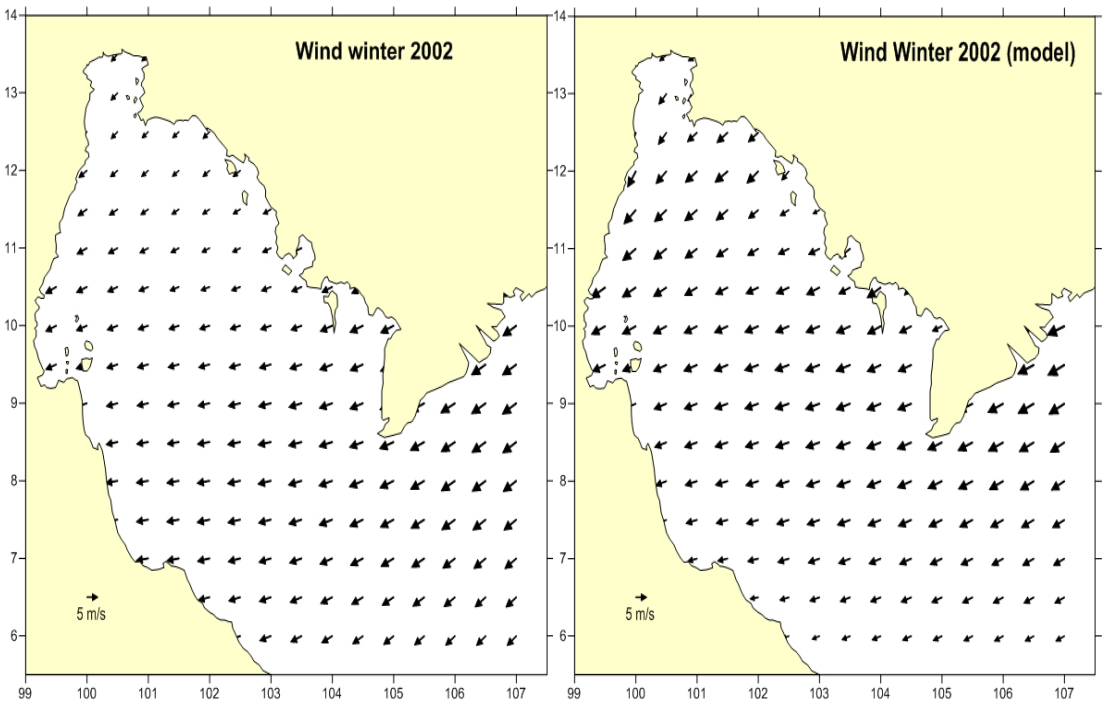

Figure 4-16 Mean sea surface wind (satellite) and simulated wind over the Gulf of Thailand in winter 2002.

Figure 4-14 to Figure 4-16 compared wind patterns from the satellite (observed) with those from the WRF model for the winter season 2000-2002. The wind blew from South China Sea in the NE direction with the mean wind speed of 4.5 m/s. The wind deflected to ENE direction in the lower gulf direction with the mean wind speed of 5.3-6.0 m/s.

From Table 4-2 wind speeds from WRF model were lower than those from the observed data. Table 4-5 paired t-test indicated that the differences in wind speed were significant for winter 2000 and 2001 only. Wind speed did not vary with El Niño – La Niña cycles. Figure 4-17 showed distribution of wind speeds and directions for the winter 2000-2002. Both the observed and simulated winds came from the NE to ENE directions. Paired t-test (Table 4-5) indicated that wind direction from the model differed significantly with that from the observed data even though the differences in wind direction were 2-4° only.

Table 4-8 Summary results of winter 2000-2002.

	Wind speed (m/s)				Wind directions (degree)			
Season	RMSE	Bias	t-test	Average	RMSE	Bias	t-test	Average
Winter 2000	1.825	-0.824	-8.07	4.413	12.3	-1.5	-2.00	56.4
Winter 2001	1.959	-0.437	-3.01	5.289	10.0	3.2	5.43	54.0
Winter 2002	2.009	-0.254	-0.20	5.223	11.0	-2.3	-3.36	64.0

Summary from Table 4-8 and Figures 4-14 to 4-16, wind in the Gulf of Thailand during winter blew mainly from the NE direction. The bias values for wind directions for winter 2000 and 2002 were negative, indicating that the average wind direction of the simulated data was lower than that of the satellite data (anti-clockwise). The bias value for the wind direction for winter 2001 was positive, indicating that the average simulated wind direction was greater than the satellite data (clockwise). While the absolute t-test values were greater than 1.65 for all 3 years, meaning that the simulated wind direction differed significantly from the observed one.

The bias values for wind speed for rainy season 2000-2002 were negative, indicating that the simulated wind was weaker than the satellite one. From the t-test values, only simulated wind speed during winter 2000 and 2001 differed significantly from the satellite ones. The average simulated wind speed during 2002 was not different from the satellite one.

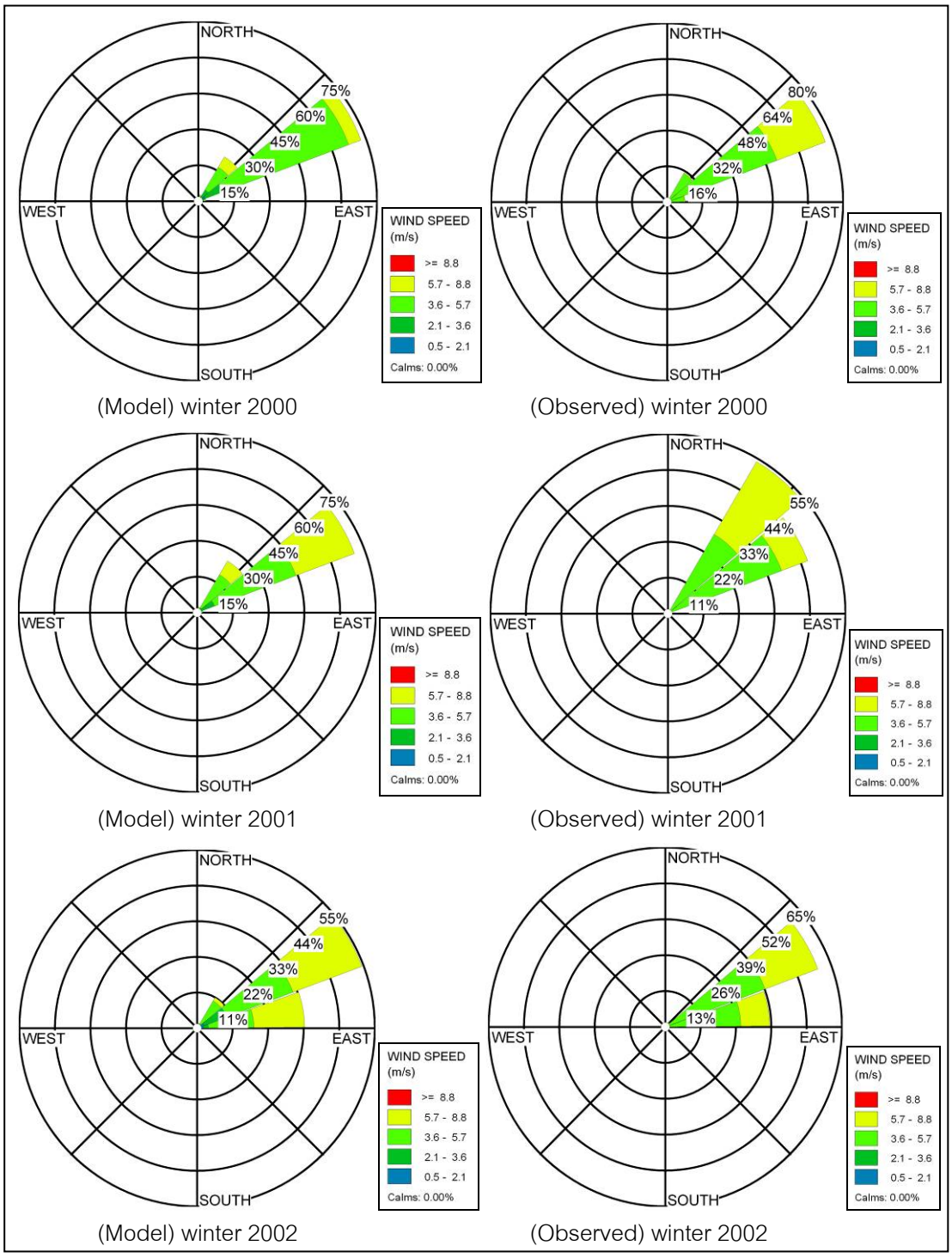

Figure 4-17 Wind rose over the Gulf of Thailand in winter season from 2000 to 2002.

4.3 Characteristics of seasonal wind-driven current in the Gulf of Thailand

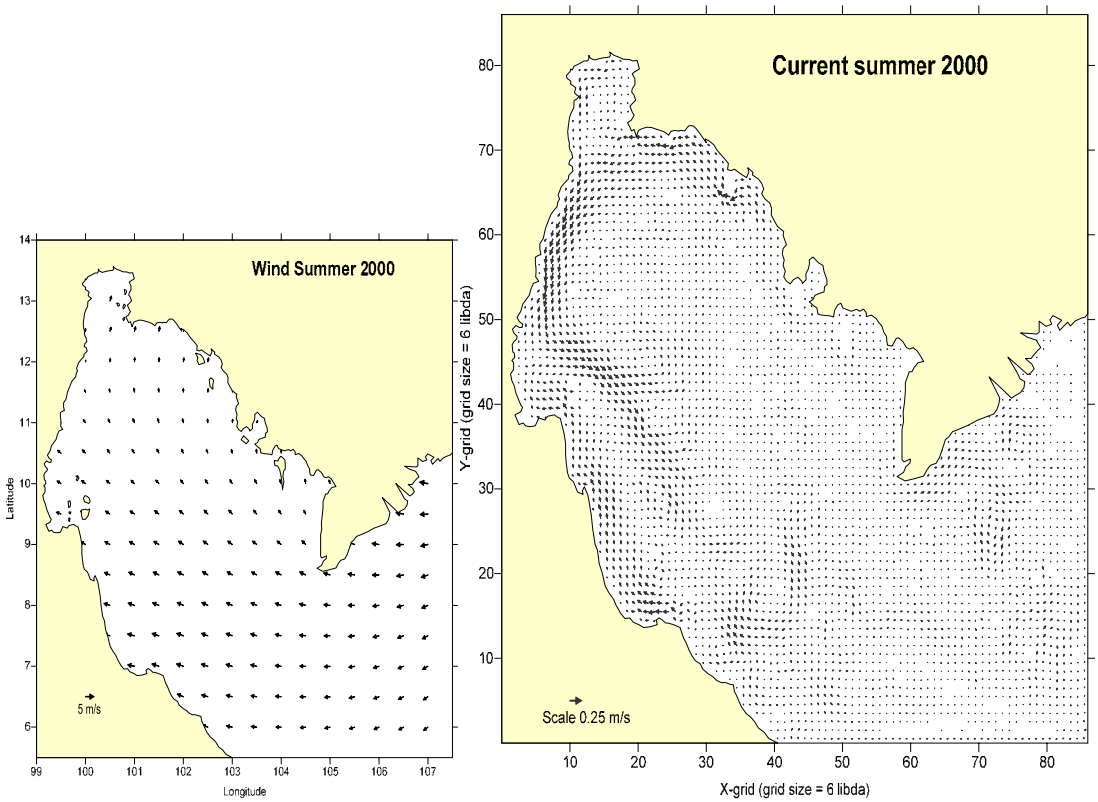

Figure 4-18 Simulated wind and wind-driven current in summer 2000.

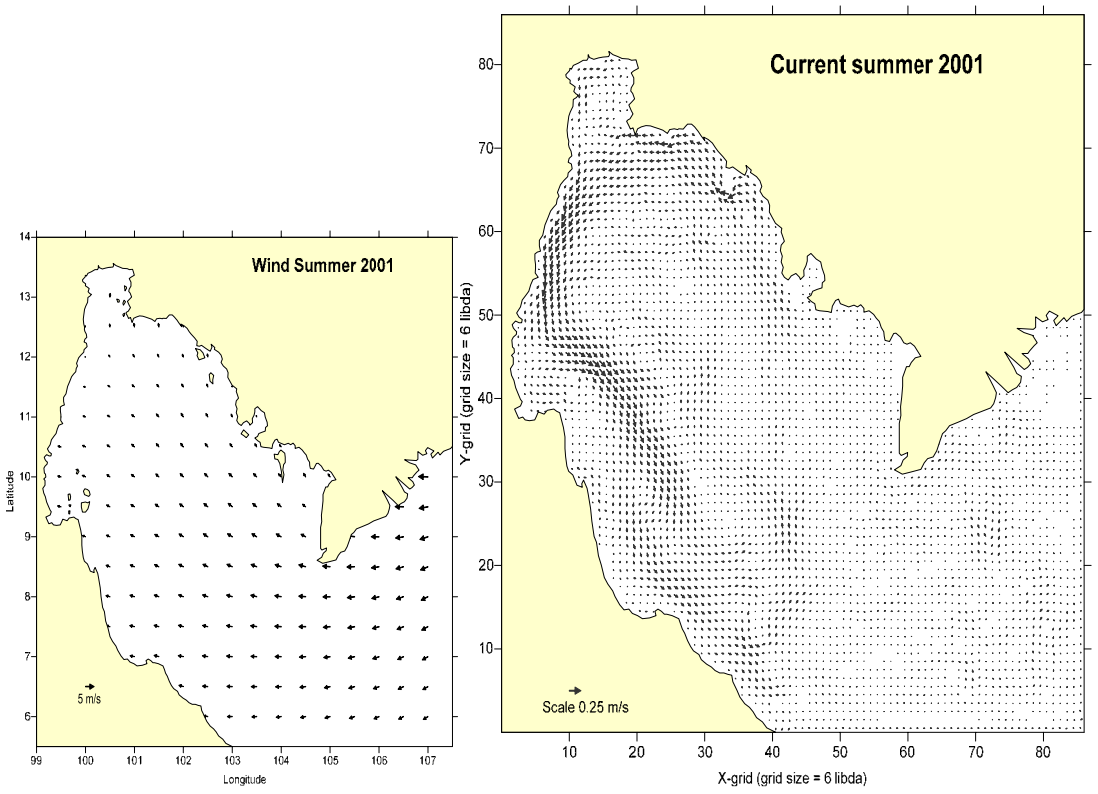

Figure 4-19 Simulated wind and wind-driven current in summer 2001.

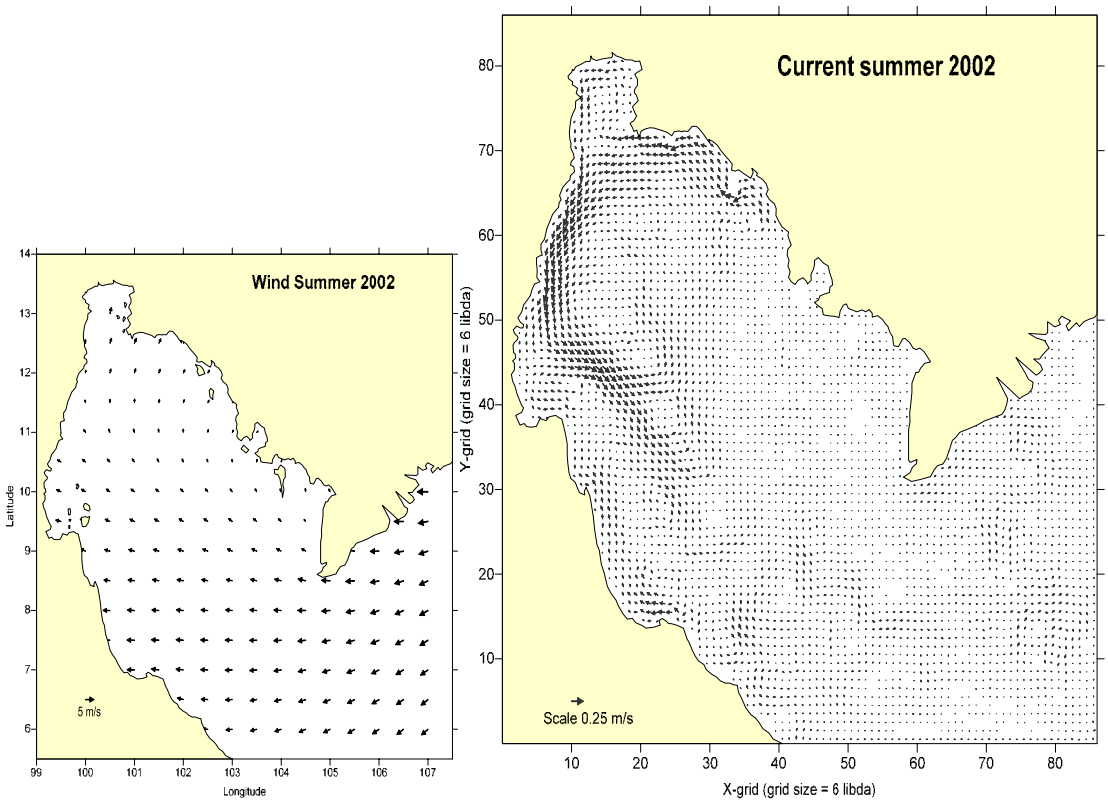

Figure 4-20 Simulated wind and wind-driven current in summer 2002.

During summer (March-April, Figure 4-18 – Figure 4-20), the E and SE surface wind caused the water in the Gulf of Thailand to move in a big CCW loop. The loop current started near Cambodia coast, than flowed northward and eastward along Thai eastern coast. The water mass crossed to the western coast and then flowed south along 40-m to 50-m depth contour to the gulf's entrance. Some water mass flowed in the upper gulf along the western coast to the inner gulf. Then the water mass turned south along the coast and reconnected with the CCW gyre along the western coast. The northward flow along the lower western coast of the gulf occurred only during summer 2000 and 2002 when the E wind near the western coast was a little bit strong. The change in water depth and protruding coast created localize CW and CCW eddies in the gulf.

Figure 4-18 – Figure 4-20 shows characteristics of seasonal wind and wind-driven current in summer 2001 and 2002. Both periods showed similar pattern, but the horizontal gradient of sea surface wind over Gulf of Thailand were different. During

2001, wind speeds on the eastern and western side of the gulf were having similar magnitude, while the wind speed on the eastern side during 2002 was stronger than that on the western side. Different seasonal wind speed on the western side of the gulf has produced different coastal circulation pattern along the western coast of the gulf. Figure 4-18 and 4-20 showed the strong northward along the western coast during the summer of 2000 and 2002 respectively, when the southeasterly and easterly wind was strong. The results of this study confirmed the finding of Buranapratheprat (2006) who studied the difference of wind horizontal gradients in the E-W and N-S directions over upper gulf and concluded that the circulation patterns in the gulf was controlled not only by wind direction but also by its gradient.

Booncherm, *et al*., (2001) also studied sea surface residual flow and water circulation in the Gulf of Thailand using data from oceanographic buoy network. He analyzed the current data from the upper gulf during 1996 and 1998 and the data from the lower gulf during 1993 and 1994.

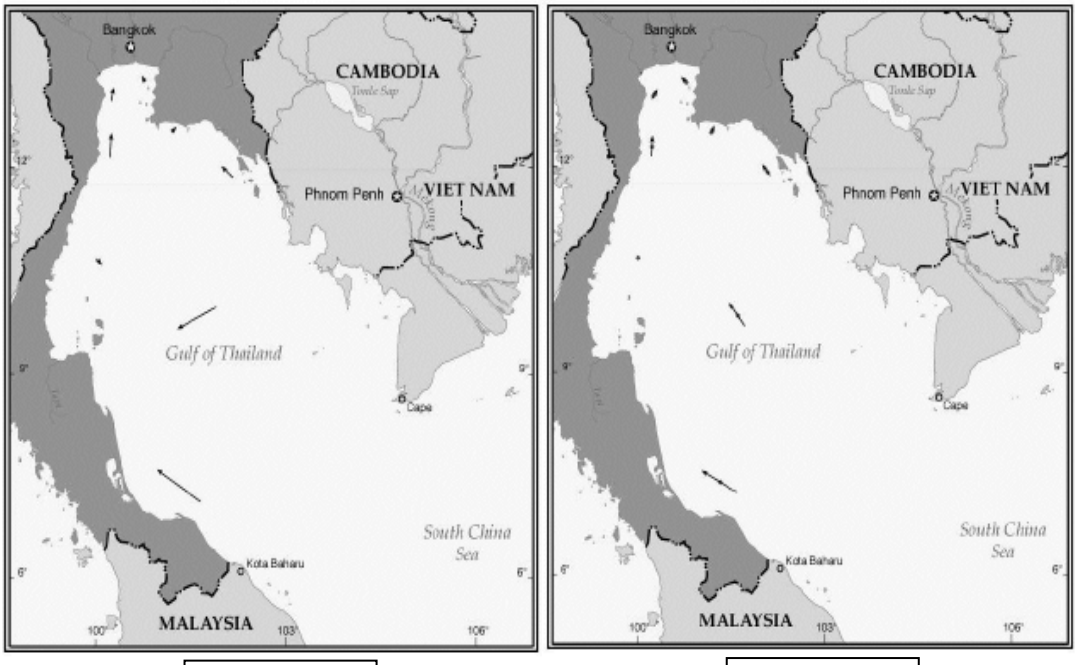

Figure 4-21 Vector charts show total annual average net surface currents in the Gulf of Thailand (March and April, Booncherm, *et al*., 2001).

The southeasterly and Southerly wind induced water near Cambodia coast to flow northward to the upper gulf then the water flowed in counterclockwise circulation over the Gulf of Thailand. Near the lower western coast of the gulf there was a northward flow along the coast. The simulation flow matched up with the average current vectors from the oceanographic buoy. But there was one contrast along the western part of the upper gulf, where the simulated flow and the current vectors from the buoys directed in the opposite way. The discrepancy in the flow direction might be that the simulated wind differed from the real wind.

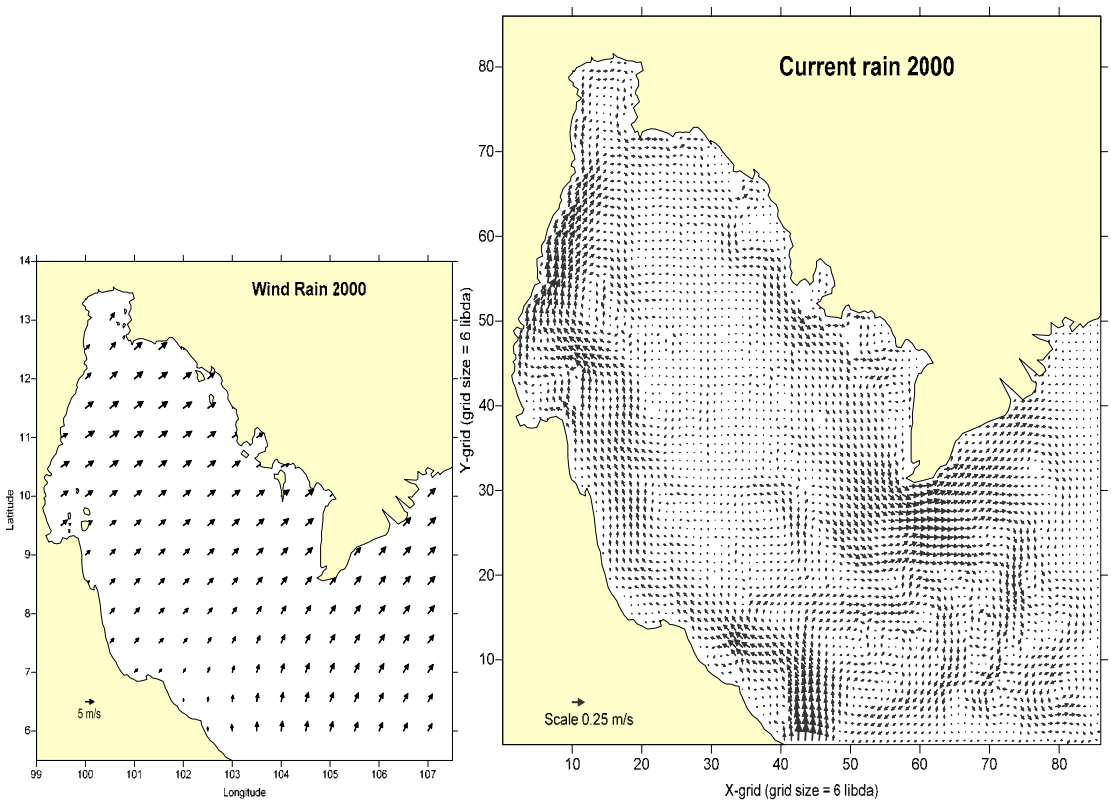

Figure 4-22 Simulated wind and wind-driven current in rainy season 2000.

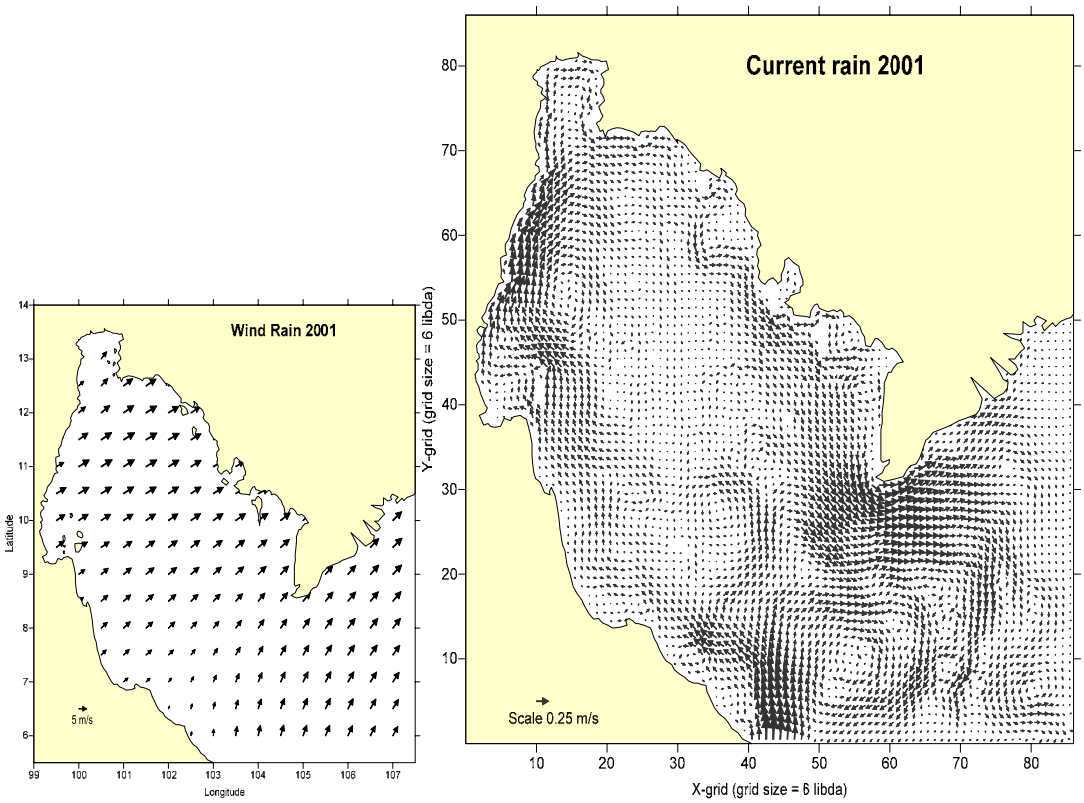

Figure 4-23 Simulated wind and wind-driven current in rainy season 2001.

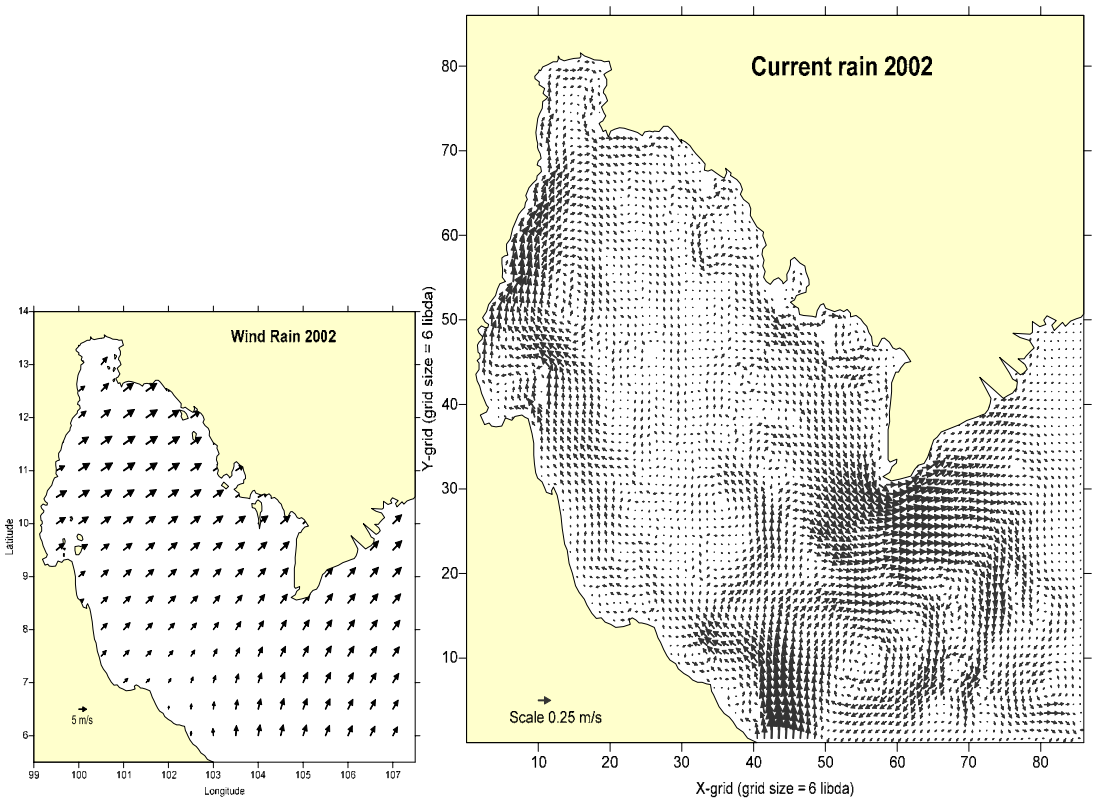

Figure 4-24 Simulated wind and wind-driven current in rainy season 2002.

During the rainy season (June-September, Figure 4-22 – Figure 4-24), the wind blew from W to SW directions and it created basin-wide CW loop in the GOT. The loop current started along the western coast of Malaysia, then move northward along the coast. The current turned right near the mouth of the upper GOT and then flowed along the gulf's eastern coast to the gulf's entrance. The water mass then flowed around Cape Camau and moved northward along Vietnam coast. The CW eddies at Latitude 6.5°, Longitude 104.5° and Latitude 10.5° and longitude 100.5° together with CCW eddy at Latitude 8°, Longitude 102.5° persisted in all 3 years. The CW loop also occurred in the upper GOT due to wind and may be induced by the bigger CW loop in the lower gulf.

Singhruck (2001) Study circulation features in the Gulf of Thailand inferred from SeaWiFS data during September 1996 to February 2001 was processed to images of chlorophyll_a concentration according to standard OC4 algorithm.

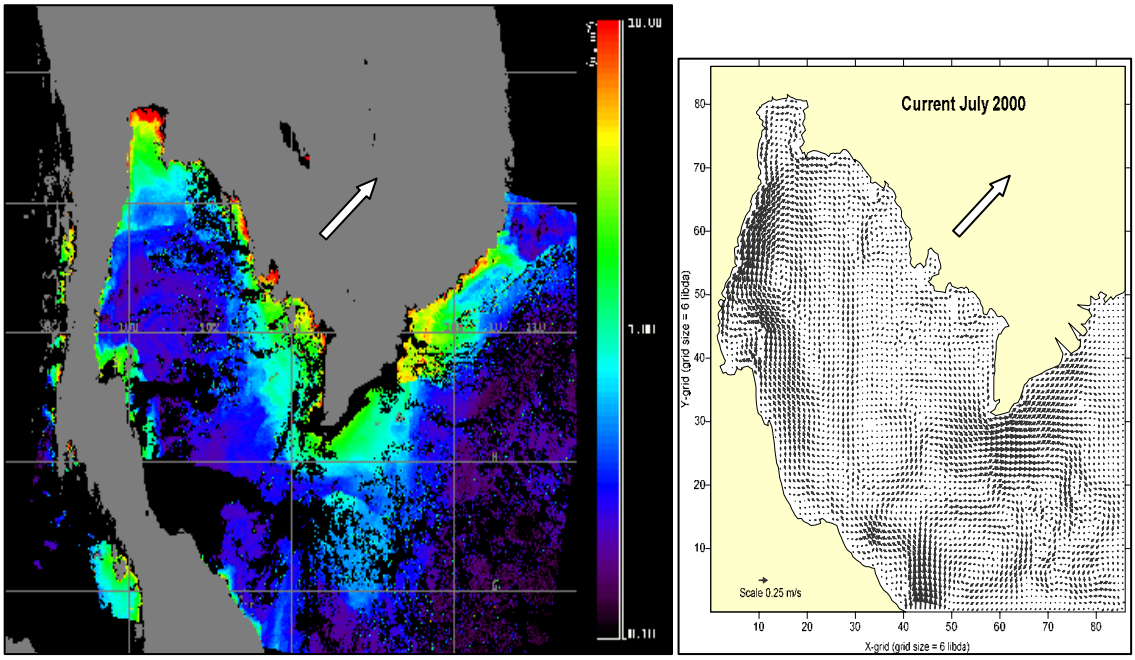

Figure 4-25 Image of chlorophyll_a concentration derived from SeaWiFS on 30 July 2000 (Singhruck, 2001). On the right is the simulated wind-driven current on July 2000 from our 2-D model (shown in appendix A). White arrows indicate wind direction.

Figure 4-25 indicated three areas of high chlorophyll_a concentration during July 2000; namely the upper gulf, the Cambodia coast and Vietnam eastern coast respectively. The upper gulf high chlorophyll_a moved to the eastern side by the SW wind. High chlorophyll_a near the Cambodia coast flowed to Cape Camau, and that at the Vietnam eastern coast flowed northward along the coast to the South China Sea. Distribution of the chlorophyll_a concentration suggested basin-wide CW circulation occurring in the upper gulf and the lower Gulf of Thailand. Our simulated wind-driven circulation for the same period confirmed the circulation pattern inferred from the chlorophyll_a concentration. The interaction of southwest wind with the coastline and topography could generate CW sea surface circulation in this season.

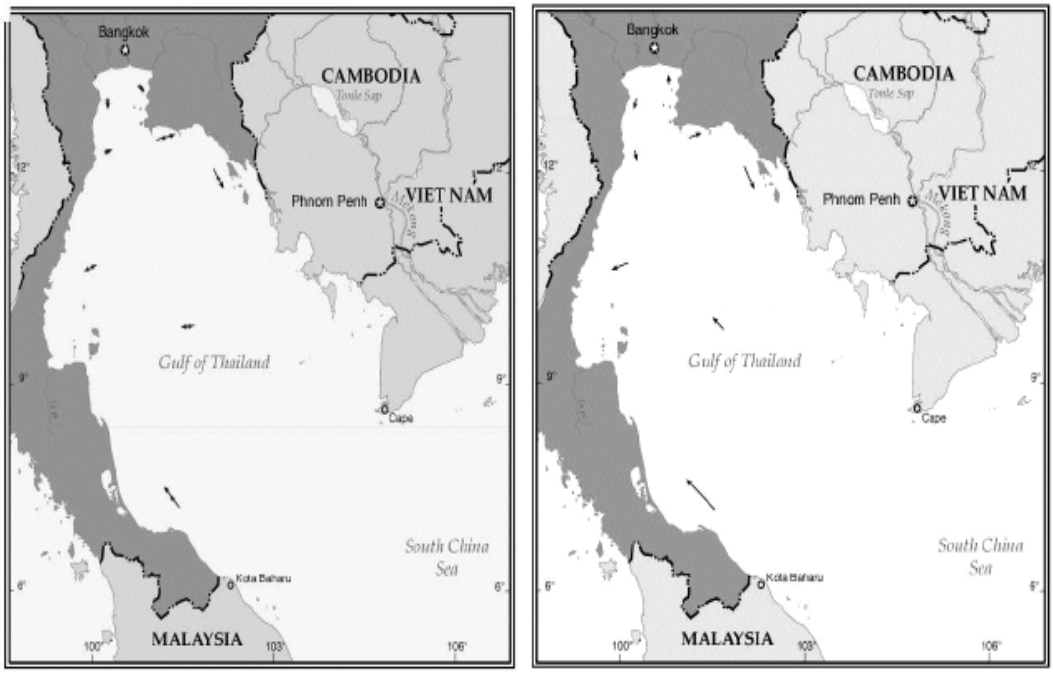

Figure 4-26 Vector charts show total annual average net surface currents in the Gulf of Thailand (June and July, Booncherm, *et al*., 2001).

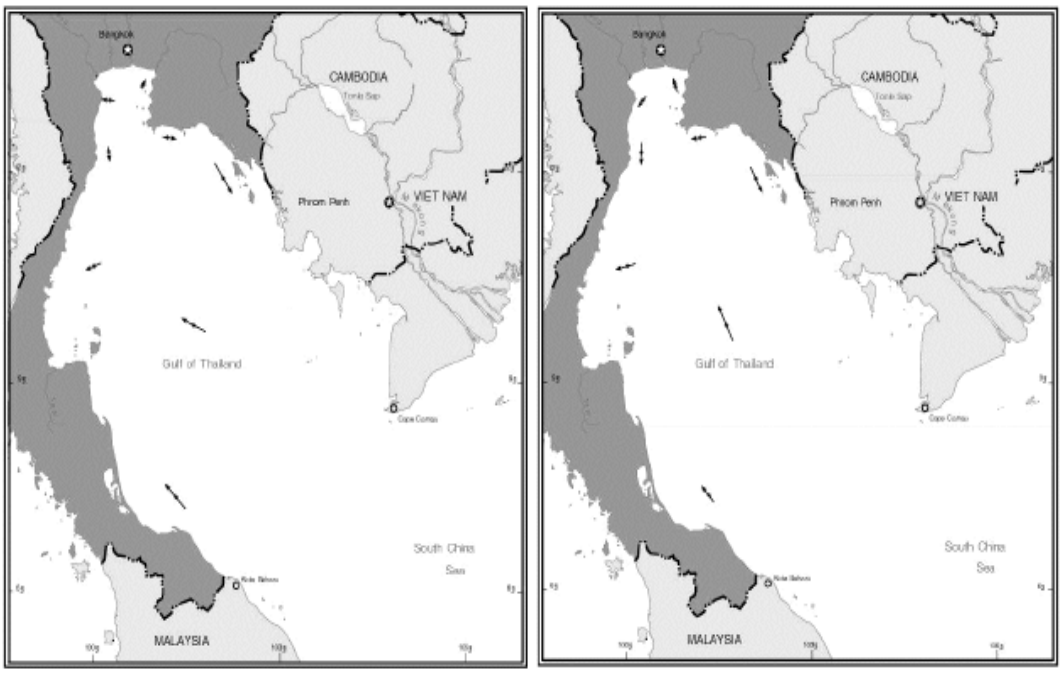

August September

Figure 4-27 Vector charts show total annual average net surface currents in the Gulf of Thailand (August and September, Booncherm, *et al*., 2001).

The Westerly and Southwesterly wind induced water near the coast of Malaysia to flow northward along the gulf's west coast. Then the water flowed in clockwise direction over the Gulf of Thailand. The pattern of the flow (Figure 4-22 – Figure 4-24) matched up with the average currents from oceanographic buoys. Contrast water circulation still existed in the upper gulf of Thailand (Figure 4-26 and 4-27).

Buranaprateprat (2006) tested the response of water circulation in the upper Gulf of Thailand to the E-W wind stress gradient. He concluded that when wind on the eastern side of the gulf was stronger than that on the western side, the CCW circulation would occur in the upper gulf. This happened during the SW monsoon (rainy) season. The difference in wind stress distribution together with river discharge from 4 major rivers in the upper gulf might give rise to the discrepancy of circulation pattern in the model from the buoy data.

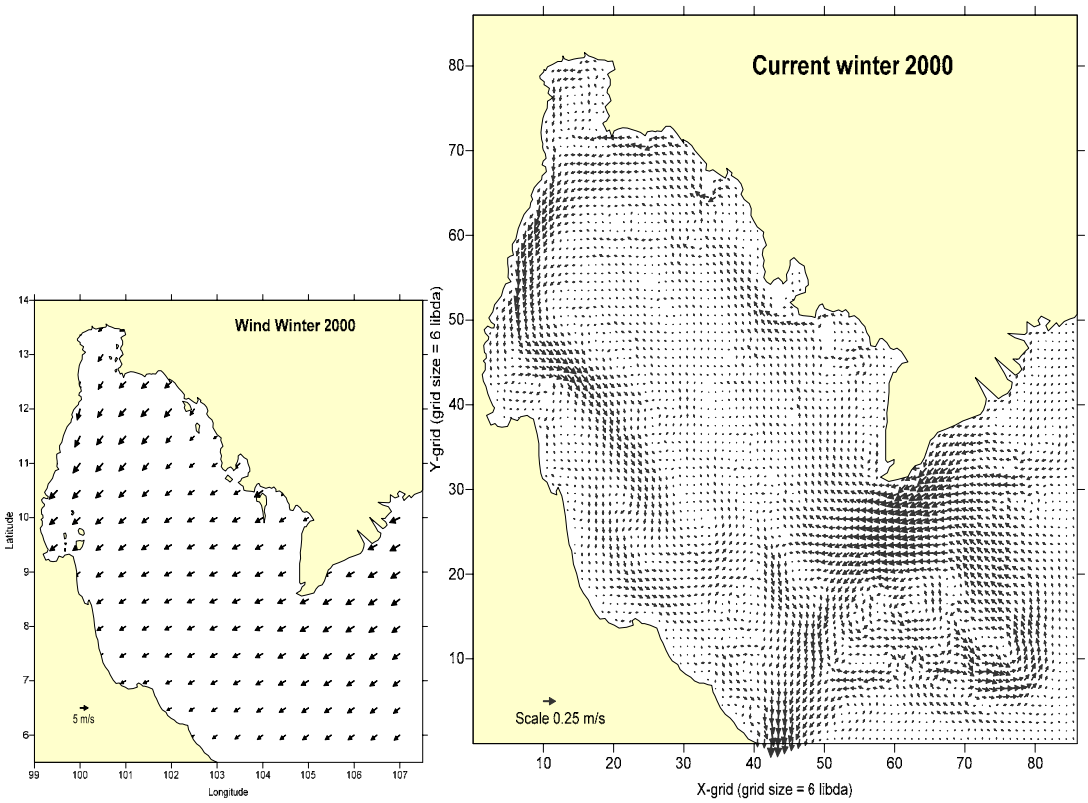

Figure 4-28 Simulated wind and wind-driven current in winter 2000.

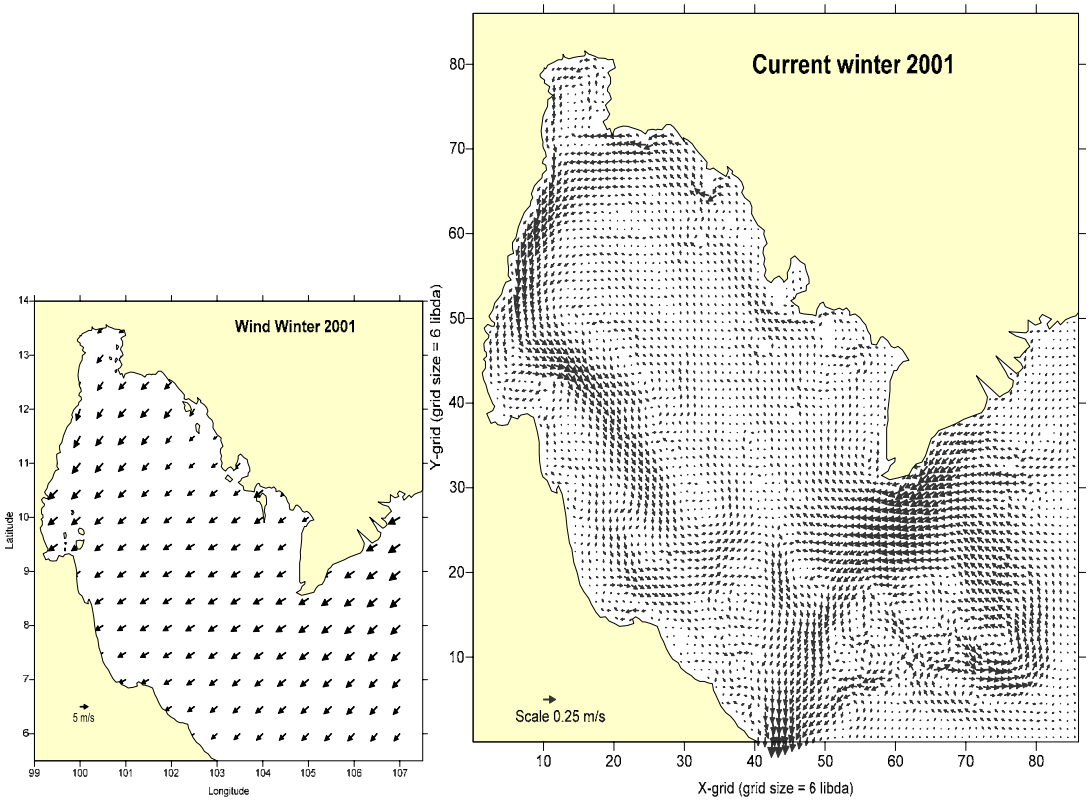

Figure 4-29 Simulated wind and wind-driven current in winter 2001.

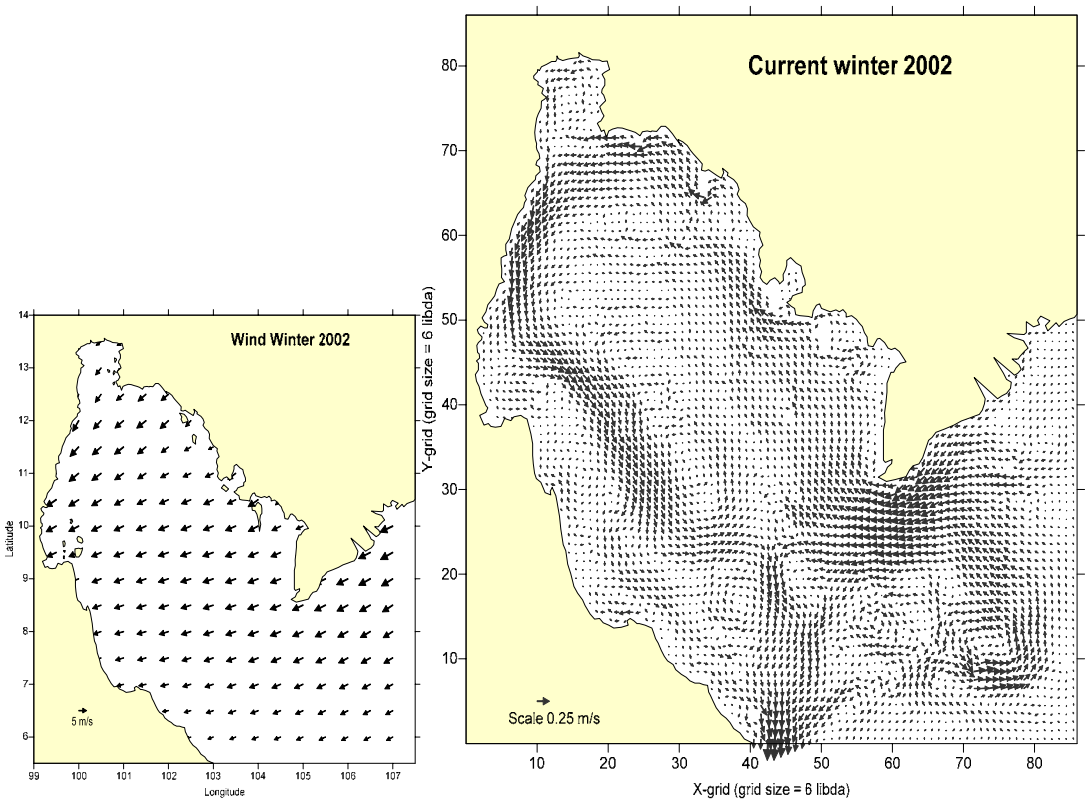

Figure 4-30 Simulated wind and wind-driven current in winter 2002.

During the winter (June-September, Figure 4-28 – Figure 4-30), the wind blew from NE to E directions and it created basin-wide CCW loop in the GOT. The loop current started from the water mass moving along the southern coast of Vietnam, and then entered the gulf on the eastern side. The current flowed along the gulf's east coast then turned left and south near the mouth of the upper GOT and then flowed along 40-m to 50-m depth contour along the gulf's western coast down to the gulf's entrance. CCW eddy and meander current from NE to SW direction also existed in front of the gulf entrance in all 3 years of study. The CW and CCW eddies also presented in the gulf. The northward flow along lower western coast occurred only in winter 2002 when NE wind change to E wind near the coast was blowing strong. The CCW loop also occurred in the upper GOT due to wind and may be induced by the bigger CCW loop in the lower gulf.

Figure 4-28 – Figure 4-30 showed basin-wide CCW circulation occurring in the lower gulf and the upper gulf during winter 2001-2002. Small CW and CCW eddies also presented in the lower gulf. The circulation pattern was confirmed by the study of Singhruk (2001). The simulated circulation pattern from this thesis matched nicely with the chlorophyll_a concentration pattern (see Figure 4-31).

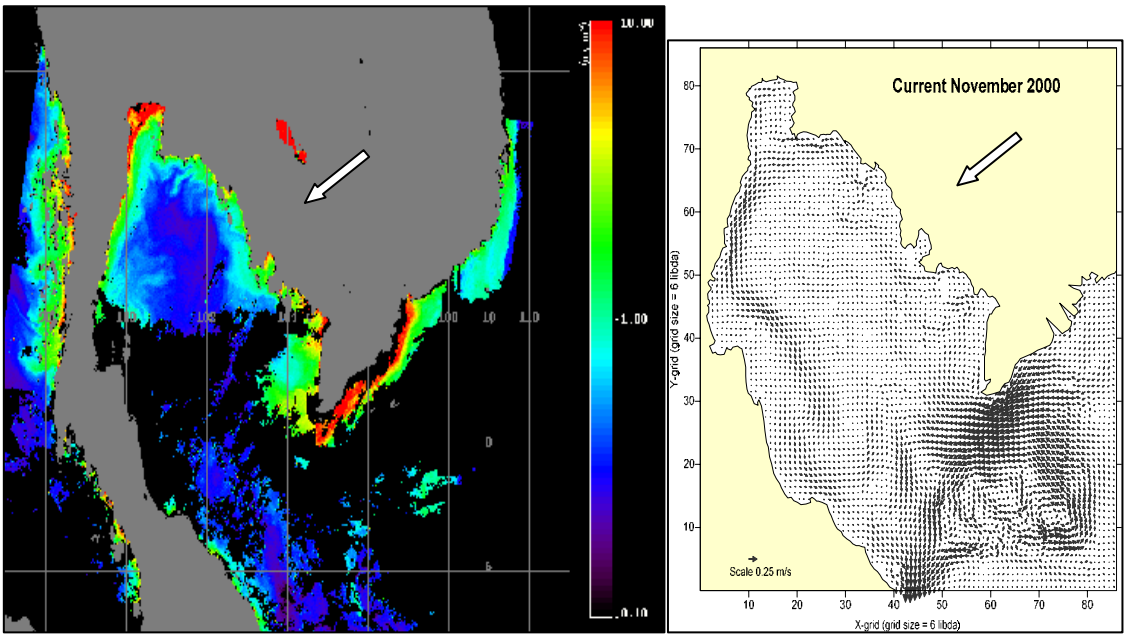

Figure 4-31 Image of chlorophyll_a concentration derived from SeaWiFS on 5November 2000 (Singhruck, 2001). On the right is the simulated wind-driven current for November 2000 from our 2-D model (shown in appendix A). White arrows indicate wind direction.

Singhruck (2001, see Figure 4-31) showed two areas where water exhibited high chlorophyll_a concentration; namely the upper gulf of Thailand and Cape Camau, while changes in Chlorophyll_a concentration corresponded to changes in prevailing wind directions. In the upper gulf of Thailand, high chlorophyll_a concentration travelled along the inner and along the western coasts. While near Cape Camau, high chlorophyll_a concentration was influenced by the Mekong River and this water mass flowed downward along the coast to the Gulf of Thailand. The chlorophyll_a pattern in these two areas indicated that the CCW circulation pattern should exist in the Gulf of

Thailand. The results from 2-D circulation model for November 2000 also confirmed the large-scale CCW circulation pattern occurring in the Gulf. The interaction of the NE wind with the coastline and topography could generate CCW sea surface circulation during this season.

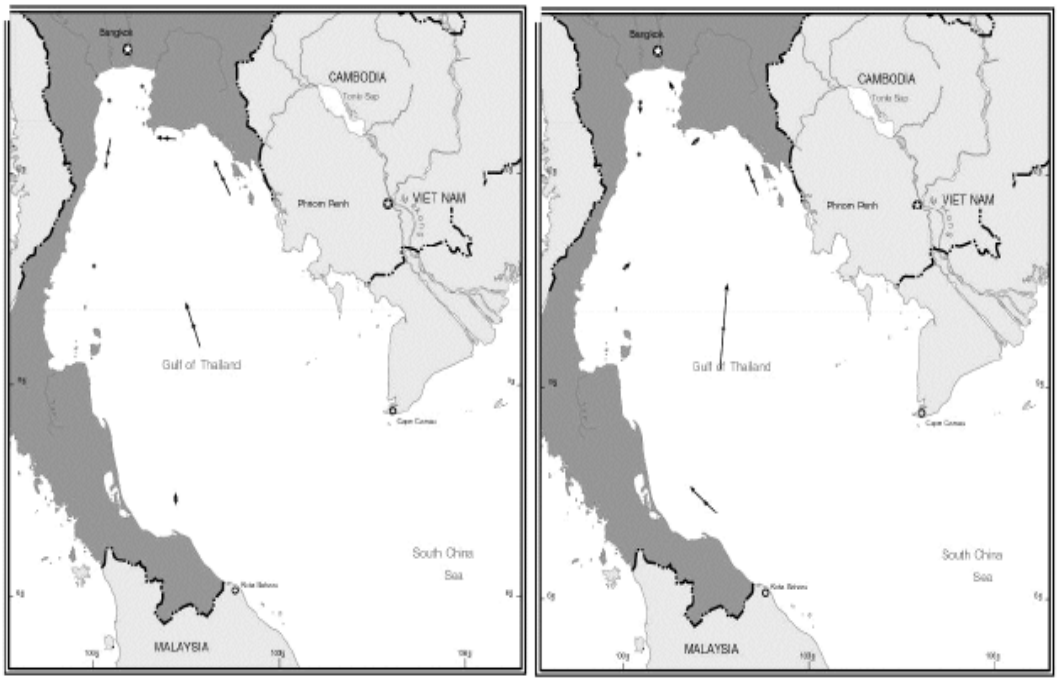

Figure 4-32 Vector charts showing total annual average net surface currents in the Gulf of Thailand (November and December, Booncherm, *et al*., 2001).

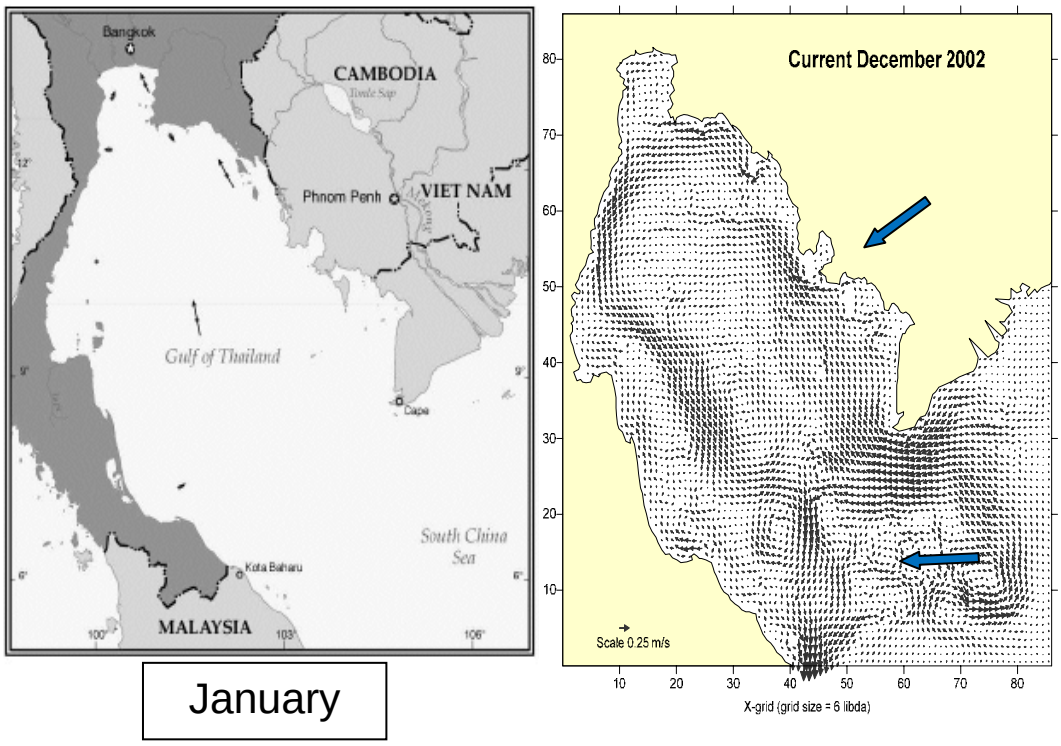

Figure 4-33 Vector charts showing total annual average net surface currents in the Gulf of Thailand (January, Booncherm, *et al*., 2001). On the right is the simulated wind-driven current for December 2000 from our 2-D model (shown in appendix A). Blue arrows indicate wind direction.

The pattern of the water circulation during winter was similar to that during summer, but the current was stronger due to stronger wind speed. Water flowed in a CCW direction in the Gulf of Thailand and in the upper gulf. The circulation in the upper gulf matched up with the data from the oceanographic buoy. In addition, the northward flow occurred along the lower western coast of the gulf in some months or years due to stronger E wind near the western coast. The data from the oceanographic buoy also indicated the existence of the northward (December) flow along the lower western coast (Booncherm, *et al*., 2001).

From the above discussion, the wind-driven circulation from this study was similar to the water circulation in the Gulf of Thailand derived from the oceanographic buoy data and the Chlorophyll_a distribution. Next, the results from this study will be compared with the numerical model results from other studies.

Lowwittayakorn (1998) used SEAWATCH 3D numerical model to simulate the tidal and wind-driven circulation in the Gulf of Thailand. He found clockwise circulation during the SW monsoon (rainy) season and anti-clockwise circulation during the NE monsoon (winter) season. The circulation patterns during the SW and NE monsoon seasons were similar to the circulation patterns from this study. But the circulation pattern was different during the summer period which might be due to differenced of wind forcing used in each study.

Aschariyaphotha (2008) used POM (Princeton Ocean Model) to simulate monthly wind-driven current in the Gulf of Thailand, using wind stress from the European Center for Medium-Range Weather Forecasts (ECMWF). The temperature and salinity fields were taken from Levitus94 data sets. And the climatologically monthly mean fresh water flux data was also used. Only the circulation pattern during the SW monsoon was similar to that of this study.

Sojisuporn (2010) simulated the geostrophic current in the Gulf of Thailand during 1995-2001 using the temperature and salinity data derived from the world ocean database, the monthly dynamic heights anomaly from TOPEX/Poseidon and the ERS-2 altimetry data. The circulation patterns in the gulf for each season were different from the results of this study. Only the meandering current at the mouth of the gulf was similar. One conclusion was that the geostrophic current in the gulf was not driven solely by wind, but the bathymetry, shape of the gulf and water density also influenced the geostrophic current in the gulf.

Idris and Mohd (2007) simulated tidal circulation in South China Sea including the Gulf of Thailand using the tidal amplitudes from co-tidal charts, the sea level anomaly and the wind speed from the Jason-1 satellite altimetry data. The circulation patterns in the gulf during the SW and NE monsoon were similar to the results of Sojisuporn (2010) study but different from the results of this study. Only the circulation pattern during summer was similar to the result of this study.

4.4 Effected of El Niño and La Niña to seasonal wind

Paired-difference Test or Paired Samples t-test or Two Related Samples t-test or paired t-test is used to test the mean of two samples that correlate to each other. In this case we will use the paired t-test to test the mean of wind speed and direction during the normal even with those during the El Niño or La Niña events. The t-test has been performed on both the satellite (observed) data and the WRF model (simulated) data. Results of t-test were given in Table 4-9. The wind characteristics varied from year to year regardless of the El Niño and La Niña events. Phuwieng (2000) stated that there is a tendency for higher pressure variation occurring during the El Niño event than during the normal year. On the other hand, less pressure variation occurs during the La Niña event.

During summer 2000-2002, the t-test results on observed and simulated data indicated that wind speed during the La Niña event (summer 2000) was weaker than that during the normal event (summer 2001), and wind direction during the La Niña event veered to the right (clockwise) from the normal event. On the other hand, the wind speed during the El Niño event (summer 2002) was stronger than that during the normal event (summer 2001) and the wind direction during the El Niño event veered to the left (anti-clockwise) of the normal event even though the t-test results were not conclusive (same direction for observed data .vs. different direction for simulated data). The test results for summer period implied that wind speed during the La Niña (El Niño) event would be weaker (stronger) than the normal event while wind direction during the La Niña (El Niño) event turned clockwise (anti-clockwise) from the normal event.

During rainy period (June-September) 2000-2002, the t-test results on observed and simulated data indicated that wind speed during the La Niña event (rain 2000) was weaker than that during the normal event (rain 2001). On the other hand, the wind speed during the El Niño event (rain 2002) was stronger than that during the normal event (rain 2001). The wind direction during both the La Niña and El Niño events veered to the left (anti-clockwise) from the normal event. The test results for rainy period implied that wind speed during the La Niña (El Niño) event would be weaker (stronger)

than the normal event while wind direction during both the La Niña and EL Niño event turned anti-clockwise from the normal event.

During winter period (November-February) 2000-2002, the t-test results on observed and simulated data indicated that wind speed during both the La Niña event (winter 2000) and the El Niño event (winter 2002) was weaker than that during the normal event (winter 2001). The wind direction during both the La Niña and El Niño events veered to the right (clockwise) from the normal event. The test results for winter period implied that the La Niña and El Niño event slowed down the NE monsoon wind and the wind direction during both the La Niña and El Niño events would turn clockwise from the normal event.

Summary from the t-test results was that the wind speed would be weaker than normal during the La Niña event and stronger than normal during the El Niño event. The exception occurred during winter when both the La Niña and El Niño events slowed down the NE monsoon wind. The wind direction turned clockwise or anti-clockwise due to the La Niña and El Niño events, though the angle difference was in the order of 0 to 10 degree.

Table 4-9 Paired t-test of observed wind speed and direction during 2000-2002.

Wind speed	Summer 2000/ 2001	Summer 2002/2001	Rainy 2000/2001	Rainy 2002/2001	Winter 2000/2001	Winter 2002/2001
t-test	-3.98	20.05	-49.16	48.97	-16.11	-5.01
Average	2.48/2.60	3.55/2.60	5.06/5.62	6.14/5.62	5.24/5.63	5.48/5.63
SD	0.51	0.75	0.18	0.17	0.38	0.47
Sig(2-tailed)	-1.65	1.65	-1.65	1.65	-1.65	-1.65
α	0.05	0.05	0.05	0.05	0.05	0.05
Wind direction	Summer 2000/ 2001	Summer 2002/2001	Rainy 2000/2001	Rainy 2002/2001	Winter 2000/2001	Winter 2002/2001
t-test	1.73	0.43	-38.80	-19.68	17.81	55.37
Average	127/120.5	120.6/120.5	238.4/244	237.8/244	58/50	65/50
SD	71.06	76.95	2.61	5.47	6.29	4.33
Sig(2-tailed)	1.65	1.65	-1.65	-1.65	1.65	1.65
α	0.05	0.05	0.05	0.05	0.05	0.05

Table 4-10 Paired t-test of simulated wind speed and direction during 2000-2002.

Wind speed	Summer 2000/ 2001	Summer 2002/2001	Rainy 2000/2001	Rainy 2002/2001	Winter 2000/2001	Winter 2002/2001
t-test	3.95	11.08	-38.54	10.28	-30.43	-1.43
Average	2.52/2.40	2.87/2.40	4.09/5.14	5.27/5.14	4.41/5.28	5.22/5.28
SD	0.48	0.67	0.43	0.20	0.45	0.70
Sig(2-tailed)	1.65	1.65	-1.65	1.65	-1.65	-1.65
α	0.05	0.05	0.05	0.05	0.05	0.05
Wind direction	Summer 2000/ 2001	Summer 2002/2001	Rainy 2000/2001	Rainy 2002/2001	Winter 2000/2001	Winter 2002/2001
t-test	14.12	7.04	-17.43	-24.63	8.30	29.52
Average	114.4/104.7	102.8/104.7	227.2/230	227.8/230	56.4/54	64/54
SD	15.86	30.71	3.06	2.03	4.34	5.15
Sig(2-tailed)	1.65	1.65	-1.65	-1.65	1.65	1.65
α	0.05	0.05	0.05	0.05	0.05	0.05

The study of El Niño and La Niña event on wind speed and direction were presented in Table 4-9 and Table 4-10. La Niña event occurred in year 2000 while El Niño event occurred in year 2002 and normal condition occurred in year 2001. The year 2000 and 2002 were not the year with strong La Niña or strong El Niño event respectively. Thus, solid conclusion cannot be reached. Special care is needed to select the month/season with strong El Niño / La Niña events so that we can see the difference in wind regime and wind-driven current under the El Niño / La Niña events.

CHAPTER V
CONCLUSION AND RECOMMENDATIONS

5.1 Conclusions

The tests with the WRF meteorological model were performed, aiming to evaluate the use of different physical options in the simulation of the near surface wind speed and direction. The different sets of parameterizations schemes regarding fixed boundary layer (SL, PBL and LSM) and radiation scheme (SW and LW) which deal with cumulus scheme and microphysics scheme were tests for winter season. The cumulus and microphysics parameterizations set composed by the schemes WSM6-class and Betts-Miller-Janjic were the one that gave better performance for winter season. This option was later used for summer and rainy seasons. The simulated seasonal wind agreed well with the observed (satellite) data. High deviation occurred during the summer season due to weaker wind speed and variable wind direction.

The seasonal wind from the WRF model gave similar pattern with the observed data with relationship R^2 = 0.37. The wind-driven current varied with seasonal wind pattern. The simulated wind-driven circulation conformed very well with the results from earlier studies.

Wind speed during summer during 2000-2002 (March-April) was rather weak with the average wind speed of 2.6 m/s. The wind direction varied between 80 to 180 degrees with the average of 107 degree. The main wind blew from South China Sea in the SE direction and gradually changed to S direction when it entered the Gulf of Thailand.

During the rainy season during 2000-2002 (June to September), the wind came from the SW direction (between 200-250 degrees with the average of 230 degree). The wind speed was quite strong with the average wind speed of 4.8 m/s.

During the winter season during 2000-2002 (November to January), the wind came from the NE direction (between 40-80 degrees with the average of 58 degree). The wind speed was quite strong with the average wind speed of 4.9 m/s.

The basin-wide CCW circulation occurred in the upper gulf and lower gulf during the winter season while the basin-wide CW circulation occurred during the rainy season. The CCW circulation also prevailed during summer, but the circulation was rather weak due to weaker wind.

Wind-driven circulation was salient in the Gulf of Thailand. The circulation pattern in the gulf was also controlled by the gulf's shape and topography. The wind-driven circulation was also influence by the El Niño – La Niña event.

The results of this study suggested that the sea surface wind curl plays a very important role in the determination of residual flow pattern in the Gulf of Thailand. We have to elucidate the detailed horizontal distribution of sea surface wind over the Gulf of Thailand in order to simulate the water circulation in the gulf.

5.2 Recommendations

This study simulated seasonal wind and wind-driven current. The results can be applied for other study such as oil spill dispersion.

Best atmospheric options should be determined for each season. Discharge, tidal forcing and density-driven current should be prescribed in the 2-D circulation model.

Optimum options from other study together with pre-selected schemes have been used with this study which might not give the best result for the Gulf of Thailand. Thus, WRF model experiments must be further performed using various schemes in order to come up with the best option for the area of study.

The circulation pattern in the upper Gulf of Thailand from this study did not conform to data from the oceanographic buoys. Fine-scale circulation model for the upper gulf must be implemented which might give real wind-driven circulation for the upper gulf.

This study used only 2-D circulation model. Since the water in the gulf is divided into 2 layers, the 3-D model would be better to produce the circulation pattern for each layer.

Influence of El Niño and La Nina effects on wind and circulation in the Gulf of Thailand was not conclusive. Further study should focus on time duration when strong El Niño and La Nina condition exist.

REFERENCES

Amnuaylojaroen, T.,and Kreasuwun, J., 2012.Investigation of fine and coarse particulate matter from burning area in Chiang Mai, Thailand using the WRF/CALPUFF. Chiang Mai Journal.39, 2: 311-326.

Aschariyaphotha, N., Wongwises, P., Wongwises, S., Humphries, U.W.,and Xiaobao, Y., 2008.Simulation of seasonal circulations and thermohaline variabilities in the Gulf of Thailand. Advances in atmospheric sciences, 25, 3: 489-506.

Australian Government. Southern Oscillation ndex (SOI). [Online]. http://www.bom.gov.au/climate/glossary/soi.shtml [2013, April 12]

Blumberg, A.F., 1977.Numerical tidal model of Chesapeake Bay. Journal of the Hydraulics Division, Proceedings of the American Society of Civil Engineers, 103(HY1):1-10.

Booncherm, C., Vongpintu, V.,and Nutpramoon, R., 2001.The characteristic of the sea surface residual flow and the circulation in the Gulf of Thailand from the long term collected data of the SEAWATCH Thailand program. Proceedings of the 39th Kasetsart University Annual Conference: Science, Natural Resources and Environmental Economics, Bangkok (Thailand), 39: 315-325.

Buranapratheprat, A.,and Bunpapong, M., 1998.A two dimensional hydrodynamic model for The Gulf of Thailand. Proceedings of the IOC/WESTPAC Fourth International Scientific Symposium, 469-478.

Buranapratheprat, A., Yanagi, T.,and Sawangwong, P.,2002.Seasonal variations in circulation and salinity distributions in the gulf upper of Thailand: Modeling Approach. La mer, 40: 147-155.

Buranapratheprat, A., Yanagi, T., Sojisuporn, P.,and Booncherm, C., 2006.Influence of local wind field on seasonal circulations in the upper Gulf of Thailand. Coastal Marine Science, 30, 1: 19 - 26.

Buranapratheprat, A., 2008.Circulation in the upper Gulf of Thailand: a review. Burapha Science Journal, 13, 1: 75 - 83.

Buranapratheprat, A., Niemann, K.O., Yanagi, T., Matsumura, S.,and Sojisuporn, P., 2009.Circulation in the Upper Gulf of Thailand Investigated using a three-dimensional Hydrodynamic Model. Burapha Science Journal, 14, 1: 99-113.

Buranapratheprat, A., Niemann, K.O., Matsumura, S.,and Yanagi, T., 2009.Meris imageries to investigate surface chlorophyll in the upper gulf of Thailand. Coastal Marine Science, 33, 1:000-000.

Carvalho, D., Rocha, A., Gomez-Gesteira, M.,and Santos, C., 2012.A sensitivity study of the WRF model in wind simulation for an area of high wind energy. Environmental Modeling & Software, 33: 23-24.

Chotamonsak, C., Salathe, E.P., Kreasuwan, J.,and Chantara, S., 2012.Evaluation of Precipitation simulations over Thailand using a WRF regional Climate model. Chiang Mai Journal.39, 4: 623-638.

Danielson E. W., Levin, J.,and Abrams, E. Meteorology. 2nd ed. Kemp: Margaret, J. Publisher; 2003.

"El Niño-La Niña". [Online].Available from: http://www.physicalgeography.net/fundamentals/7z.html [2012, August 2]

Emery, C. *et al*., 2001.Enhanced Meteorological Modeling and Performance Evaluation for Two Texas Ozone Episodes, Environ, International Corporation.

Idris, N.H., and Mohd, M.L.S., 2007.Total sea surface current circulation pattern in the South China Sea derived from satellite altimetry.Asian Conference on Remote Sensing, Kuala Lumper Malaysia, PWTC: (12-17 November 2007).

Jutakorn, J., 2010. El Nino and La Nina phenomenon effected on southwest monsoon in Thailand. Meteorological Department Weather report, No.551.577.

Kwun, H. J., Kim, Y.K., Seo, J.W.,and Jeong, J.H., 2009.Sensitivity experiments of winds prediction with planetary boundary layer parameterizations. Scientific and Technical Symposium on Storm Surge, COREE, 51: 63-77.

Menendez, F.J. *et al*., 2012. Using WRF to generate high resolution offshore wind climatolocies. Climate dynamics, 85-91.

Manomaiphiboon, K., 2009. Performance of wind resource prediction by a Mesoscale Meteorological Model for selected four areas in Thailand.7th Eco-Energy and Materials Science and Engineering Symposium, Chiang Mai, Thailand, 7: (17-20 November).

Mesoscale and Microscale Meteorology Division of NCAR. WRF model. [Online]. Available from: http://www.mmm.ucar.edu/wrf/users/ [2011, April 26]

Papanastasiou, D.K., Melas, D., and Lissaridis, I., 2010.Study of wind field under sea breeze conditions; an application of WRF model. Atmospheric Research, 98: 102-117.

Phaksopa, J., and Sojisuporn, P., 2006.Storm Surge in the Gulf of Thailand Generated by Typhoon Linda in 1997 Using Princeton Ocean Model (POM).Kasetsart journal. (Nat. Sci.) 40: 260-268.

Phuwieng Prakhammintara, 2000. Impacts of ENSO on rainfall, temperature and tropical cyclone frequency in coastal areas of Thailand. Master's Thesis, Department of Marine Science, Faculty of Science, Chulalongkorn University. 132pp.

Phuwieng Prakhammintara, 2007.Correlation between heat flux, moisture and wind pattern over the Indian Ocean and southwest monsoon intensity in Thailand by using MM5 numerical model. Doctoral dissertation, Department of Marine Science, Faculty of Science, Chulalongkorn University. 140pp.

Qi, Y., Zhang, Z.,and Shi, P.,2010.Extreme wind, wave and current in deep water of South China Sea. The International Society of Offshore and Polar Engineers, 20, 1: 18-23.

Singharuck, P., 2001. Circulation features in the Gulf of Thailand inferred from SeaWiFS data. The Asian Conference on Remote Sensing, 22: (5-9 November 2001), Singapore.

Singharuck, P., 2002. Numerical modeling of eddies in the Gulf of Thailand comparing with satellite remote sensing data. Doctoral dissertation, Department of Marine Science, Faculty of Science, Chulalongkorn University. 94 pp.

Snidvongs, A.,and Sojisuporn, P., 1997.Numerical simulation of the net circulation in the Gulf of Thailand under different monsoon regimes. In Proceeding of the first Technical Seminar on marine fishery resources survey in the South China Sea, Area I: Gulf of Thailand and Peninsular Malaysia, Samutprakarn, Thailand: Training Department, Southeast Asia Fisheries Development Center, 1: 54-72.

Sojisuporn, P., Morimoto, A.,and Yanagi, T., 2010.Seasonal variation of sea surface current in The Gulf of Thailand. Coastal Marine Science, 34, 1: 000-000, 2010.

Somyod Lowwittayakorn, 1998. Analysis of sea surface temperature and salinity from oceanographic buoys with circulation patterns in the Gulf of Thailand from mathematical model. Master's Thesis, Department of Marine Science, Faculty of Science, Chulalongkorn University. 137pp.

"Tidal current". [Online]. Available from: http://msi.nga.mil/MSISiteContent/StaticFiles/NAV_PUBS/APN/Chapt-09.pdf [2012, May 17]

"Wind-driven current". [Online]. Available from: http://www.tpub.com/weather1/6m.htm and http://www.ehow.com/how-does_4685844_what-causes-winddriven-currents.html [2012, January 24]

Yanagi, T.,and Takao, T., 1998.Seasonal variation of three-dimensional circulations in the Gulf of Thailand. La mer, 36: 43-55.

Yanagi, T., Sachoemar, I. S., Takao, T.,and Fujiwara, S., 2001.Seasonal variation of stratification in the Gulf of Thailand. Journal of Oceanography, 57: 461-470.

APPENDICES

Appendix A

Results of Monthly mean simulated wind and wind-driven current over the Gulf of Thailand

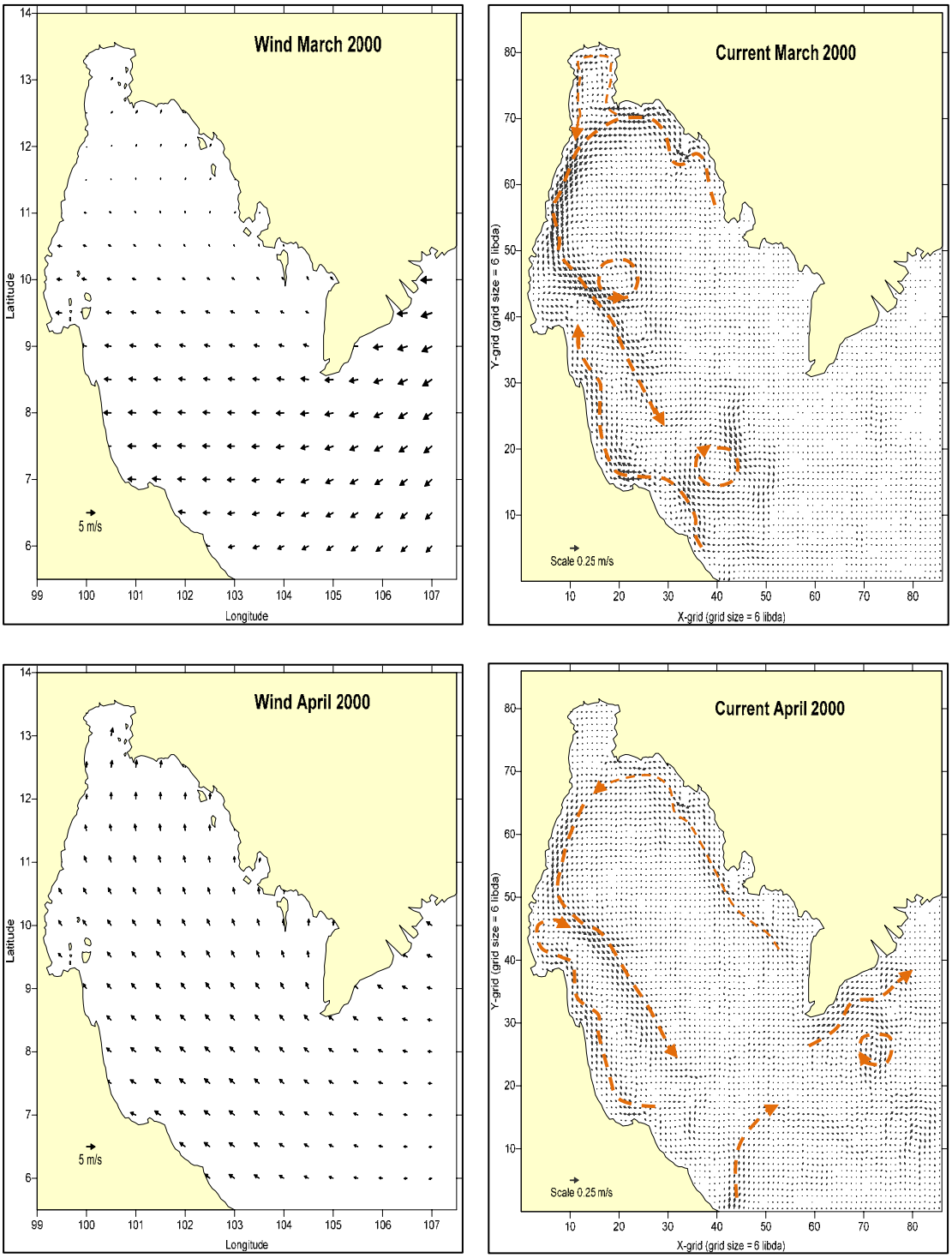

Monthly mean simulated wind and wind-driven current over the Gulf of Thailand in March and April 2000.

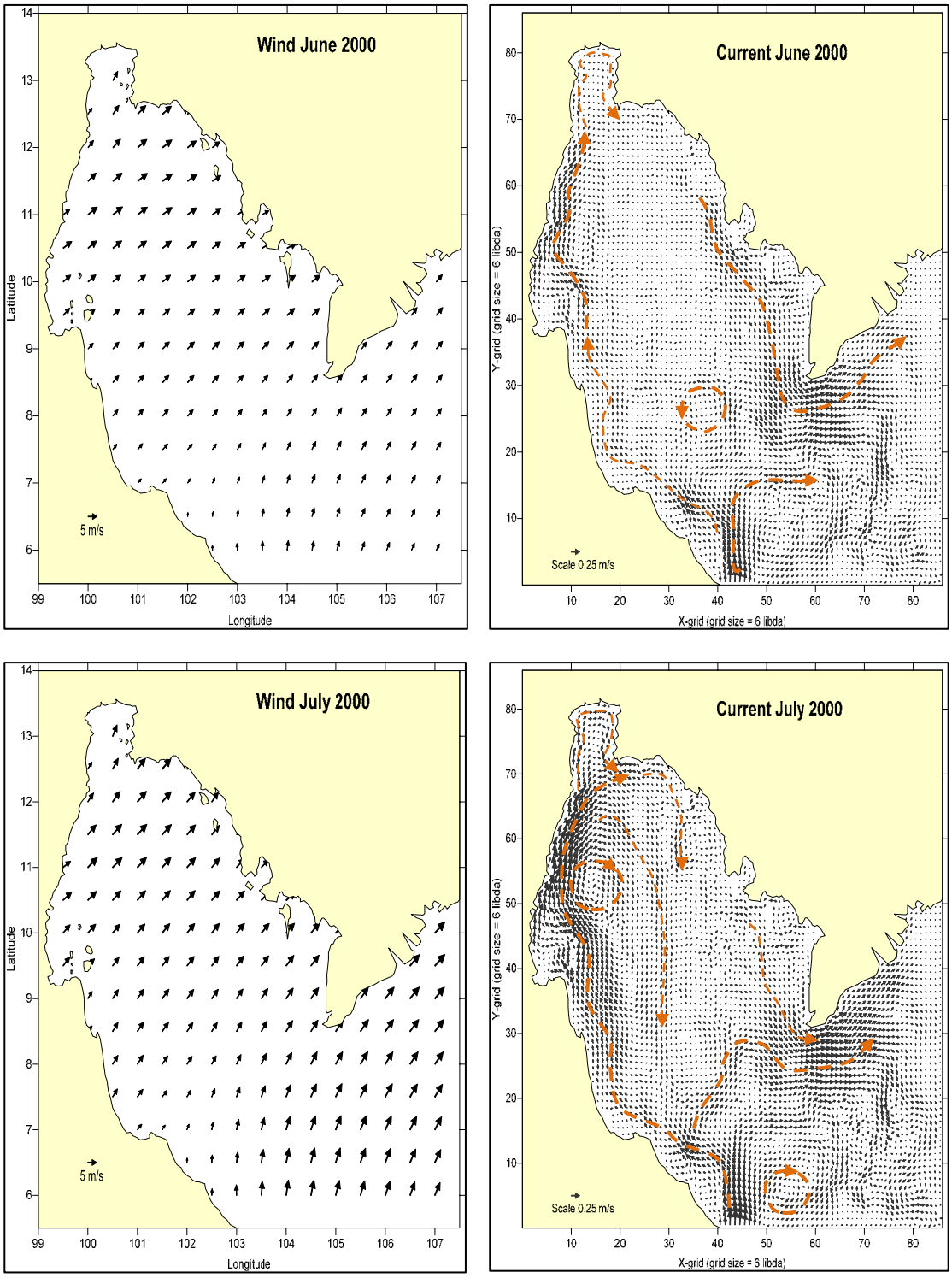

Monthly mean simulated wind and wind-driven current over the Gulf of Thailand in June and July 2000.

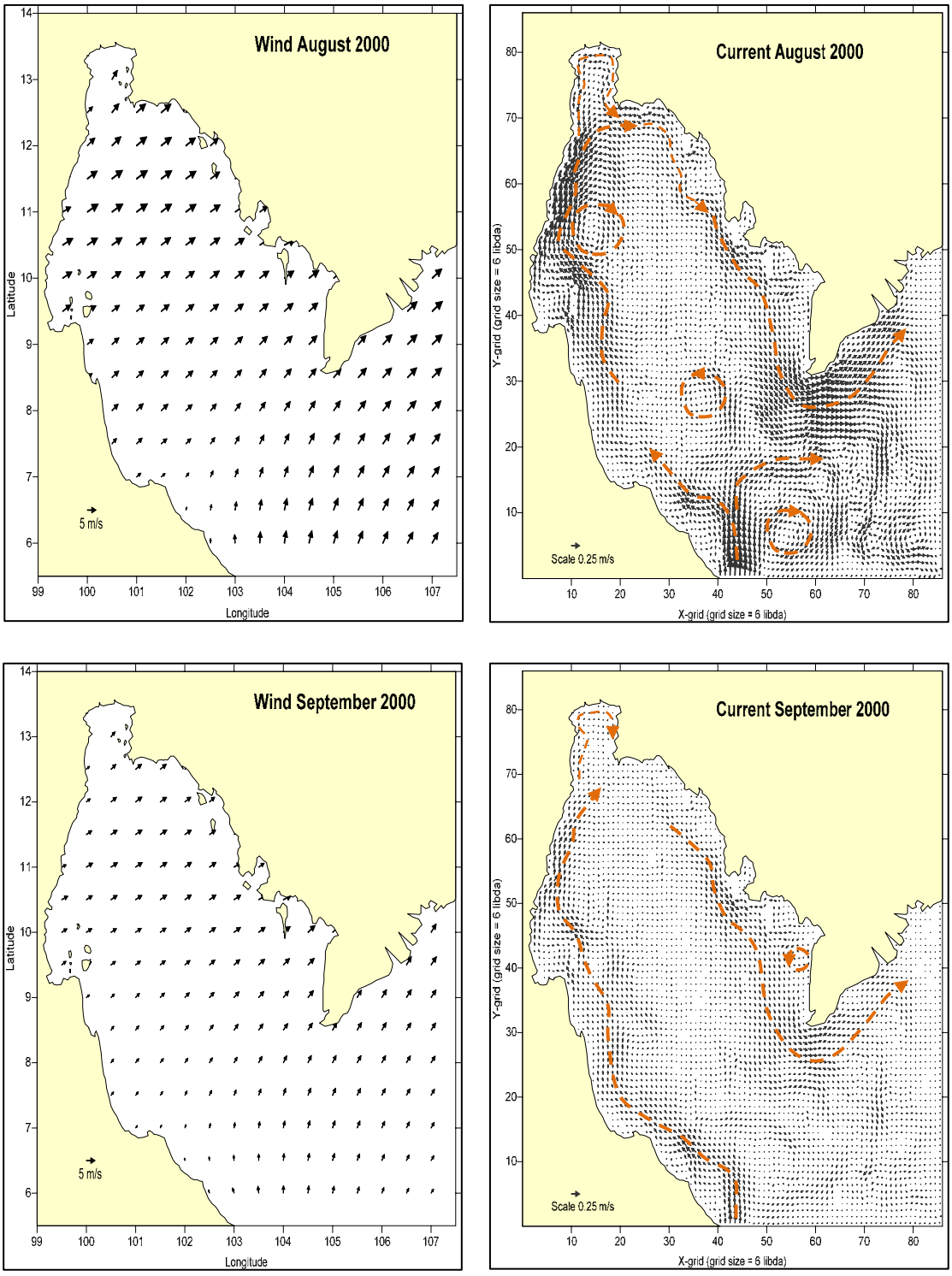

Monthly mean simulated wind and wind-driven current over the Gulf of Thailand in August and September 2000.

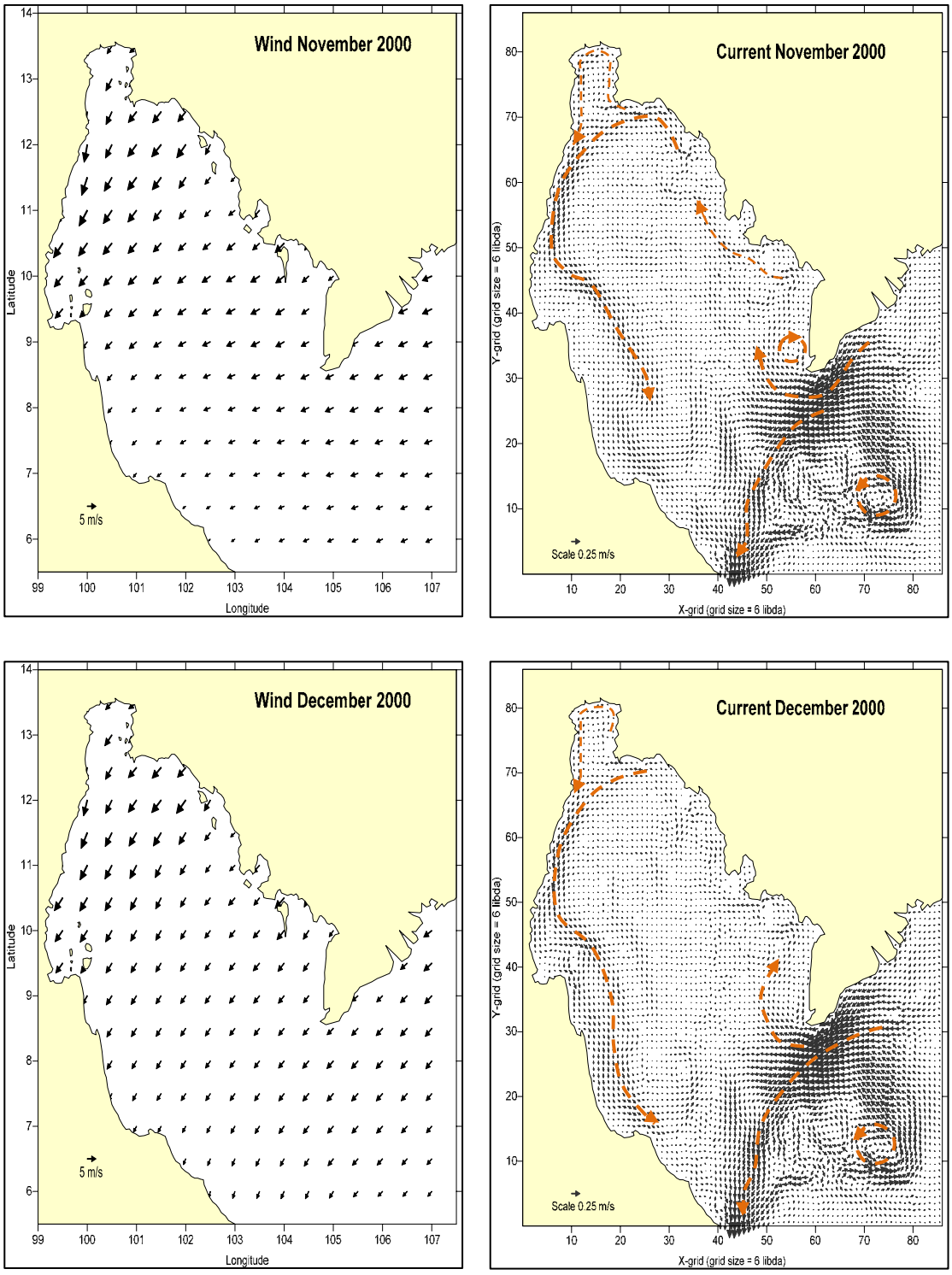

Monthly mean simulated wind and wind-driven current over the Gulf of Thailand in November and December 2000.

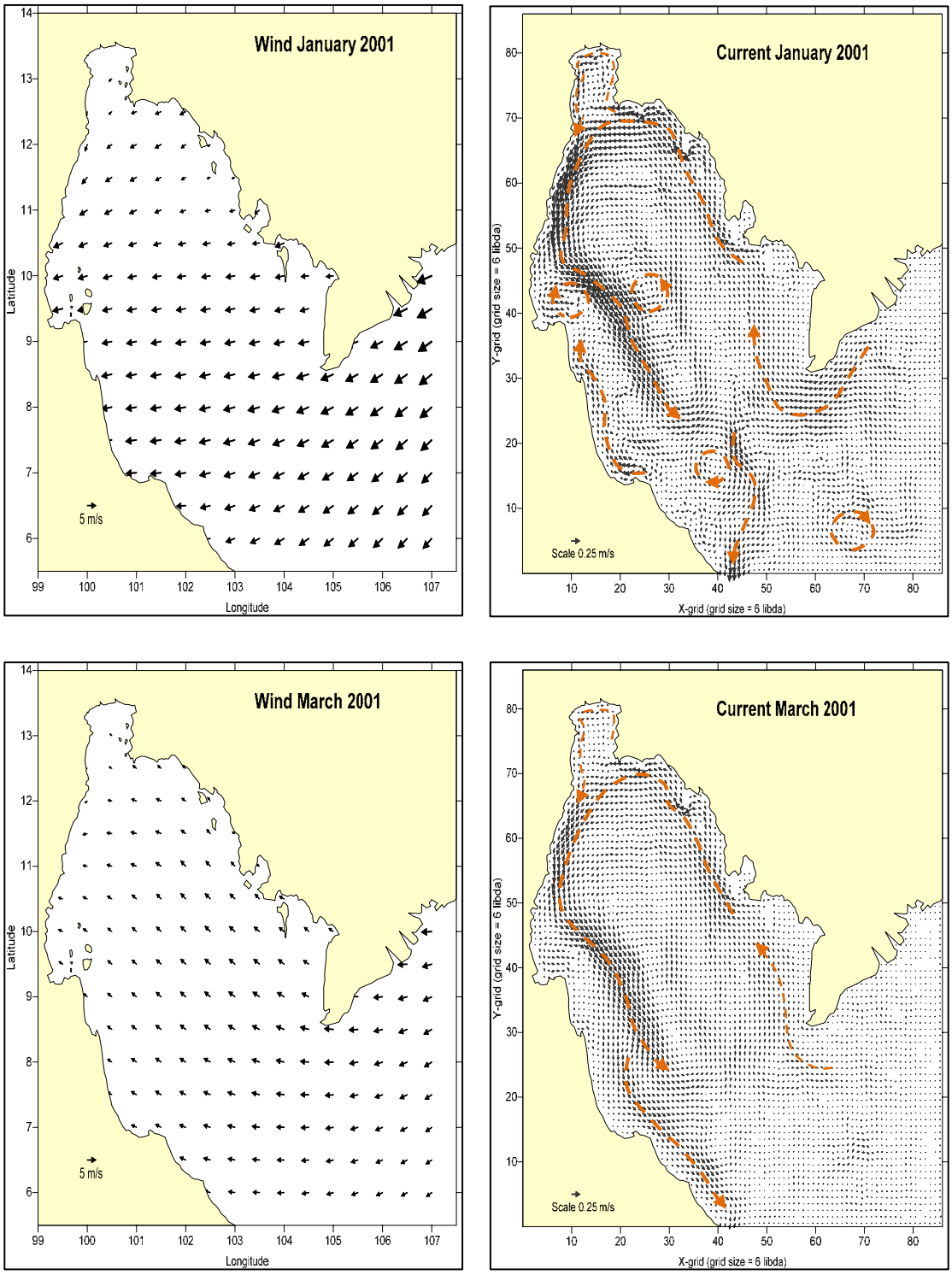

Monthly mean simulated wind and wind-driven current over the Gulf of Thailand in January and March 2001.

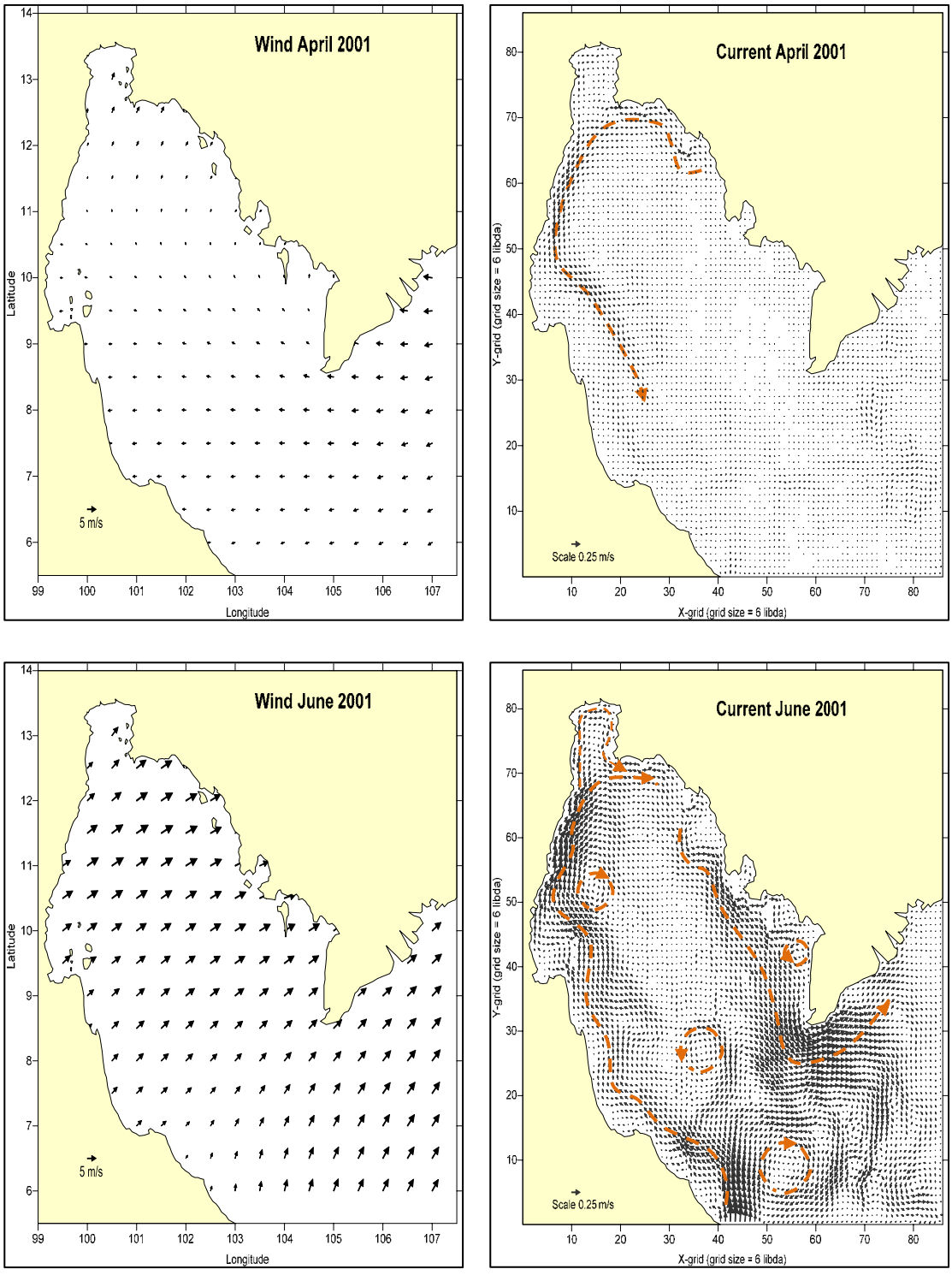

Monthly mean simulated wind and wind-driven current over the Gulf of Thailand in April and June 2001.

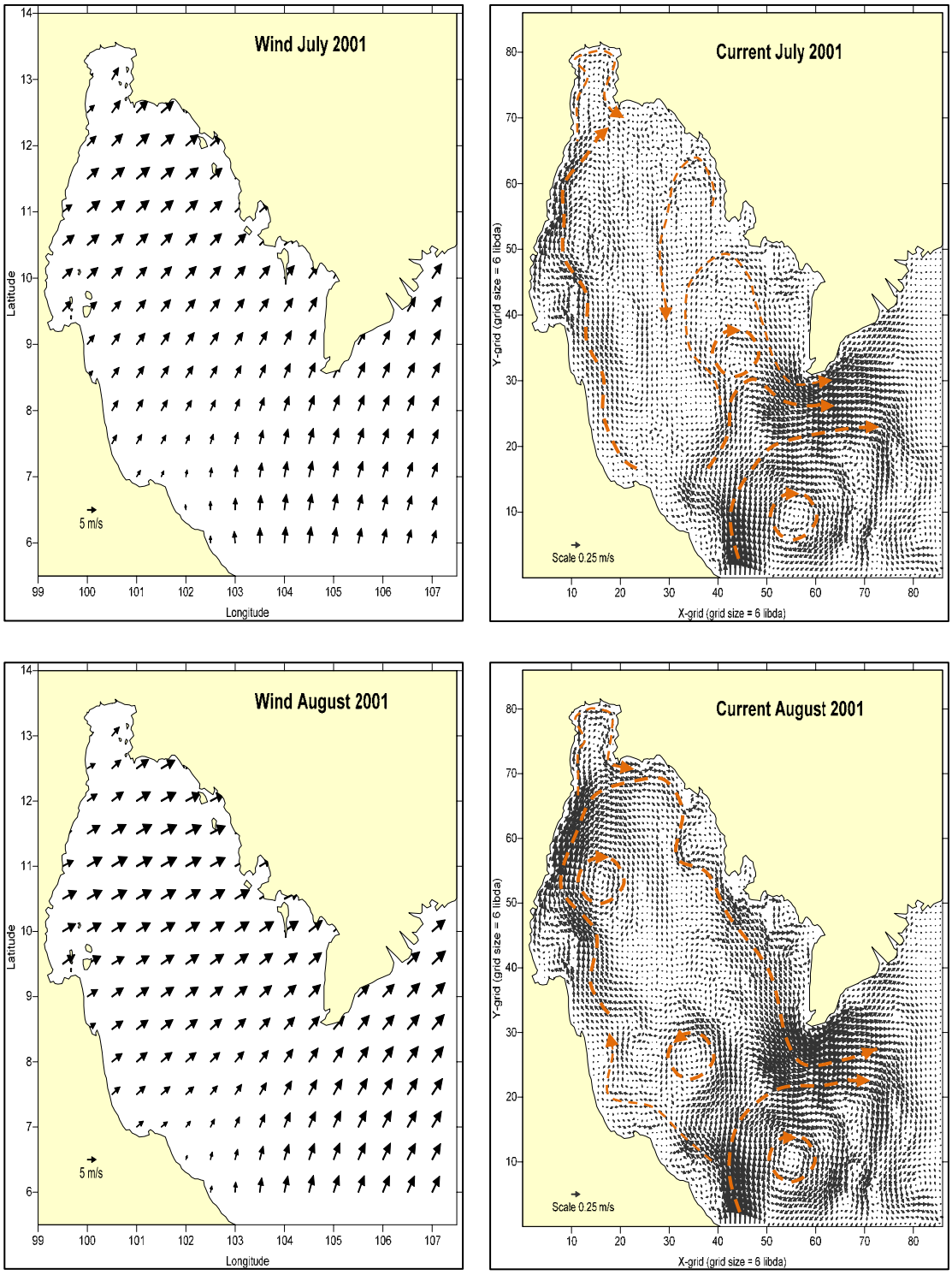

Monthly mean simulated wind and wind-driven current over the Gulf of Thailand in July and August 2001.

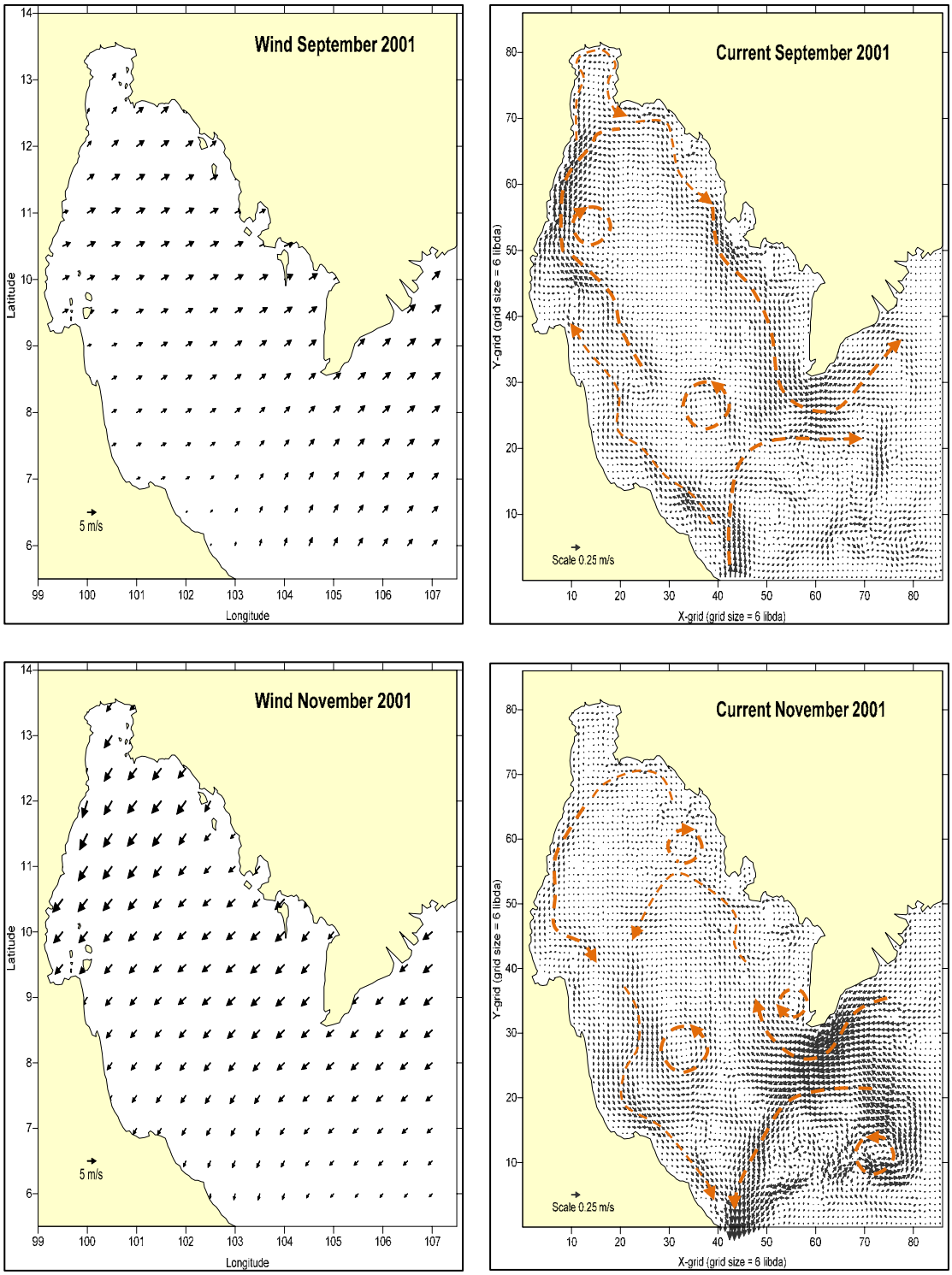

Monthly mean simulated wind and wind-driven current over the Gulf of Thailand in September and November 2001.

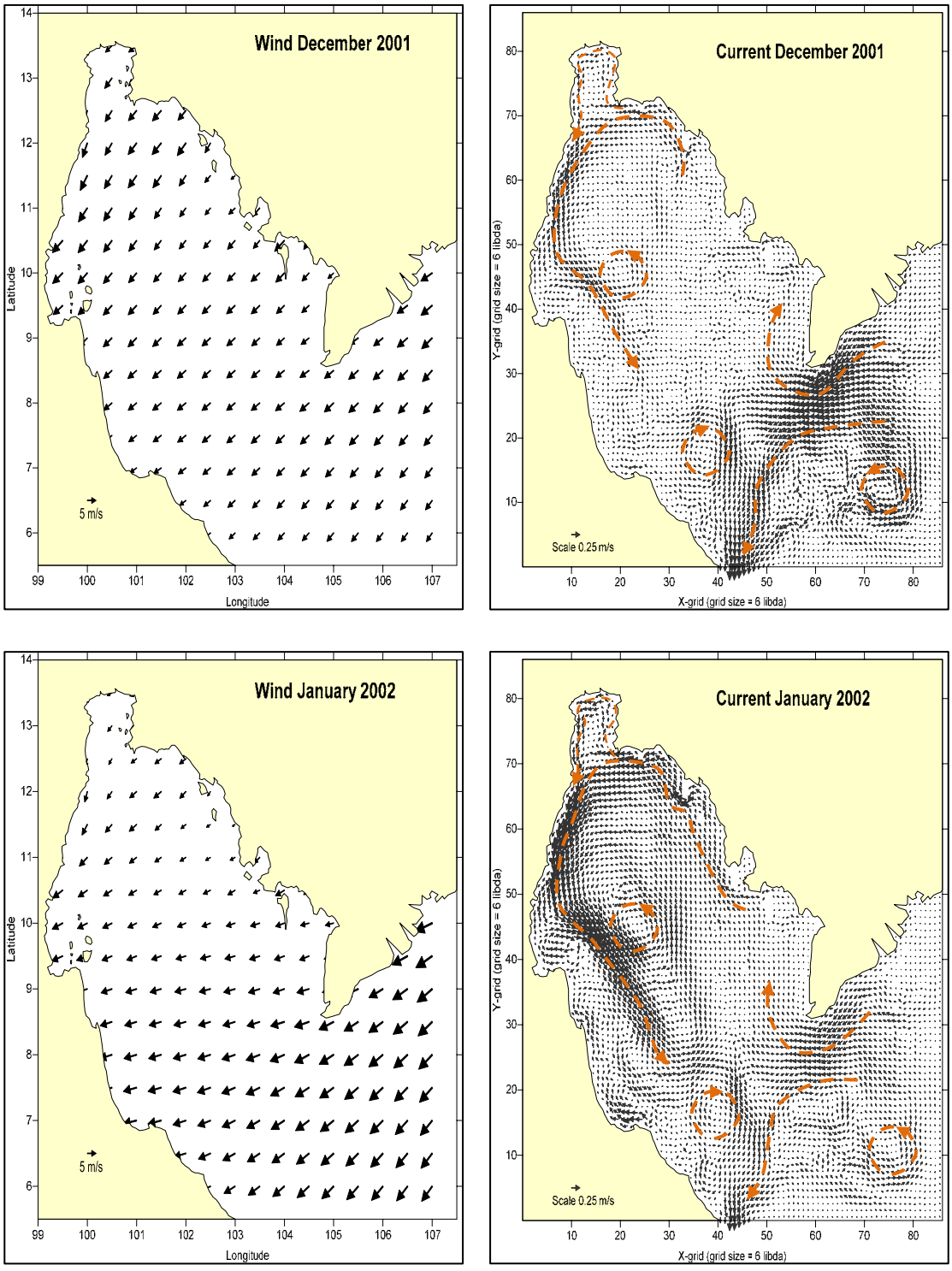

Monthly mean simulated wind and wind-driven current over the Gulf of Thailand in December 2001 and January 2002.

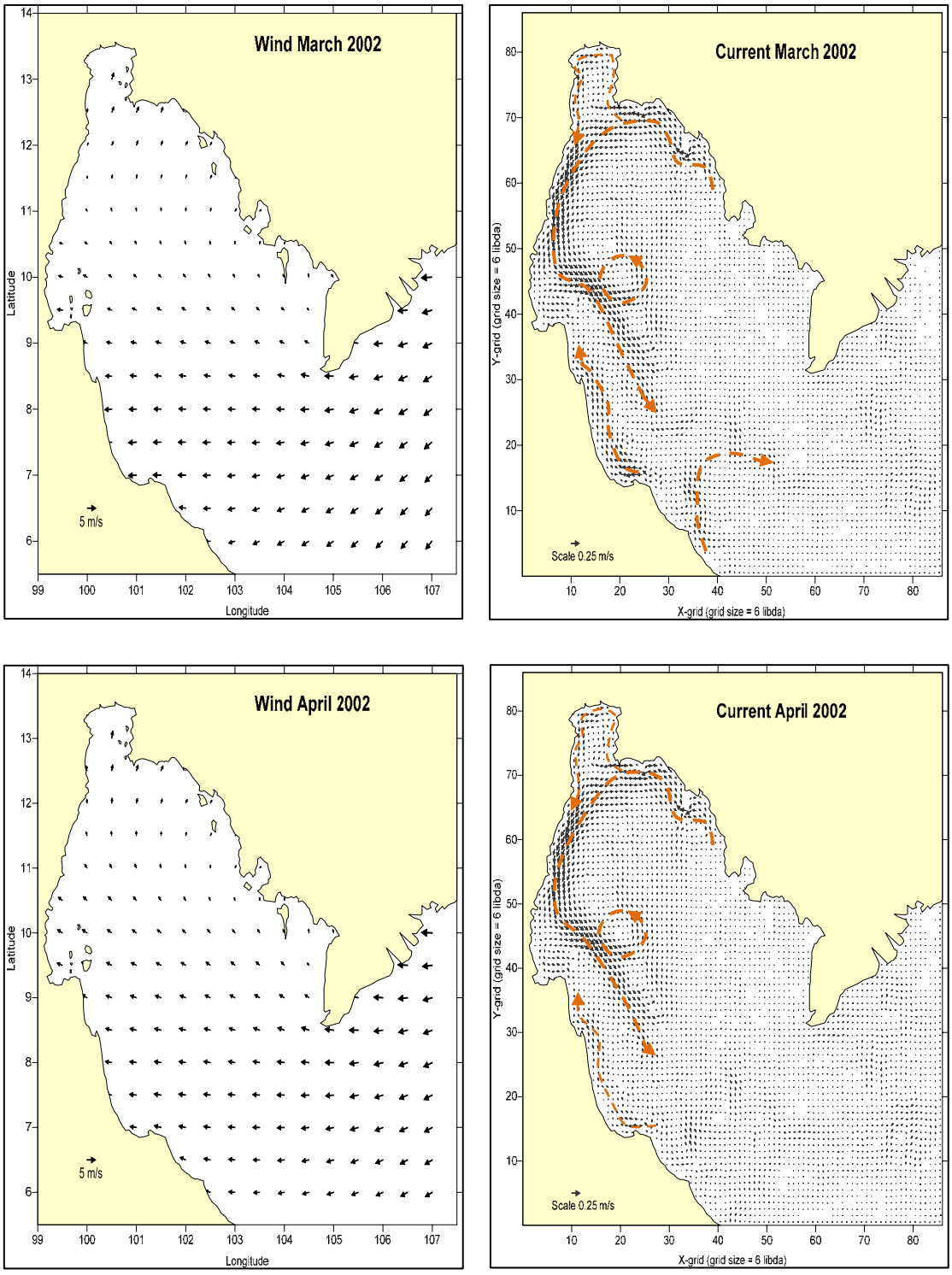

Monthly mean simulated wind and wind-driven current over the Gulf of Thailand in March and April 2002.

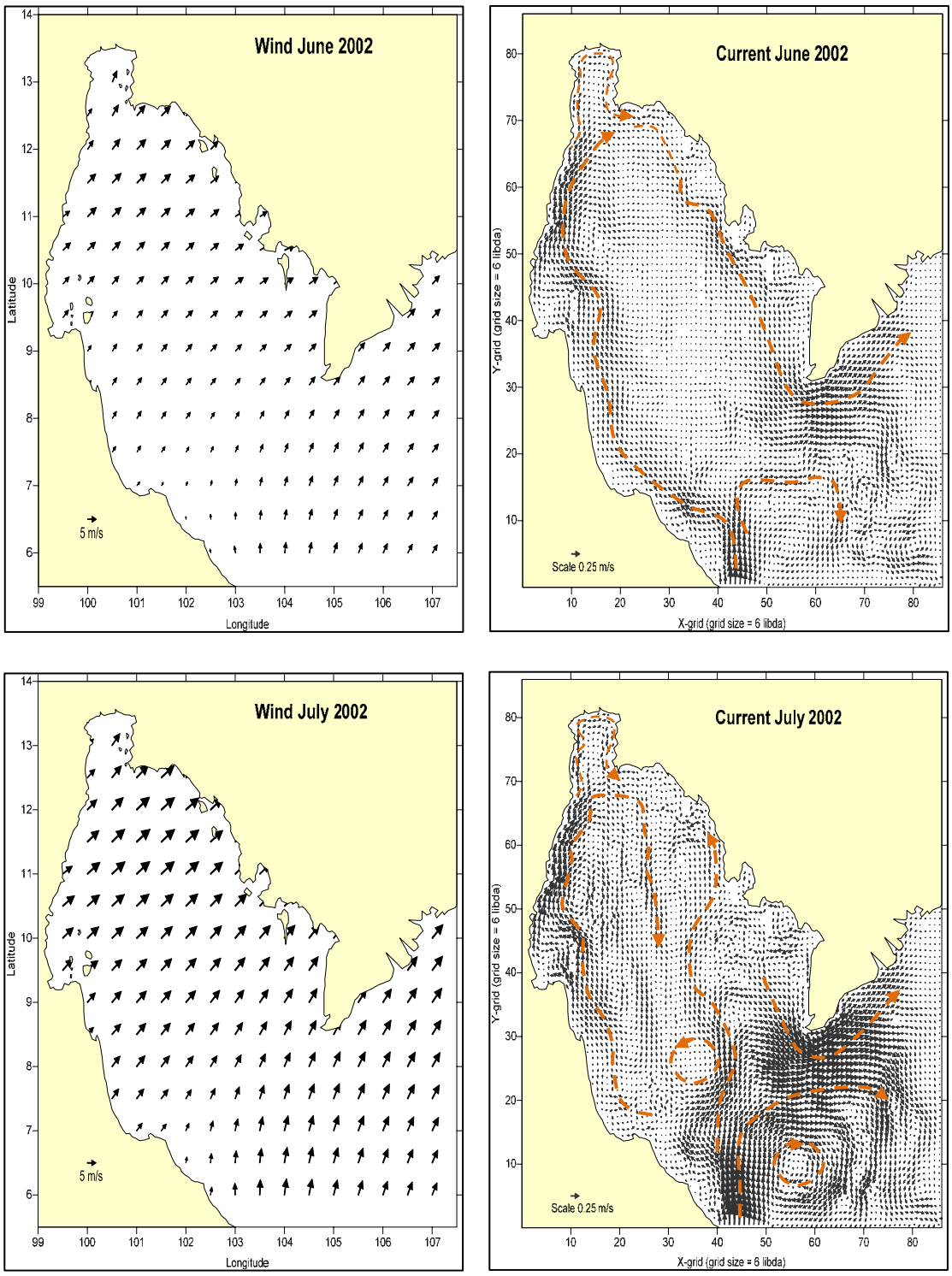

Monthly mean simulated wind and wind-driven current over the Gulf of Thailand in June and July 2002.

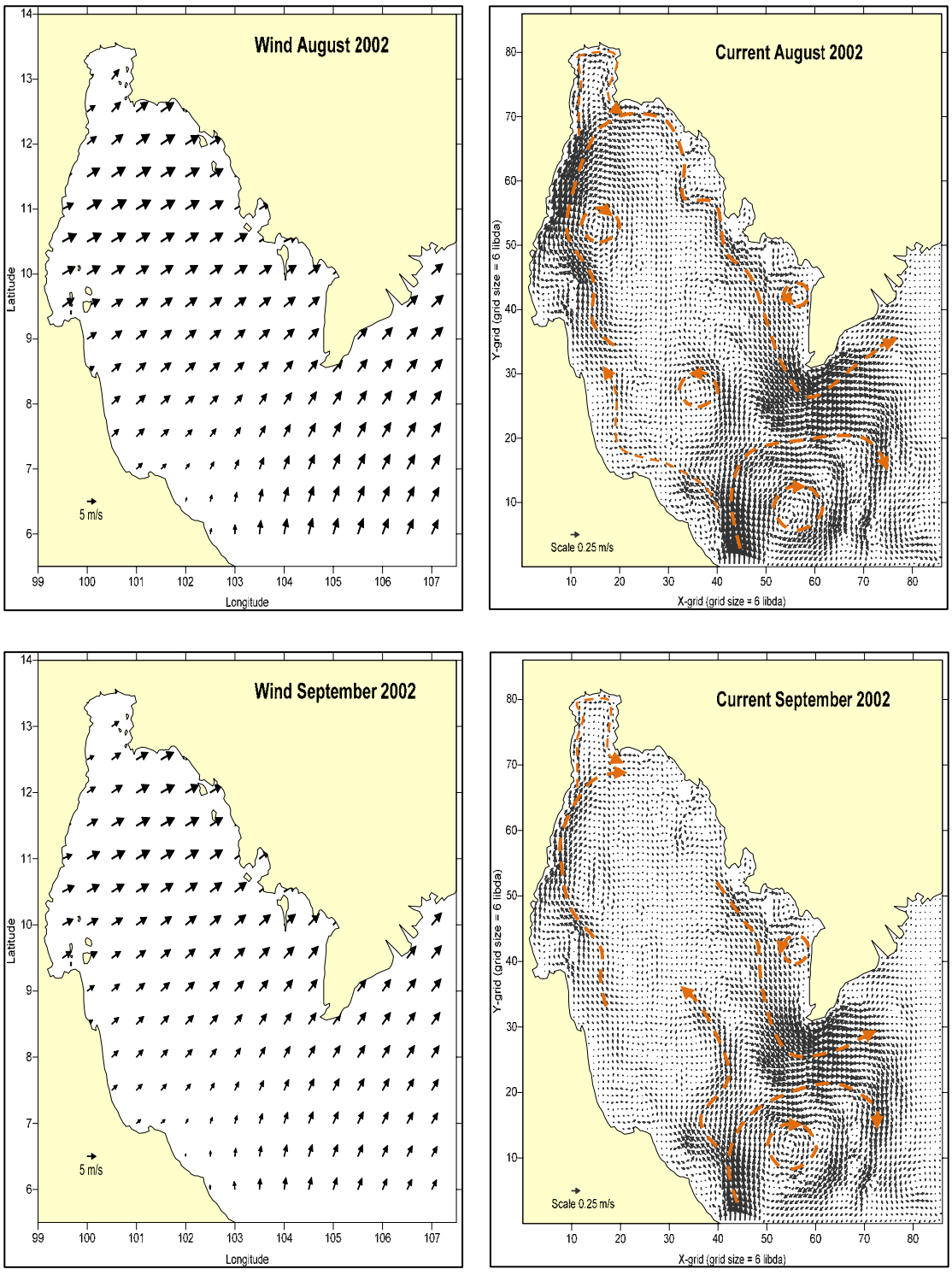

Monthly mean simulated wind and wind-driven current over the Gulf of Thailand in August and September 2002.

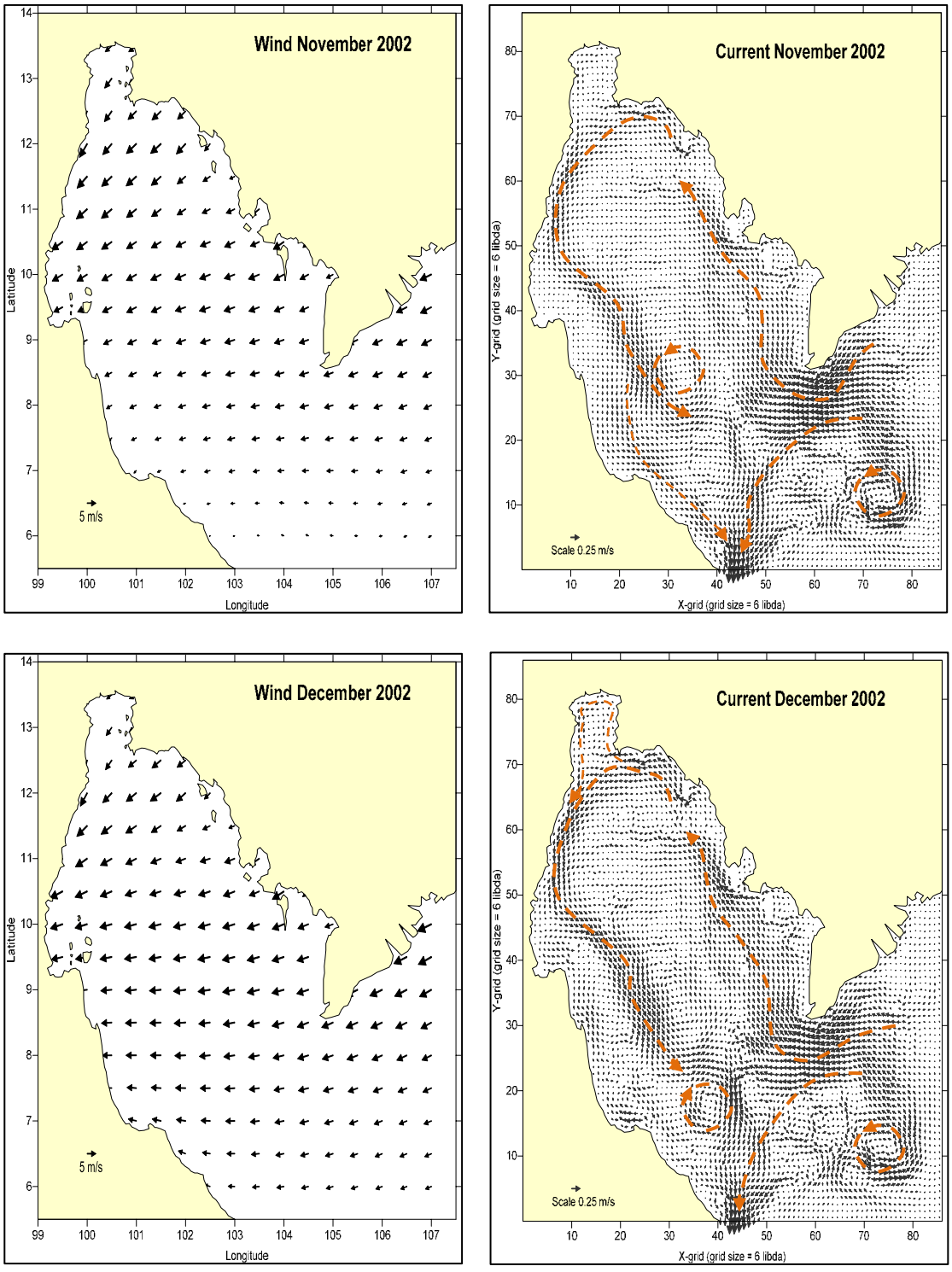

Monthly mean simulated wind and wind-driven current over the Gulf of Thailand in November and December 2002.

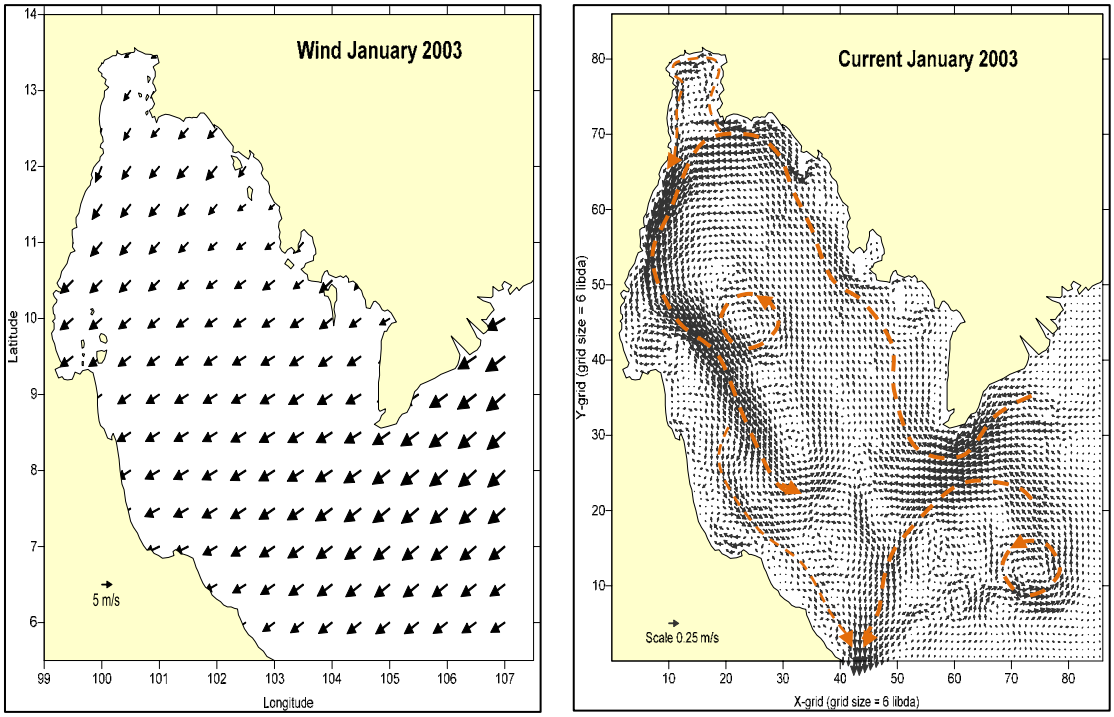

Monthly mean simulated wind and wind-driven current over the Gulf of Thailand in January 2003.

Appendix B

El Niño, La Niña, and Normal year in 1951-2010

ปีเอลนีโญ	ปีลานีญา	ปีปกติ
ส.ค.-ธ.ค.1951(15 เดือน)	ม.ค.1950-มี.ค.1951(15 เดือน)	เม.ย.-ก.ค.1951(4 เดือน)
เม.ย.1957-ม.ค.1958(15 เดือน)	เม.ย.1954-ม.ค.1957(34 เดือน)	ก.พ.-มี.ค.1957(2 เดือน)
ก.ค.1963-ม.ค.1964(7 เดือน)	ก.ย.1962-ม.ค.1963(5 เดือน)	ก.ค.1958-ส.ค.1962(50 เดือน)
มิ.ย.1965-เม.ย.1966(11 เดือน)	เม.ย.1964-ม.ค.1965(10 เดือน)	ก.พ.1963-มิ.ย.1963(5 เดือน)
ธ.ค.1968-มิ.ย.1969(8 เดือน)	ธ.ค.1967-เม.ย.1968(5 เดือน)	ก.พ.-มี.ค.1964(2 เดือน)
ก.ย.-ธ.ค.1969(4 เดือน)	ก.ค.1970-ม.ค.1972(19 เดือน)	ก.พ.-มี.ค.1965(4 เดือน)
พ.ค.1972-มี.ค.1973(11 เดือน)	พ.ค.1973-พ.ค.1976(37 เดือน)	มี.ค.1966-พ.ย.1967(19 เดือน)
ก.ย.1976-ก.พ.1977(6 เดือน)	ต.ค.1984-ก.ย.1985(12 เดือน)	มี.ค.-ต.ค.1968(6 เดือน)
ก.ย.1977-ม.ค.1978(5 เดือน)	พ.ค.1988-พ.ค.1989(13 เดือน)	ก.ค.-ส.ค.1969(2 เดือน)
มี.ค.1982-มิ.ย.1983(14 เดือน)	ก.ย.1995-มี.ค.1996(7 เดือน)	ม.ค.-มิ.ย.1970(6 เดือน)
ส.ค.1986-ก.พ.1988(19 เดือน)	ก.ค.1998-ก.พ.2001(32 เดือน)	ก.พ.-เม.ย.1972(3 เดือน)
พ.ค.1991-ก.ค.1992(15 เดือน)	ก.ย.2007-พ.ค.2008(9 เดือน)	เม.ย.1973(1 เดือน)
พ.ค.1994-มี.ค.1995(11 เดือน)		มิ.ย.-ส.ค.1976(3 เดือน)
พ.ค.1997-พ.ค.1998(13 เดือน)		มี.ค.-ส.ค.1977(6 เดือน)
พ.ค.2002-มี.ค.2003(11 เดือน)		ก.พ.1978-เม.ย.1982(51 เดือน)
มิ.ย.2004-ก.พ.2005(9 เดือน)		ก.ค.1983-ก.ย.1984(15 เดือน)
ส.ค.2005-ม.ค.2006(6 เดือน)		ต.ค.1985-ก.ค.1986(10 เดือน)
มิ.ย.2009-ม.ค.2010(8 เดือน)		มิ.ย.1989-เม.ย.1991(23 เดือน)
		ส.ค.1992-เม.ย.1994(21 เดือน)
		เม.ย.-ส.ค.1995(5 เดือน)
		เม.ย.1996-เม.ย.1997(13 เดือน)
		มิ.ย.1998(1 เดือน)
		มี.ค.2001-เม.ย.2002(14 เดือน)
		เม.ย.2003-พ.ค.2004(14 เดือน)
		มี.ค.2005-ก.ค.2006(17 เดือน)
		ก.พ.-ส.ค.2007(7 เดือน)
		มิ.ย.2008-พ.ค.2009(12 เดือน)

Jutakorn, J., 2010.

BIOGRAPHY

Mr. Pracha Chiongkarn was born in Phayao, Thailand on October 9, 1986. He received a B.Sc. (Physical Oceanography) in 2008 from the Department of Marine Science, Faculty of Science, Chulalongkorn University. In 2009, he enrolled for his M.Sc. degree (Earth Sciences program) at the Department of Geology, Faculty of Science, Chulalongkorn University.